Synthesis and properties of colloidal heteronanocrystals†

Celso de Mello Donegá*

Received 27th July 2010
DOI: 10.1039/c0cs00055h

Colloidal heteronanocrystals (HNCs) can be regarded as solution-grown inorganic–organic hybrid nanomaterials, since they consist of inorganic nanoparticles that are coated with a layer of organic ligand molecules. The hybrid nature of these nanostructures provides great flexibility in engineering their physical and chemical properties. The inorganic particles are heterostructured, *i.e.* they comprise two (or more) different materials joined together, what gives them remarkable and unique properties that can be controlled by the composition, size and shape of each component of the HNC. The interaction between the inorganic component and the organic ligand molecules allows the size and shape of the HNCs to be controlled and gives rise to novel properties. Moreover, the organic surfactant layer opens up the possibility of surface chemistry manipulation, making it possible to tailor a number of properties. These features have turned colloidal HNCs into promising materials for a number of applications, spurring a growing interest on the investigation of their preparation and properties. This *critical review* provides an overview of recent developments in this rapidly expanding field, with emphasis on semiconductor HNCs (*e.g.*, quantum dots and quantum rods). In addition to defining the state of the art and highlighting the key issues in the field, this review addresses the fundamental physical and chemical principles needed to understand the properties and preparation of colloidal HNCs (283 references).

Debye Institute for Nanomaterials Science, Utrecht University, Princetonplein 5, 3584 CC Utrecht, Netherlands. E-mail: C.demello-donega@uu.nl; Fax: 31-30-2532403; Tel: 31-30-2532226

† Electronic supplementary information (ESI) available: Slow-motion movie showing the fast injection of a cold solution of precursors (TOP-Se and $Cd(CH_3)_2$ in TOP) into a hot coordinating solvent (TOPO and HDA diluted in ODE). The movie is a fragment of a documentary series broadcast by the Discovery Channel in 2007, in which our group participated (*Update 2056*: *The world in 50 years*, Episode 03, Copyright 2007 Discovery Channel). See DOI: 10.1039/c0cs00055h

Celso de Mello Donegá

After degrees in Chemistry from the State University of São Paulo (Brazil), Celso de Mello Donegá moved to the Netherlands, where he worked under the supervision of Prof. G. Blasse from 1991 to 1994, being awarded a PhD degree in Chemistry from Utrecht University in 1994. Upon his return to Brazil in 1995, he was appointed Associate Professor at the Federal State University of Pernambuco. He moved back to the Netherlands in 2000 to join the Condensed Matter and Interfaces Group of the Debye Institute for Nanomaterials Science (Utrecht University), initially as a Post-doctoral associate, and later as tenured Assistant Professor. His research is focused on the synthesis and optical spectroscopy of luminescent nanomaterials.

1. Introduction

The novel and extraordinary properties of complex materials outperform those of the individual components, and emerge from an intricate architecture involving organization of matter at several levels. Colloidal heteronanocrystals (HNCs) provide an example of such complex materials, as they consist of inorganic heterostructured nanocrystals (NCs) that are coated with a layer of organic molecules. The hybrid inorganic–organic nature of these nanomaterials greatly expands the possibilities for property control, since both components can be independently manipulated to achieve or optimize a desired property. Moreover, synergistic interactions may give rise to novel properties.

An essential feature of colloidal NCs and HNCs is that, owing to their nanoscale dimensions, size effects can be fully exploited to engineer the material properties (Fig. 1). Spatial confinement effects become increasingly important as the dimensions of a NC decrease below a certain critical limit, leading to size- and shape-dependent electronic structure.[1,2] Further, as the NC size decreases, the number of atoms is reduced from a few thousand to a few hundred and therefore the surface to volume ratio increases dramatically (*e.g.*, from 5% to 50% for a reduction from 20 to 2 nm in diameter).[1,2] Consequently, the contribution of the surface to the total free energy of a NC becomes significant and increases with decreasing size, making the interaction between the surface atoms and surfactant molecules crucially relevant (Fig. 2). This has important consequences, one of them being that the NC becomes easily dispersible in solvents (Fig. 1), making fabrication and processing in solution possible, which is an essential advantage of colloidal NCs over nanomaterials

Fig. 1 Suspensions of colloidal CdSe NCs of different sizes (1.7 to 4.5 nm diameter, from left to right) under UV excitation. This iconic image of colloidal nanoscience provides a beautiful visual demonstration of two fundamental nanoscale effects: quantum confinement (size dependent luminescence colours) and large surface to volume ratio (colloidal stability).

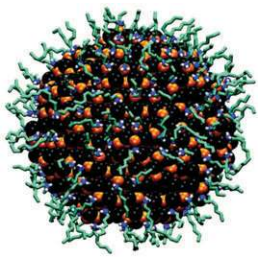

Fig. 2 Molecular simulation snapshot of a colloidal CdSe NC capped by hexylamine molecules. Colour coding: black, Se; orange, Cd; light blue, C; dark blue, N; white, H; yellow, S; brown, P; red, O. The simulation methodology is described in ref. 3. Courtesy of P. Schapotschnikow (Delft University of Technology, Netherlands).

prepared by other techniques (*e.g.*, molecular beam epitaxy). Colloidal chemistry methods are also cheaper and easier to upscale, and are highly versatile in terms of composition, size, shape and surface control. Moreover, colloidal NCs can be used as building blocks for complex nanostructures, such as NC superlattices.[4,5]

The combination of ease of fabrication and processing and flexibility in property-tailoring has turned colloidal NCs and HNCs into promising materials for a multitude of applications (optoelectronics, photonics, spintronics, catalysis, solar energy conversion, thermoelectrics, information processing and storage, sensors, and biomedical applications),[4–18] spurring an intense research activity over the past decades. As a result, a remarkable degree of control over the composition, size, shape and surface of colloidal NCs has been achieved. Several excellent reviews and books covering various aspects of colloidal NC research have been published recently.[4–9,16–47] Therefore, this *critical review* is not intended as a comprehensive treatise, but rather as an enticing overview of the field, in which the fundamental principles are highlighted and the current state-of-the-art is outlined and discussed.

2. Properties of colloidal heteronanocrystals: when the whole is greater than the sum of its parts

The properties of colloidal HNCs emerge from their hybrid organic–inorganic nature, and are dictated not only by the individual characteristics of the inorganic and organic components, but also by their mutual interaction. The organic–inorganic interface and the interplay between the organic surfactant molecules are also of crucial importance during the synthesis of colloidal HNCs, being the driving forces behind the remarkable control achieved in recent years over the size, shape and architecture of HNCs (section 3 below). This has yielded an exquisite variety of colloidal HNCs, spanning from concentric core/(multi)shell quantum dots (QDs) of various shapes to intricate multipod HNCs, *via* heterodimers, nanodumbbells and heteronanorods (Fig. 3).[25–30]

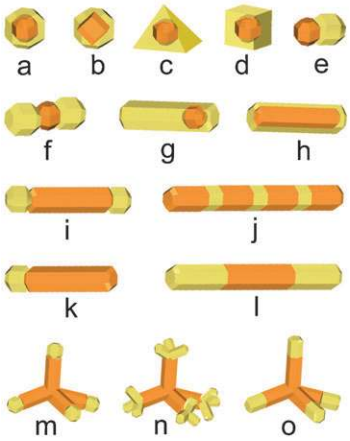

Fig. 3 Schematic survey of colloidal HNC architectures (for clarity the surfactant layer is not represented). The diversity of possible material combinations for each category can be illustrated by a few examples: (a) CdSe/ZnS,[30] InP/ZnS,[30] Co/CdSe;[48] (b) PbSe/CdSe;[49] (c) CdTe/CdSe;[50] (d) Au/Fe_3O_4;[51] (e) Au–Fe_3O_4,[52] CdSe–Fe_2O_3,[53] CdSe–Au,[54] FePt–CdSe,[55] FePt–PbS,[55] CdS–Fe_2O_3;[56] (f) Au–Fe_3O_4–Au;[51] (g) CdSe/CdS,[57–59] ZnSe/CdS;[59] (h) Au/Ag;[29] (i) CdTe–CdSe–CdTe,[60] PbSe–CdSe–PbSe,[61] Au–CdSe–Au,[62] Co–TiO_2–Co;[63] (j) CdS–Ag_2S;[64] (k) PbSe–CdSe,[61] Co–TiO_2;[63] (l) CdSe–CdS–CdSe,[65] CdTe–CdSe–CdTe;[66] (m) CdSe–Au;[62] (n) CdSe–CdTe;[65] (o) CdSe–CdTe.[65] TEM images of some of these HNCs will be provided later. Courtesy of M. Casavola (Utrecht University, Netherlands).

2.1 The inorganic component

The inorganic nanoparticle (NP) dictates the optoelectronic and magnetic properties, which are defined by the composition, size and shape of the HNC. These properties may be further modulated or modified by the organic ligand layer, as will be discussed below (section 2.2).

A HNC comprises two (or more) materials that share one or more interfaces. The nature of the materials connected by the heterojunction can be widely different.[25–30] Consequently, HNCs can be made combining metals (*e.g.*, Ag–Au), metals and semiconductors (*e.g.*, Au–CdSe), metals and insulators (*e.g.*, Co–Fe_3O_4 or Au–SiO_2), metal alloy and metal oxides (*e.g.*, FePt–Fe_3O_4), and different semiconductors or insulators (*e.g.*, CdSe-ZnS or ZnS-Fe_3O_4). Multicomponent colloidal HNCs combining different types of materials have also been obtained (*e.g.*, CdSe/(Cd,Zn)S/ZnS core/multishell QDs embedded in SiO_2 NPs[67]).

The ability to join different materials in the same HNC opens up a rich realm of possibilities for property engineering. For example, magnetic and optical functionalities can be

combined in a single HNC (*e.g.*, FePt/PbSe dumbbell and core/shell HNCs[26,68]) or two different magnetic materials may be coupled (*e.g.*, Co/Fe_2O_3).[69] Alternatively, an inert material can be used to add chemical stability and/or modify the solubility of a colloidal HNC without affecting its optical properties (*e.g.*, encapsulation of QDs in amorphous silica[67]). Moreover, novel properties may arise from the interaction between the different components of the HNC, as will be discussed below.

2.1.1 Confinement effects. The nanoscale dimensions of HNCs can be exploited to further expand the gamut of properties originating from a given combination of materials. However, the impact of spatial confinement is not the same for different materials and/or different properties, as it depends on characteristic length scales of a given physical property, which are ultimately determined by the material's composition and structure. For example, confinement effects on magnetic properties will only be observed for dimensions comparable to (or smaller than) the critical magnetic single domain size.[2,8]

The profound impact of spatial confinement on the optical properties of semiconductor NCs is illustrated in Fig. 1. The relevant length scale in this case is the exciton Bohr radius (a_0), a dimension describing the spatial extension of excitons (*i.e.*, electron-hole pairs) in solids, which ranges from ~2 to ~50 nm depending on the material.[1] As the NC size approaches a_0, confinement begins to affect the exciton wave function, inducing changes in the density of electronic states and in the energy level separation,[1] which are manifested in an increase of the bandgap (HOMO–LUMO gap, E_g) with decreasing size and the appearance of discrete energy levels near the band edges (Fig. 4). As a result, the optoelectronic properties of semiconductor NCs become strongly size- and shape-dependent, making it possible to tune the photoluminescence (PL) of semiconductor NCs through a wide spectral window by choosing the composition, size and shape of the NC. It is worth noting that a_0 and E_g are correlated, so that materials with narrower E_g have larger a_0, and therefore experience quantum confinement (QC) at larger NC sizes.

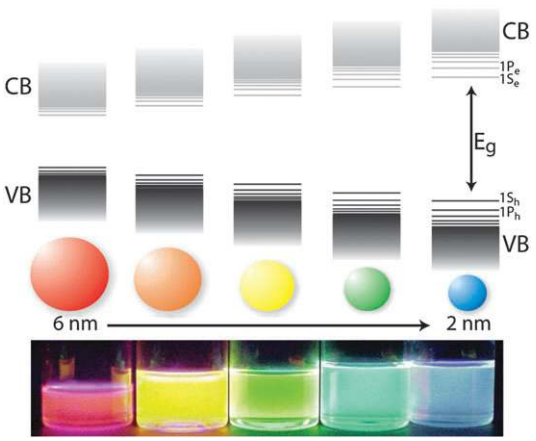

Fig. 4 Schematic representation of the quantum confinement effect on the energy level structure of a semiconductor material. The lower panel shows colloidal suspensions of CdSe NCs of different sizes under UV excitation. Courtesy of R. Koole (Philips Research Laboratories, Netherlands).

In contrast, insulators (*e.g.*, $E_g \geq 4$ eV, Lu_2O_3) possess very small a_0 (<1 nm), and are thus affected by QC only for sizes already in the cluster regime (<20 atoms).[70] Further, the degree of QC may vary along different directions depending on the NC shape.[1] For instance, a NC with all dimensions comparable to or smaller than a_0 is referred to as a quantum dot (QD), since it confines the exciton in all directions, therefore being experienced as a 0-dimensional (0D) object. Similarly, NCs in which the exciton is confined only in the diameter direction are referred to as quantum wires (1D), while in a quantum well QC occurs only in the thickness direction (2D). Quantum rods (QRs) are NCs in transition from 0D to 1D confinement regime.

2.1.2 Surface and trap states. Surface atoms have fewer neighbours than their interior counterparts, and therefore possess unsatisfied chemical bonds (dangling bonds). These unshared atomic orbitals give rise to energy levels within the HOMO–LUMO gap of the NC.[1,2] This is detrimental to the PL quantum yield (PL QY) of the NC, because exciton relaxation into localized surface states reduces the overlap between the electron (*e*) and hole (*h*) wave functions, thereby making radiative recombination less likely. Surface defects give rise to even lower energy states, known as trap states, since they lead to strong carrier localization. Due to this localization the *e*–*h* wave function overlap nearly vanishes, and the exciton relaxation proceeds primarily *via* nonradiative pathways (*i.e.*, energy dissipation as heat by coupling to vibrations). For these reasons, it is essential to control the surface quality and to eliminate dangling bonds, a process known as surface passivation. This can be achieved either by overgrowing a shell of a wider band gap semiconductor or by coating the surface with suitable organic ligands (see sections 2.1.4 and 2.2, respectively).

2.1.3 Doped nanocrystals. The intentional introduction of impurities (doping) is vital to a large number of technologies, since the properties of materials for lighting, electronic and optoelectronic applications are largely controlled by dopants. Doping of bulk materials has therefore evolved into a very mature field. In contrast, the ability to precisely control the doping of NCs was until recently rudimentary. However, the possibility to impart new properties (optical or magnetic) to colloidal NCs by means of doping has stimulated efforts to develop methods to incorporate dopants into a variety of NCs (both semiconductor and insulator materials). This has lead in recent years to great advances in the fundamental understanding of doping in NCs,[71,72] and to several novel nanomaterials (*e.g.*, LaF_3 : Yb,Er;[73] $NaYF_4$: Yb,Er;[74] ZnO : Li;[75] CdSe : Mn;[76,77] ZnSe : Mn;[72] ZnO : Co;[71] and ZnO : Mn doped NCs;[78] and ZnSe : Co/CdSe;[79] and ZnSe : Mn/CdSe[79,80] doped core/shell HNCs).

2.1.4 Excitons in semiconductor heteronanocrystals. The ability to create novel optoelectronic properties can be extended further by using semiconductor HNCs instead of single composition NCs. The band alignment between the materials that are combined at the heterojunction is of paramount importance. Depending on the energy offsets between the HOMO and the LUMO levels of the two adjoining materials,

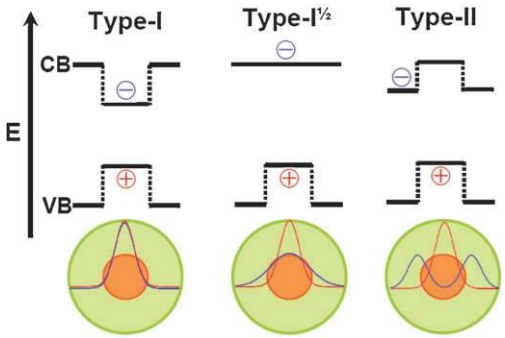

Fig. 5 Schematic representation of the three limiting charge carrier localization regimes in core/shell semiconductor HNCs. The conduction and valence band edges (*i.e.*, the LUMO and HOMO energy levels) are indicated by CB and VB, respectively. The plus and minus signs represent the charge carriers (hole and electron, respectively). The electron and hole ground-state wave functions are schematically depicted in the lower panel. Courtesy of M. Vis and A. G. M. Brinkman (Utrecht University, Netherlands).

different charge carrier localization regimes will be observed after photoexcitation. Three limiting cases can be identified: Type-I, Type-I$^{1/2}$ and Type-II (Fig. 5).[81] In the Type-I regime the band gap of one semiconductor lies entirely within the gap of the other material. Therefore, after photoexcitation *e* and *h* are confined primarily in the same part of the HNC (the narrower gap material), resulting in a direct exciton. In the Type-II case the staggered energy level alignment results in the spatial separation of *e* and *h* on different sides of the heterojunction, leading to the formation of a spatially indirect exciton. In the Type-I$^{1/2}$ regime (also known as "*quasi* type-II" regime[82]) one carrier is confined in one of the components, while the other is delocalized over the whole HNC.

The band offsets in the bulk limit can be obtained from the band positions of the bulk semiconductors, which are known only for a limited number of materials (Fig. 6). Since the position and the density of energy states in quantum confined semiconductor NCs is governed by size and dimensionality (section 2.1.1),[1] the energy offsets in semiconductor HNCs can be tuned by a judicious control of the composition, size and shape of each component. This offers the possibility of directly controlling the *e*–*h* wavefunction overlap, thereby tailoring the

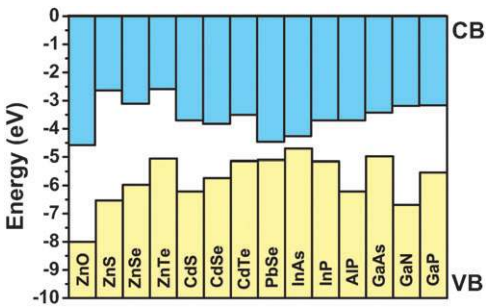

Fig. 6 The energy of the electronic band edges relative to the vacuum level of selected semiconductors (VB: valence band, CB: conduction band). The space between the solid bars gives the band gap. Bulk values are used, except for PbSe, which have been estimated from NC results.[71]

material optoelectronic properties. This flexibility in engineering the properties of colloidal HNCs has important consequences for a number of technologies, and opens up interesting application possibilities: low-threshold lasers, light-emitting diodes, photovoltaic devices, fast optical switches, IR detectors, fast access memories, spintronic devices, and labels for biomedical imaging.[5,12–14,82–90] This has turned the investigation of semiconductor HNCs into a captivating research topic, which is attracting increasing attention worldwide. An overview of the properties associated with each type of HNC will be given below.

Type-I HNCs. Type-I concentric core/shell QDs (*e.g.*, CdSe/ZnS, CdS/ZnS, InP/ZnS) are the most investigated colloidal semiconductor HNCs.[30,91–99] This large interest stems from the fact that the exciton is confined to the core, and therefore is protected from interaction with the surface and the environment. Moreover, the exciton no longer probes dangling orbitals since the interface core atoms are bound to the shell atoms. Consequently, the PL QYs are high ($\geq$ 50%) and the stability against photodegradation is enhanced.[30] The properties of a direct exciton in a type-I HNC are dictated primarily by the narrow gap material. This means that upon the shell overgrowth the emission and absorption spectra of the core should remain unaffected, except for the appearance of new high energy absorption peaks associated with the shell material. However, the energy offsets between the two materials are finite and therefore the exciton wave function partially extends into the shell (this is usually referred to as "exciton leakage"). Consequently, a small redshift will be observed for all exciton transitions, both in emission and absorption (see, *e.g.*, CdSe/ZnS in Fig. 7b). The redshift is proportional to the reduction in exciton confinement and therefore is larger for smaller offsets. The energy difference between the maxima of the emission band and of the lowest energy absorption band (the so-called "non resonant Stokes shift") is not affected, and remains $\leq$20 meV (Fig. 7d).[83] The exciton radiative lifetime also remains essentially the same (Fig. 7c),[92,96] although the observed PL decay time will typically be longer, due to the reduction of the non-radiative recombination rates, since the exciton no longer probes the surface.

In practice, the exciton leakage into the shell implies that thick shells (and larger offsets) are needed to effectively prevent the exciton from probing the surface. However, interfacial strain induced by lattice mismatch between the core and shell materials becomes a serious issue for thick shells, and may severely limit the maximum thickness. For example, from the viewpoint of energy offsets, ZnS is the best shell material for CdSe based core/shell QDs, but the large lattice mismatch (12%) makes it difficult to grow shells thicker than 2–3 monolayers (MLs). ZnSe and CdS give smaller lattice mismatches (6.3% and 3.9%, respectively), but also smaller energy offsets. The solution is to grow multiple shells of different compositions around a central core, so that the energy offsets progressively increase towards the surface, but with small lattice mismatches between subsequent shells (*e.g.*, CdSe/CdS/(Cd,Zn)S/ZnS core/multishell QDs[30,97]). The use of gradient alloy shells (the so-called graded shells, *e.g.*, (Cd,Zn)S) is particularly effective, as it allows the lattice

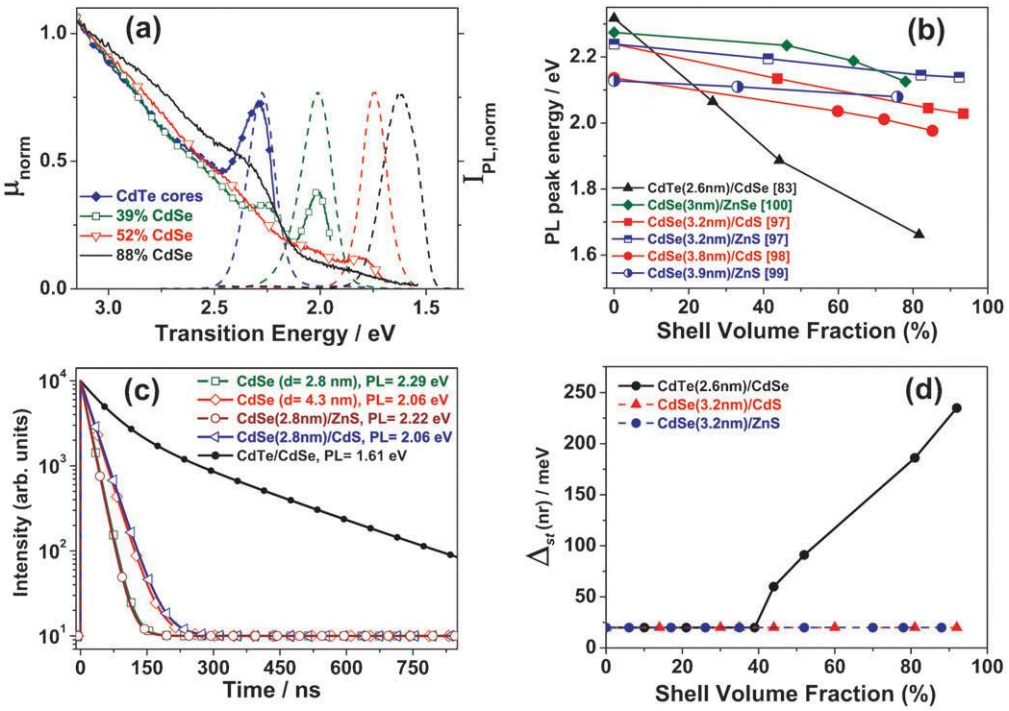

Fig. 7 (a) Photoluminescence (PL, dashed lines) and PL excitation (PLE, solid lines) spectra of colloidal CdTe/CdSe HNCs with a 2.6 nm CdTe core and increasing CdSe volume fraction (39% to 88%) (data from ref. 83). PL spectra are normalized at the peak. PLE spectra are normalized to 1 at 3.1 eV. The symbol μ_{norm} gives the normalized absorption cross section per Cd(Te,Se) ion pair unit. The evolution from Type-I$^{1/2}$ (39% CdSe) to Type-II (88%CdSe) localization regimes is clearly observed. (b) PL peak position of colloidal core/shell HNCs of different compositions as a function of the shell volume fraction. The diameter of the core NC is indicated between brackets. The compositions were chosen as representative examples of different carrier localization regimes (*viz.*, Type-I: CdSe/ZnS and CdSe/thin shell ZnSe; Type-I$^{1/2}$: CdSe/CdS, CdSe/thick shell ZnSe, CdTe/thin shell CdSe; Type-II: CdTe/thick shell CdSe). (c) PL decay curves of CdSe QDs and three different core/shell HNCs.[83] To facilitate comparison, only the initial 850 ns of the decay curve of CdTe/CdSe are shown. (d) Non-resonant Stokes shift ($\Delta_{ST}(nr)$) as a function of the shell volume fraction for different core/shell HNCs.[83]

parameters and energy offsets to be smoothly tuned from the small mismatch and small offset material to the large mismatch and large offset material (Fig. 8). In this way, the exciton no longer probes the surface, while undesirable interfacial strain is minimized. Shell growth strategies will be discussed in more detail below (section 3).

The multishell strategy has greatly increased our ability to control the epitaxial shell growth and has yielded sophisticated HNCs (both Type-I and Type-II) in which shells of various compositions are sequentially grown around a central core. Interesting recent examples are the so-called "giant"

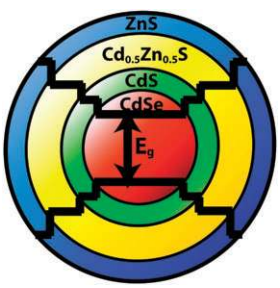

Fig. 8 Schematic representation of a core/multishell colloidal QD. The gradual increase in the band gap (E_g) from the core (CdSe) to the outer shell (ZnS) is also illustrated. Courtesy of R. Koole (Philips Research Laboratories, Netherlands).

CdSe/CdS core/shell NCs,[86] consisting of a 3 nm CdSe core overcoated by 19 MLs of CdS, and (Cd,Zn)Se/ZnSe core/shell HNCs,[91] which consist of a (Cd,Zn)Se gradient alloy NC overcoated with a ZnSe shell. In both cases, Auger recombination processes are largely suppressed, resulting in non-blinking NCs (*i.e.*, without PL intermittency at the single NC level)[86,91] and optical amplification at low excitation thresholds.[86] Further, CdSe/ZnS/ZnSe/CdSe core/multishell QDs have been recently synthesized, allowing the intraband relaxation rates of hot electrons to be slowed down by orders of magnitude.[84]

Type-I$^{1/2}$ HNCs. The most investigated Type-I$^{1/2}$ HNC composition is CdSe/CdS, although it is usually referred to as a "Type-I" core/shell QD.[30] However, it is well established that the energy offset for the electron is too small to confine it to the CdSe core, and, consequently, the *e* wave function will delocalize over the entire HNC, while the *h* is confined in the CdSe core.[95,98] Anisotropic CdSe/CdS HNCs (*e.g.*, CdSe/CdS dot core/rod shell nanorods) have also been recently obtained,[57–59] and shown to exhibit intriguing optical properties, such as linearly polarized PL that can be manipulated by external electric fields.[101] Further, the exciton radiative lifetimes were observed to be longer in these anisotropic HNCs than in CdSe/CdS concentric core/shell QDs. These optical properties were interpreted as signature of decreased *e*–*h* overlap due to localization of the hole in the CdSe core and electron

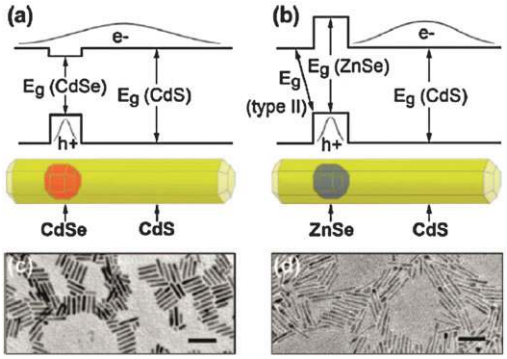

Fig. 9 Schematic illustration of the predicted band structures and the electron and hole ground-state wave functions of (a) Type-$I^{1/2}$ CdSe/CdS and (b) Type-II ZnSe/CdS dot core/rod shell HNCs. TEM images of the (c) CdSe/CdS and (d) ZnSe/CdS core/shell nanorods. Scale bars: 50 nm. Reproduced with permission from ref. 59. Copyright 2008 American Chemical Society.

delocalization over the whole HNC (Fig. 9).[101] This picture has been partially challenged by recent scanning tunneling spectroscopic investigations, which led to the conclusion that the electron ground-state wave function is primarily localized in the CdSe core, while higher energy electron states extend over the whole HNC.[59]

Other examples of Type-$I^{1/2}$ HNCs are ZnSe/CdSe core/shell QDs (*e* localized in CdSe shell, *h* delocalized over the HNC),[82,100] CdTe/CdSe core/thin shell HNCs (*h* is confined to core, *e* is delocalized),[83] and PbSe/CdSe core/thin shell QDs (*h* in core, *e* delocalized).[102] The redshift observed in the PL and absorption spectra upon shell overgrowth (*viz*., up to 200–400 meV, depending on the core diameter) is much larger than that observed for Type-I HNCs (Fig. 7b), due to the loss in confinement energy of the carrier that is delocalized over the entire volume of the HNC.[83] The Stokes shift, however, remains small ($\leq$20 meV) and is comparable to that observed for single component NCs and Type-I HNCs (Fig. 7d).[83] The absorption peaks remain distinct and well-defined (Fig. 7a), in contrast to the behaviour observed for Type-II HNCs (see below).[83,95] The delocalization of one of the carriers reduces the *e*–*h* overlap, leading to longer exciton radiative lifetimes. The PL QYs can be as high as 80%.[30,82,83]

Type-II HNCs. The properties of the spatially indirect exciton can be manipulated by choosing suitable combinations of semiconductors.[30,82,83] It should be noted that complete spatial separation occurs only for the physically unrealistic case of infinite offsets. For finite offsets the wave functions of the carriers partially extend across the heterojunction, leading to non-zero *e*–*h* overlap. The indirect nature of the exciton leads to longer radiative lifetimes,[82–83,103] increased exciton polarisability,[82] and emission at lower energies than those of the band-gaps of both materials,[82,83] thus allowing access to wavelengths that would otherwise not be available. It has also been reported to make single exciton lasing possible.[88] Further, the rates for Auger recombination,[103] hot carrier relaxation,[84] and spin flip[104] decrease, as a consequence of the (partial) spatial separation of the photoexcited carriers. In some systems charge separation rates in the sub-ps time regime have been observed (<0.35 ps for photoexcited electrons in ZnSe/CdS nanobarbells[105]). The potential of colloidal type-II HNCs has attracted increasing attention over the last few years, leading to the investigation of HNCs of various compositions (*viz*., CdTe–CdSe,[50,60,66,83,85,103,106–109] CdSe—ZnTe,[109,110] ZnTe–ZnSe,[111] and ZnSe–CdS,[59,82,84,105,112] Fig. 9) and shapes (*viz*., core/shell NCs,[50,82–84,103,107,109,110] rods and multipods,[59,66,83,85,106,108,110,112] and dumbbells[60,105]).

The redshift observed in the PL and absorption spectra upon shell overgrowth is very large (*e.g*., up to 0.5–0.8 eV for CdTe/CdSe HNCs, depending on the CdTe core diameter, Fig. 7b),[83,103,109] making Type-II HNCs promising near-IR emitters. It should be noted that thick shells (>1 nm) are needed to achieve the Type-II localization regime.[82–83,103] Thin shells yield Type-$I^{1/2}$ HNCs. The onset of the Type-II regime is characterized by the loss of structure of the lowest energy absorption band (*i.e*., a featureless absorption tail develops), accompanied by a simultaneous increase in the Stokes shift (up to 200–300 meV) and bandwidths (Fig. 7).[83] Also, the absorption cross section at emission energies decreases dramatically and the exciton radiative lifetime becomes much longer (0.2–2 μs, 1–2 orders of magnitude longer than that of a direct exciton in the same materials).[83] Until recently, low PL QYs have been seen as an intrinsic limitation of Type-II HNCs, since the slower indirect exciton radiative recombination can result in the dominance of faster nonradiative processes. However, pioneering work by several groups has recently demonstrated that improved synthesis methodologies can lead to highly luminescent Type-II HNCs, with PL QYs as high as 50–80% (CdS/(Cd,Zn)Se/ZnSe,[82] CdTe/CdSe/ZnS,[107] and CdTe/CdSe HNCs[50,83]).

2.1.5 Alloy nanocrystals. Research into semiconductor alloy NCs (alloy QDs) has been limited, and only a few compositions have been investigated (*viz*., Cd(Te,Se), Cd(S,Se), (Cd,Zn)Se, (Cd,Zn)S, (Cd,Zn)(S,Se)).[113–117] Alloy QDs can consist of homogeneous alloys or gradient alloys.[113–116] In terms of carrier localization, homogeneous alloy QDs are equivalent to single composition QDs, while gradient alloy QDs appear to be either Type-I or Type-$I^{1/2}$. The photochemical stability and PL QYs of alloy QDs are higher than those of single component QDs.[113–116]

2.1.6 Metal-semiconductor heteronanocrystals. Metal NCs have the ability to localize and strongly enhance the incident electromagnetic field when excited at their plasmon resonance.[118,119] The optical properties of metal-SC HNCs are determined by a complex interplay between the enhancement of the local excitation field and the modification of radiative and nonradiative exciton decay rates, thereby inducing a change of the exciton lifetimes and the PL QYs.[118] This may lead to either quenching or enhancement of the PL, depending on a number of parameters.[118] The plasmon-exciton coupling may also affect the non-linear optical (NLO) properties of HNCs. For instance, synergetic effects on second harmonic generation (SHG) by CdSe–Au nanodumbbells have been recently observed, leading to reduced SHG response for shorter dumbbells.[120] Further, electron transfer may occur from the SC to the metal segment. This quenches the PL,

but has been reported to enhance photocatalytic processes on a number of colloidal HNCs (*viz*., CdSe–Au and CdSe–Pt dumbbells,[120,121] CdSe/CdS–Pt nanorod/dot HNCs[122]).

2.2 The organic layer

The ligand molecules that coat the surface of colloidal NCs, forming the surfactant (or capping) layer, perform a number of essential roles. First, ligands strongly influence the nucleation and growth kinetics of colloidal NCs, thereby controlling their size and shape. Second, several physico-chemical properties are directly determined by the organic surfactant layer and by the organic–inorganic interface, and can thus be manipulated by a judicious choice of ligands. This section will focus on the latter aspect. The size and shape control of colloidal NCs will be addressed in Section 3 below.

2.2.1 Surfactant molecules. Amphiphilic molecules, which consist of a polar head group and a non-polar hydrocarbon tail are ideal surfactants for NCs. The functionality of the surfactant molecule depends on both domains. The apolar tail determines the interaction of the surfactant layer with the surrounding medium, while the polar head coordinates to metal atoms in solution and at the NC surface. Moreover, both domains strongly influence the diffusion rates of the free surfactant molecules. These characteristics have a large impact on the growth rates of colloidal NCs (section 3) and on their properties after the growth, and must thus be carefully considered when designing syntheses or post-preparation processing procedures.

The ability of the head group to bind to the NC surface originates from the presence of donor atoms (*e.g*., N, O, S, P), which possess unshared electron pairs and are thus capable of forming coordinating bonds with metal atoms or ions. This is why the surfactant molecules employed during the colloidal synthesis of NCs are commonly referred to as coordinating ligands or coordinating solvents. The variety of chemicals suitable for use as coordinating ligands is very large: alkylamines (R–NH_2, *e.g*., hexadecylamine, HDA), fatty acids (R–COOH, *e.g*., oleic acid, OA), alkylphosphine oxides (R_3PO, *e.g*., trioctylphosphineoxide, TOPO), phosphonic acids (R–POOH, *e.g*., *n*-octadecylphosphonic acid, ODPA; *n*-tetradecylphosphonic acid, TDPA), alkylthiols (R–SH, *e.g*., hexanethiol, HT). These chemicals bind primarily to metal atoms (*e.g*., Cd, Zn, In). The choice of coordinating ligands for the non-metal components of the NC (*e.g*., Se, Te) is quite limited, being restricted to alkylphosphines (R_3P, *e.g*., trioctylphosphine, TOP; tributylphosphine, TBP). It is also possible to use ligands with two polar heads separated by a hydrocarbon chain (*e.g*., dithiols, HS–R–SH; mercapto *n*-alkyl acids, HS–R–COOH; hydroxyalkylphosphines, or peptides). These ligands are used to cross-link NCs together,[5,123] or to render them water soluble.[9] Rigid chains have been shown to be better to cross-link NCs, since long and flexible aliphatic chains very often bind both end groups to same NC facet.[123] Amphiphilic multidentate polymeric ligands and dendrons may also be used, leading to NC encapsulation.[9,124] It should be mentioned that fully inorganic surfactant molecules (metal chalcogenide complexes such as, *e.g*., $Sn_2S_6^{-4}$) have been recently developed, and shown to be advantageous for the fabrication of NC superlattices with improved conductivity.[125]

The binding strength between the surfactant molecule and the metal atom is a very important parameter, being largely responsible for its effectiveness. For example, a strong bond may be useful to provide stability and surface passivation to the NC after the synthesis, but may hinder its growth, therefore being undesirable during the synthesis. On the other hand, too weak bonds result in uncontrolled growth and/or insufficient colloidal stability. Despite the wealth of experimental data available in the literature, a rigorous quantitative description of the binding between the surfactant layer and the NC surface has yet to emerge. Nevertheless, coordination chemistry and organic chemistry provide a number of useful principles that can be used as guidelines for the rational choice of surfactants (see, *e.g*., ref. 126 and 127).

The bond between the donor atom of the polar head group and the metal atom can be rationalized in terms of a Lewis acid–base interaction, whose strength is determined by both electrostatic and covalent contributions. Smaller and/or more charged metal ions (*i.e*., hard Lewis acids, *e.g*., Zn^{2+}) will form stronger bonds with donors capable of strong electrostatic interactions (*i.e*., hard Lewis bases, which are characterized by large electronegativities and small polarisabilities, *e.g*., Oxygen). Conversely, larger and/or less charged metal ions (*i.e*., soft acids, *e.g*., Cd^{2+} or Pb^{2+}) will favour larger and more polarisable ligand atoms (*i.e*., soft bases, *e.g*., Sulfur). Phosphines differ from the other commonly used surfactants because they bind to metals by a combination of σ donation from the P atom and π back-bonding from the metal atom. Therefore, they will bind strongly to chalcogenides and transition metals in their low oxidation states, but interact only very weakly with IIB, IIIA and IVA metals (*e.g*., Cd, Zn, In, Pb). Further, the bond strength increases with the number of donor atoms (*i.e*., monodentate < bidentate < tridentate, and so forth). It can thus be anticipated that the strength of the surfactant-NC interaction for, *e.g*., Cd based NCs increases in the sequence $R_3P \ll$ R–NH_2 < R_3PO < R–SH < R–COOH < R–POOH. The length of the hydrocarbon tail is also an important parameter, since shorter alkyl chains result in weaker metal–ligand bonds and weaker interactions between the surfactant molecules, leading to more dynamic NC-surfactant interactions and higher diffusion rates at relatively lower temperatures. Steric effects are also relevant and should be considered when utilizing bulky surfactants, such as tertiary phosphineoxides and amines.

2.2.2 Solubility and colloidal stability. The term "solubility" is used here to indicate the ability of a NC to form stable colloidal suspensions. This is a direct consequence of the surfactant layer, which prevents aggregation and fusion of the NCs. The stability of colloidal suspensions is due to repulsion between the NCs, which can result from van der Waals or electrostatic interactions (steric or charge stabilization, respectively). The first mechanism is responsible for the colloidal stability of NCs coated with hydrophobic surfactants in apolar solvents, while the second confers stability to dispersions of NCs coated with hydrophilic or charged ligands in polar media. Recently, amphiphilic CdTe NCs that

are readily soluble both in water and apolar solvents have been prepared by using methoxypolyethylene glycothiol as capping ligand.[128] The ability to control the solubility of colloidal NCs is essential for applications, in which the NCs are used either directly in solution (*e.g.*, labels for biomedical imaging[9]) or embedded in other materials, such as organic polymers (*e.g.*, LED's,[12,13] solar cells,[14] lasers,[12] and solar concentrators[15]).

The surfactant layer also controls the interaction potential between the NCs, which can have a large impact on the formation of superstructures using colloidal NCs as building blocks.[4,5] The interaction between the NCs can also be manipulated to narrow the size dispersion of ensembles of NCs *via* post-preparative size-selective precipitation. This is achieved by slowly adding a non-solvent to a colloidal suspension of NCs (*e.g.*, methanol to a colloidal suspension of NCs in toluene). Larger NCs exert greater attractive forces over each other and thus destabilize with smaller volumes of non-solvent than smaller NCs. Therefore, the gradual addition allows different NC sizes to be sequentially separated.

2.2.3 Ligand exchange. Colloidal NCs are typically synthesized with a hydrophobic surfactant layer, making them readily dispersible in apolar solvents. However, some applications (*e.g.*, biomedical imaging) require water-dispersible NCs. This can be achieved by simply exchanging the native hydrophobic ligands by hydrophilic or charged ones.[9] Further, the most widely procedure for surface functionalization of colloidal NCs involves the displacement of the native surfactant with difunctional molecules containing a surface-binding head group at one end and the desired functional group at the other end. This is also useful to attach NCs to surfaces (*e.g.*, mesoporous oxide layers in QD sensitized solar cells[14]). As will be discussed below, the surfactant layer affects several properties of colloidal NCs. Therefore, ligand exchange is a valuable and widely used tool for property control.[5]

The native surfactant molecules can easily be exchanged by stronger ligands (*e.g.*, amines by thiols).[129,130] In this case, the capping exchange can be carried out immediately after the synthesis, with the NCs still in the original crude reaction mixture. To exchange the native ligand by a weaker one (*e.g.*, fatty acids by amines) or by one with a comparable binding strength (*i.e.*, the same functional head group) it is necessary to use a large excess of the new ligand,[131] which requires the purification of the NCs by precipitation prior to adding the new ligand. After allowing the exchange reaction to reach equilibrium (which may take from several hours for stronger ligands[130] to several days for weaker ligands) the NCs can be precipitated and isolated. To ensure complete exchange, the NCs must be subjected to several cycles of ligand exchange. Several techniques can be used to check the degree of ligand exchange (section 2.3). Further, surfactants with low boiling points (*e.g.*, pyridine or allylamine) can also be used, since the ligand exchange procedure is carried out at mild temperatures (≤ 50 °C). Pyridine is often used as a weak and labile ligand that can be easily replaced by other surfactants of interest (regardless of their affinity for the NC surface) or stripped off the surface by vacuum treatment.[5]

The control over the ligand exchange process also allows the fabrication of complex HNCs. For example, the first step in the incorporation of hydrophobic NCs in amorphous silica by a reverse microemulsion method is a rapid ligand exchange, in which hydrolized triethylorthosilane replaces the native hydrophobic ligands.[67] This enables the transfer of the NCs to the hydrophilic interior of the micelles where the silica growth takes place. By selectively hindering the exchange process using stronger ligands (thiols), the position of the incorporated NC in the silica NPs can be controlled.[67]

2.2.4 Ligand dynamics. The success of ligand exchange protocols provides a clear demonstration that the surfactant layer is very dynamic. Nevertheless, the dynamics of ligands bound to NC surfaces have only recently been quantitatively investigated.[130,132,133] The results show that the surfactant molecules bind and unbind to the NC surface on a time-scale that is dependent on their binding strength.[132] Weaker ligands, such as amines, bind on and off the surface at faster rates (*viz.*, ≥ 0.05 ms^{-1}), while stronger ligands (*e.g.*, oleic acid) have much longer residence times at the surface (*viz.*, s^{-1} range).[132,133] Therefore, the exchange rates of amines can be orders of magnitude faster than those of more tightly bound ligands (*viz.*, seconds *vs.* hours).[130] Ligand–ligand interactions are also important and are reflected in slower exchange rates for bulkier ligands, due to a combination of more pronounced steric hindrance and slower diffusion times away from the surface (or towards the surface, for incoming ligands).[130] It is also clear that the tendency of leaving the NC surface increases with decreasing chain length for a given head group.[134] It has also been demonstrated that the ligand exchange rates are strongly site-dependent, being much faster at defect sites in the surfactant monolayer (*e.g.*, at vertices,[135] or at the poles of the NC[136]).

2.2.5 Surfactants and self-assembled monolayers. Amphiphilic molecules are known to form self-assembled monolayers (SAM's) on surfaces.[137] The surfactant layer that coats a colloidal NC can be envisioned as a three-dimensionally constrained SAM of tightly packed organic amphiphilic molecules.[138] It is becoming increasingly evident that the morphology and organization of the surfactant layer plays an essential role in defining the properties of colloidal NCs. Recent studies have shown that surfactant monolayers on facets of Au NCs are at least as ordered as SAM's on flat bulk surfaces.[136,138] Further, surfactant layers of mixed composition have been observed to undergo phase separation, yielding ordered patterns of single-composition domains.[136,138] Moreover, phase transitions in the surfactant layer have been shown to affect the optical properties of CdSe and CdTe QDs,[92,131,139] (see section 2.2.8 for details) and the kinetics of heteronucleation of Au NCs on CdSe/CdS dot core/rod shell nanorods.[140]

2.2.6 Surfactants as anchors for new functionalities. Van der Waals, electrostatic or covalent interactions with the native surfactant layer can be utilized to assemble new molecules around the colloidal NC, thereby introducing new functionalities or modifying properties. For example, the van der Waals interactions between lipid molecules and the

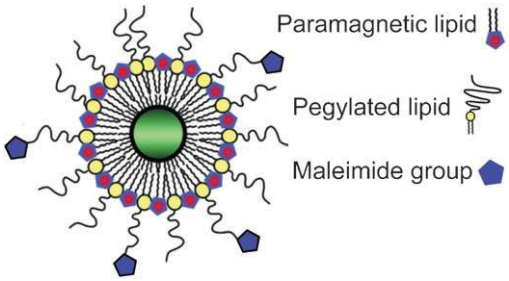

Fig. 10 Schematic representation of a nanolabel for bimodal (optical and MRI) biomedical imaging, obtained by self-assembly of a multifunctional lipid monolayer around an organically capped CdSe/(Cd,Zn)S/ZnS core/multishell colloidal QD.[141] Courtesy of W. J. M. Mulder (Mount Sinai School of Medicine, USA).

octadecylamine coating layer of CdSe/(Cd,Zn)S/ZnS core/multishell (CSS) QDs has been successfully used to self-assemble a multifunctional lipid monolayer around the QD, yielding nanolabels for bimodal biomedical imaging (Fig. 10).[141] The CSS QDs retain their efficient PL, allowing the detection of the biolabels by optical imaging techniques, while paramagnetic Gd^{3+}-lipids make them efficient contrast agents for magnetic resonance imaging. Solubility in water is conveyed by the use of PEGylated lipids (PEG = polyethylene glycol), while lipid molecules with a maleimide head are used to covalently bind biorecognition molecules.[141] This approach has also been successful for octadecanol coated silica NPs embedding CSS QDs.[142]

2.2.7 Functionalisation with reversible switches. The ligand exchange and ligand anchoring strategies described above can be employed to functionalise NPs with molecular and supramolecular switches.[39] These switches are capable of reversibly changing their shape or other properties in response to an external stimulus (*e.g.*, light or a pH change), and thereby can endow a wealth of adaptive behaviours to functionalised NPs (*e.g.*, modulation and switching of optical, electrical and magnetic properties, or self-organization).[39]

2.2.8 Surfactants and photoluminescence quantum yields. The PL QY of colloidal NCs is strongly dependent on the nature of the surfactant layer. For example, synthesis in a TOPO/TOP surfactant mixture yields CdSe QDs with low QYs (<10%), while the HDA/TOPO/TOP mixture can yield CdSe QDs with QYs as high as 85%.[143] Post-preparative ligand exchange can also dramatically affect the PL QYs of colloidal NCs, leading to PL enhancement or quenching, depending on the chemical nature of the new surfactant and the extent of the exchange. For instance, the PL QY of CdSe QDs increases by one order of magnitude after the exchange of the native TOPO capping by primary alkylamines.[144–146] Secondary alkylamines lead to a smaller enhancement (by a factor 3), while tertiary alkylamines induce only a modest improvement (50%).[144] In contrast, several organic ligands have been reported to decrease the PL QYs of colloidal QDs.[144] Well-known examples of such ligands are thiols, which strongly quench the PL of CdSe QDs, even at low concentrations.[130,145] Impurities in solvents may also decrease the PL QYs.[96,145] It is also known that excessive purification of colloidal NCs leads to quenching.[96,146]

The influence of organic surfactants on the PL QYs of semiconductor NCs is due to a combination of mechanisms:

Surface passivation. The bond formed between the surfactant molecules and the dangling orbitals at the NC surface shifts the energy of the surface (and trap) states away from the HOMO–LUMO gap, thereby preventing nonradiative relaxation *via* these states. The effect of the surface adsorption of molecules on the PL efficiency of semiconductors has been extensively investigated for several materials, particularly for CdSe.[147] Lewis acids cause quenching, while Lewis bases cause PL enhancement.[147] However, the efficacy of the surface passivation provided by different Lewis bases varies dramatically. Linear monodentate ligand molecules (*e.g.*, primary alkylamines) provide a more efficient surface passivation than bulky ligands (*e.g.*, TOPO), because they lead to a higher surface coverage density, allowing the dangling orbitals to be fully passivated. In contrast, bulky molecules, such as TOPO or tertiary alkylamines, possess a large exclusion volume, which prevents the simultaneous occupation of neighbouring surface sites.

Surface relaxation and reconstruction. Surface states can also be shifted away from the HOMO–LUMO energy gap by a reorganization of the surface atoms in such a way that the dangling orbitals of neighbouring cations and anions partially overlap, leading to a redistribution of electronic density that makes the surface auto-compensated.[148] This is referred to as surface self-passivation (or "self-healing"), and can be achieved by surface relaxation and/or reconstruction. Surface relaxation and reconstruction have been extensively investigated for bulk semiconductors, particularly for the technologically important III–V and II–VI materials (GaAs, ZnS, CdTe, *etc.*).[148] The first process involves a shortening of the bonds between the surface atoms and those immediately underneath, while the latter results in a more extensive reorganization of the surface atoms, which changes both bond lengths and coordination geometry. Recent studies on the surface structure of Au NCs (3–5 nm diameter) have shown that surface relaxation is strongly dependent on the facet and coordination number of the atom, with edge atoms displaying the largest out-of-plane contraction (*viz.*, 0.02 nm), while atoms in {111} facets display only a small contraction (0.005 nm).[149] Moreover, reconstruction has been reported to be strongly size-dependent for CdSe NCs.[150] For NCs larger than 4 nm in diameter the reconstruction process is restricted to the surface, while smaller NCs undergo a global reconstruction.

Surfactant molecules are likely to strongly affect surface relaxation and reconstruction processes, since they modify the surface free energies and thereby may hinder or facilitate the reorganization of surface atoms. The interaction between the surfactant molecules and their collective effect are also crucial, making the surfactant layer a very active player in the relaxation and reconstruction of the surfaces of colloidal NCs.[92,131,139] Linear molecules that can form ordered SAM's, such as primary alkylamines, seem to facilitate surface relaxation and reconstruction. In contrast, bulky molecules

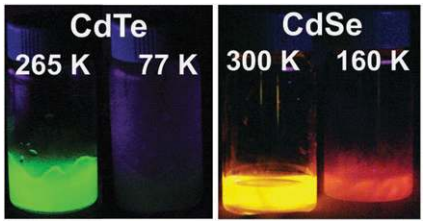

Fig. 11 Left panel: Vials containing an aqueous solution of CdTe QDs capped with aminoethanethiol under UV (365 nm) illumination at the temperatures indicated. Right panel: Solutions of colloidal CdSe QDs in toluene under UV (365 nm) illumination at the temperatures indicated. The luminescence temperature anti-quenching effect[92,131,139] is evident in both cases, since the PL intensity is dramatically reduced upon cooling.

(*e.g.*, TOPO) are unable to form ordered SAM's and therefore impose disorder to the NC surface and, possibly, also additional energy barriers for relaxation and reconstruction.

The active role of the surfactant layer in the surface reconstruction of colloidal QDs has been clearly demonstrated by the recent observation of an unusual behaviour (Fig. 11), dubbed luminescence temperature anti-quenching (LTAQ),[92,131,139] in which the exciton lifetimes and PL QYs of CdSe QDs[92,131] and CdTe QDs[139] are observed to increase sharply above a certain transition temperature T_{LTAQ}. For CdSe QDs capped by primary alkylamines T_{LTAQ} increases with the alkyl chain length, consistent with a phase transition in the surfactant monolayer.[92,131] Below T_{LTAQ} the NC surface atoms are pushed and locked into energetically unfavorable positions, resulting in PL quenching. Above T_{LTAQ} the alkyl chains regain precessional mobility, which allows the NC surface to reconstruct itself, shifting the surface states away from the HOMO–LUMO gap, and leading to PL recovery.[92,131] In the case of alkylthiol capped CdTe QDs in water, T_{LTAQ} is determined by the freezing and thawing of the solvent molecules. Due to the interaction between water and the charged heads of the capping molecules, freezing of the solvation molecules surrounding the QDs induces strain in the surfactant layer.[139] Ligands with short carbon chains (amino-ethanethiol) propagate the strain to the QD surface, creating quenching states, whereas long and flexible chains (amino-undecanethiol) dissipate the strain, thus preventing surface distortion and PL quenching.[139]

Carrier trapping. Some molecules can efficiently scavenge photogenerated electrons or holes from colloidal QDs (*e.g.*, methylviologen and alkylthiols are, respectively, efficient *e* and *h* acceptors for CdSe QDs[151,152]). This leads to PL quenching, since trapping of one the carriers precludes the *e*–*h* radiative recombination. The quenching induced by trapping is very efficient, being observable already at low acceptor concentrations,[130,152] and can be used to probe the carrier localization regime in HNCs,[83] since a carrier will be trapped only if its wave function reaches the surface. The ability of a molecule to trap photoexcited electrons (or holes) from a semiconductor NC is determined by its reduction (or oxidation) potential with respect to the size-dependent conduction band (or valence band) potential of the NC.[152]

2.2.9 Exciton-surfactant coupling. Electronic coupling between the exciton and the donor atom of the capping molecules may shift the exciton levels to lower energies, since a strong coupling will effectively relax the exciton confinement, leading to delocalization of at least one of the carriers into the surfactant shell. This ligand induced bathochromic shift has been observed for a number of systems, *e.g.*, thiol capped CdTe and CdSe QDs,[123,152,153] and CdTe/CdSe HNCs,[83] and can reach values as large as 50–220 meV, depending on the size of the NC and the nature of the ligand molecule.[83,123,152,153] The exciton can also couple to vibrational modes of the surfactant molecules. This has been reported to affect the intraband relaxation rates in colloidal QDs (*e.g.*, 30 ps, 10 ps, and <8 ps, for dodecanethiol, alkylamines, and OA capped CdSe QDs, respectively).[84,154]

2.3 The organic–inorganic interface

The interface between the surfactant layer and the inorganic NC is defined by the coordinating atoms of the surfactant molecules and the surface atoms of the NC. The driving force for its organization is the minimization of the interfacial free energies, which results from the interplay between several forces acting within and across the interface (*e.g.*, intermolecular interactions between the surfactants, attractive forces between the NC surface and the surfactant polar heads, interactions between the surface and the interior atoms of the NC, *etc.*). Therefore, the organic–inorganic interface is a very dynamic structure that strongly influences a number of key properties of colloidal NCs, making them highly responsive to their environment, during and after their preparation.

The understanding of the surface chemistry of a colloidal NC thus requires the knowledge of the composition of both the surfactant layer and the NC surface, which is rarely known with certainty. The composition of the surfactant layer is usually presumed to be the same as that of the surfactant mixture used during the growth, and the NC is typically assumed stoichiometric. However, recent work has shown that this picture is oversimplified and, in many cases, incorrect.

The stoichiometry of CdSe NCs has been observed to be primarily determined by the composition of the coordinating solvent used during the growth.[35] NCs grown in TOPO are Cd-rich (Cd : Se = 1.2), while those grown in TOPO/HDA mixture are stoichiometric, regardless of the Cd : Se ratio in the growth mixture.[35] Given that the NCs also display different faceting, the different compositions can be seen as a result of the dominance of Cd-rich facets in NCs grown in TOPO. The effect can be attributed to the impact of the different surfactants on the growth kinetics (section 3 below) and on the relative free energies of different facets of CdSe. Similarly, colloidal PbSe NCs have also been shown to be non-stoichiometric, owing to the composition of the surfactant layer, which consists mostly of OA ligands.[155] These ligands bind strongly to Pb and, as a result, the NC surface is composed mainly of Pb atoms, rendering the NCs Pb-rich.[155]

Theoretical calculations of the surface free energies of NCs have been carried out only for a few selected facets of CdSe[156,157] and PbSe.[158] The results indicate that the various crystallographic facets of a NC can have quite different free

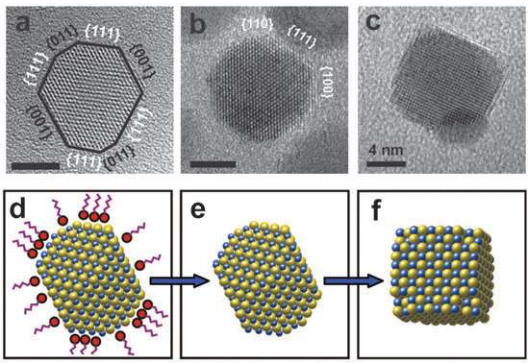

Fig. 12 High-resolution TEM images showing the morphology of PbSe NCs in a near-110 projection showing non-polar {001} and {011} surfaces and polar {111} surfaces (a), and in a 011 projection, showing the {100}, {110}, and {111} surfaces (b). Cubic NCs start to dominate after longer annealing times as the surfactants evaporate (c). The process of morphological reconstruction induced by the loss of surfactants is schematically illustrated in panels (d) to (f).[158] Courtesy of M. A. van Huis (Delft University of Technology, Netherlands).

energies, arising from different arrangements and densities of atoms, polarity and number of surface dangling bonds. Further, the energies of individual crystallographic facets can be modified differently by surface relaxation (or reconstruction) and binding of surfactant molecules. As it will be discussed below (section 3), this has important consequences for the growth kinetics and shape control of NCs, and implies that the faceting of a colloidal NC, and therefore its shape and composition, may be largely determined by the organic–inorganic interfacial energies due to the large surface to volume ratio of NCs.

The impact of surfactant molecules on the equilibrium shape of colloidal NCs has been recently demonstrated by *in situ* high-temperature HRTEM studies on PbSe QDs.[158] Hexylamine capped PbSe QDs are observed to have a nearly spherical, multifaceted morphology, in which a considerable fraction of the surface consists of {111} polar facets. Upon removal of the capping molecules through *in situ* gentle heating (393 K) under vacuum, the NCs reconstruct into cubes with predominantly {100} non-polar facets (Fig. 12). This is consistent with the theoretical prediction that the non-polar {100} surface is the most stable under vacuum, and demonstrates that the dominance of the polar {111} facets in the surface of the capped NC is due to the hexylamine surfactant molecules, which lower the free energies of these facets with respect to the {100} facets.[158] It is worth noting that if the temperature is too high sublimation of the PbSe NCs occurs,[159] with the higher energy {111} facets sublimating at a faster rate.

Theoretical modelling of the surfactant layer is also scarce and has been performed for a few cases only,[3] demonstrating that the surfactant–solvent interaction is also important. Despite these recent advances, the current understanding of the surface–ligand and ligand–ligand interactions and of the structure of the inorganic–organic interface is still quite fragmentary.

2.4 Lifting the veil: techniques to unravel the properties of colloidal nanocrystals

Size, shape and crystal structure. Transmission Electron Microscopy (TEM) and High-Resolution TEM (HRTEM) are indispensible tools for the characterization of the size and shape of colloidal HNCs. HRTEM may also yield information about the crystal structure and chemical composition of single NCs when associated to electron diffraction analysis and energy-dispersive X-ray spectroscopy (EDS), respectively (Fig. 13).[57,106] Energy filtered TEM is also an attractive technique to analyse the chemical composition of complex

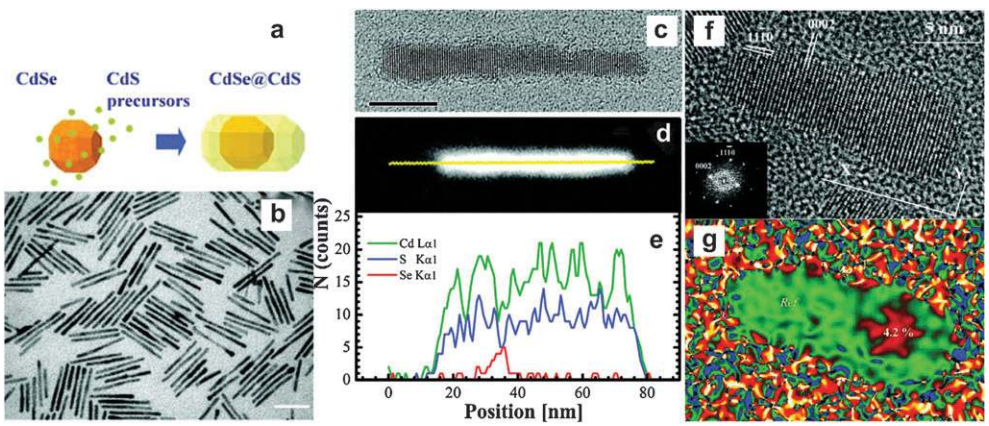

Fig. 13 Advanced structural characterization of CdSe/CdS dot core/rod shell nanorods. (a) Sketch of the seeded injection growth approach used to prepare the nanorods. (b) TEM image of CdSe/CdS nanorods (diameter: 3.8 ± 0.3 nm; length: 70 ± 4 nm). Scale bar: 50 nm. (c) HRTEM image of a CdSe/CdS nanorod grown from a 4.4 nm wurtzite CdSe seed. Scale bar: 5 nm. (d) High-angle annular dark field (HAADF) image of a CdSe/CdS nanorod and (e) corresponding elemental profiles for Cd, S, and Se obtained by recording EDS signal intensities along the line shown in yellow in panel (d). (f) HRTEM image of a CdSe/CdS nanorod. (g) Corresponding "mean dilatation" image of the same CdSe/CdS nanorod shown in (f). Areas of the same colour are regions with the same periodicity. The mean dilatation image shows an area where the lattice parameters are altered by 4.2% with respect to the reference area, situated at the opposite tip of the rod. Both the elemental profiles[57] and the dilatation mapping[58] show that the CdSe core is located closer to one of the tips of the nanorod. Panels a, b, f, and g are adapted with permission from ref. 58. Panels c, d, and e are adapted with permission from ref. 57. Copyright 2007 American Chemical Society.

HNCs, as it allows different elements to be imaged separately. Powder X-ray diffraction is very useful for the structural characterization of NCs at the ensemble level, and can also be used to estimate the sizes of NCs.[57,70,106]

Advanced structural characterization. Interfacial strain due to lattice mismatch is an important issue in nanostructures grown by heteroepitaxy (section 3.1.3.III). The investigation of core/shell QDs has clearly established that heterointerfacial strain negatively affects both the PL QY and the stability of the QD.[30] Nevertheless, the understanding of the mechanisms by which interfacial strain affects the optical properties of HNCs is still quite limited. The availability of advanced techniques, such as aberration-free high-angle annular dark field (HAADF) scanning TEM (''Z-STEM''), has made it possible to establish a clear structural basis for near-unity QY in graded core/multishell CdSe/CdS/ZnS QDs.[35,160] Z-STEM is strongly sensitive to the atomic number and can thus be exploited to achieve atomic-resolution elemental mapping of HNCs.[35,57,106] Also, aberration-free phase-contrast HRTEM images allow the core in anisotropic core/shell HNCs to be located (Fig. 13).[58,106] TEM tomography allows for full three dimensional imaging of the shape of individual NCs, and is therefore becoming increasingly important in the analysis of complex shaped NCs and HNCs (*e.g.*, hyperbranched CdTe and CdSe NCs[161] or Au tipped CdTe hyperbranched HNCs[162]). This technique is also indispensible for a quantitative in depth real space study of NC superlattices, providing accurate lattice parameters and unambiguously revealing the crystal structure.[163] Finally, recent technological advances in the fabrication of MEMS micro-hotplates have made it possible to combine HRTEM with *in situ* heating stages, allowing nanoscale phase transitions and morphology transformations to be followed in real-time with atomic resolution.[158–159,164]

Surface characterization techniques. Despite the large surface/volume ratio of NCs, the NC surface has been scarcely investigated. Techniques commonly used for the surface characterization of bulk materials, such as X-Ray photoelectron spectroscopy (XPS) and Rutherford backscattering spectroscopy (RBS), have penetration depths comparable to the typical dimensions of NCs and therefore yield information about the whole NC.[35] These techniques are thus useful to accurately determine the elemental composition of NCs,[35] but cannot distinguish between surface and interior atoms. The degree of interior strain and disorder of NCs can be directly observed by combined small-angle X-Ray scattering (SAXS) and high-energy wide-angle X-ray scattering (WAXS) measurements,[165,166] and also by extended X-Ray absorption fine structure (EXAFS).[167] For example, these techniques have been used to demonstrate that surfactant free ZnS NCs undergo a reversible structural transformation accompanying methanol desorption and water adsorption, through which surface and interior disorder are significantly reduced.[166] Evidence for surface reconstruction and relaxation in colloidal InAs NCs has been provided by both X-Ray absorption near-edge spectroscopy (XANES)[168] and photoelectron spectroscopy using synchrotron radiation.[169]

Solution Nuclear Magnetic Resonance (NMR) spectroscopy has been used to investigate *in situ* the composition of the surfactant layer of colloidal NCs (OA capped PbSe NCs,[155] TOPO-capped InP NCs,[155] TOPO-capped CdSe NCs,[35,170] thiophenol-capped CdS NCs[35]) and also to study the ligand dynamics at the surface of the NCs.[132,133] NMR methods are inherently element specific and can allow the differentiation of discrete environments within a QD by analyzing the chemical shift of the elemental sites and discriminating the signal associated with the surface *versus* the interior of a NC.[150] The combination of NMR spectroscopy and vibrational spectroscopy is particularly useful to characterize ligand exchange processes.

Optical spectroscopy. In order to unravel the photophysical properties of colloidal HNCs a combination of spectroscopic techniques is needed. Absorption, PL, and PL excitation (PLE) spectroscopy provide information about the exciton energy level structure,[50,59,82–84] and may also be used to identify radiative recombination at dopants or defects (the so-called ''trap emission''). Fig. 7 clearly illustrates the value of optical spectroscopic techniques in the investigation of colloidal HNCs. PLE spectra are better suited than absorption spectra for the identification and assignment of absorption transitions, because only emitting NCs contribute to the spectra.[83] Further, the PLE technique allows a narrow portion of the ensemble of NCs to be spectrally selected, thereby minimizing the impact of sample inhomogeneities. Absorption spectra can be used to estimate the NC size for single composition QDs, provided an empirical calibration curve is available.[96] However, in HNCs the volume probed by the lowest energy exciton state is not necessarily the same as the NC size, and therefore calibration curves are no longer useful.[83] PL QYs provide a very sensitive parameter to assess the surface and interface quality of NCs and HNCs,[82–83,92,106,107] and can be determined by comparison with suitable standard luminophores for which the absolute PL QYs are known (*e.g.*, commercial laser dyes).[83]

Time-resolved optical spectroscopy and advanced spectroscopic techniques. Time-resolved (TR) PL spectroscopy is well-established as a quantitative tool for the analysis of photoexcitation dynamics in colloidal NCs, yielding information about both radiative and non-radiative exciton recombination channels.[82–86,91–93,103,171] In combination with other spectroscopic techniques, this allows the nature of the emitting state to be elucidated (*viz.*, direct or indirect exciton states, dopants, surface or trap states),[57,82–86,91,106,109] and provides a thorough fundamental understanding of the interactions between intrinsic exciton states and the NC surface,[171] as well as the organic–inorganic interface[92,131,139] and the surrounding medium (*e.g.*, local field effects[172]).

TR spectroscopy is also essential to investigate energy transfer processes within or between NCs,[7,123,173] and from QDs or ions doped in NCs to dye molecules.[174,175] The information provided by temperature dependent studies shed light on the role of thermally activated carrier trapping (or detrapping)[92,171] and on the exciton-phonon interaction, as well as on the exciton fine-structure.[92,176–178] The magnetic

field dependence of the exciton lifetimes is also crucial for the understanding of the exciton fine-structure.[179–181] TR PL spectroscopy allows the temporal evolution of the PL spectrum to be followed after excitation, making it possible to distinguish emission originating from different centres (*e.g.*, from the dopant Mn^{2+} ion or the exciton in ZnS : Mn NCs[182]) or states (*e.g.*, the exciton or biexciton emission[42]).

At the single-NC level colloidal QDs have been observed to display PL intermittency (blinking). Since blinking is detrimental to the performance of QDs in a number of applications (*e.g.*, LEDs, biomedical labels, *etc.*), significant efforts have been devoted to its understanding and control.[86,91,177,183,184] Although the suppression of QD blinking has been recently achieved in colloidal HNCs (*e.g.*, CdSe/CdS core/shell QDs,[86,185] CdSe/(Zn,Cd)Se core/alloy shell QDs,[91] and CdTe/Cd(Te,Se)/CdSe core/shell QDs[186]), the blinking mechanism is still not fully understood. It has long been thought that the dark periods were due to charging of the QDs as a result of Auger ionization and trapping of one of the carriers.[177,183] However, recent work on multiexciton blinking in colloidal QDs has challenged this model, pointing out the need for a deeper reevaluation of the nature of the off-state in colloidal QDs.[184]

To probe the dynamics of fast processes, such as intraband relaxation, multiexciton generation and decay, and exciton spatial separation, a combination of ultrafast TR techniques must be used (*viz.*, transient absorption, fs fluorescence up-conversion and THz time-domain spectroscopy). These techniques provide complementary information regarding the fast relaxation of electrons and holes, and have been successfully applied by several groups to probe the exciton relaxation dynamics in colloidal QDs and HNCs.[84,88,105,187–190] These techniques are also essential to probe charge injection dynamics[151,191–193] and multiexciton generation (MEG) in QDs,[18,42,194–196] and have therefore attracted increasing attention in recent years, given that both topics are very relevant for solar energy related applications. The occurrence of MEG in QDs has been subject to intense debate in recent years regarding its mechanism and efficiency.[194–199] Although a consensus is emerging in the literature that MEG is not significantly more efficient in NCs than in bulk semiconductors, the issue is yet far from being settled.

Non-linear optical spectroscopic techniques. NLO properties, such as harmonic generation, wave-mixing or refractive index modulation, are promising for a number of applications (*e.g.*, optical switching). Colloidal NCs and HNCs have been anticipated to have enhanced NLO properties as a result of higher electronic polarizabilities, higher surface/volume ratio and shape anisotropy. Several techniques have been used in recent years to investigate the NLO properties of NCs, with particular emphasis on the Hyper-Rayleigh scattering (HRS, useful to quantify 2nd order NLO properties[115,120,200]) and *Z*-scan (useful to quantify 3rd order NLO properties[201]) techniques.

Magnetic resonance spectroscopic techniques. NMR spectroscopy was already discussed above, in the context of surface characterization techniques. Electron paramagnetic resonance (EPR) spectroscopy has been mostly applied to characterize paramagnetic ions (*e.g.*, Mn^{2+}) in QDs and HNCs, as it allows dopants at surface to be distinguished from those in the interior of the NC.[71–72,76,80] The technique can also be applied after photoexcitation of the sample, allowing the interaction between the exciton and paramagnetic impurities to be observed,[76,80] as well as photoexcited carriers bound to impurities (*i.e.*, donor and acceptor centres),[202,203] or even coupled donor–acceptor pairs.[204] In combination with electron nuclear double resonance (ENDOR) it offers the unique possibility of identifying the nature of the trapping impurity and its position in the NC.[204] Optically detected magnetic resonance spectroscopy (ODMR) detects changes in optical processes (absorption, emission or photoconductivity) induced by the application of magnetic fields, being therefore five orders of magnitude more sensitive than conventional EPR.[46] This technique has been successfully applied to colloidal NCs, yielding a wealth of information over the influence of surface and interface defects on their optical properties.[46]

Scanning tunneling spectroscopy (STS). STS is a powerful technique to unravel the electronic energy levels of individual NCs and has been applied to both metallic and semiconductor NCs.[44,45] This technique is complementary to optical spectroscopy, but is inherently different in the sense that it separately probes conduction and valence band states, thereby yielding direct information on the density of hole and electron states. For example, STS has been recently used to determine the band offsets and carrier localization regimes in CdSe/CdS and ZnSe/CdS dot core/rod shell nanorods,[59] and to measure the electron-hole interaction energy of PbSe/CdSe core/shell QDs.[102]

3. The challenge of heteronanocrystal synthesis

Colloidal NCs are typically synthesized by combining precursors that contain the constituent elements (*viz.*, organometallic compounds or inorganic salts) at sufficiently high temperatures, in the presence of organic surfactant molecules. Thermal decomposition of the precursors leads to nucleation and growth of NCs. Colloidal HNCs are obtained if NCs of a different material are already present when the precursors of the second component are added. The surfactants control the nucleation and growth rates by dynamically binding to the surface of the NCs and to the constituent elements in solution, and are thus essential to control the size and shape of the NCs and HNCs. The functionality of the surfactant molecules depends on both the polar head and the apolar tail. Surfactants can be introduced explicitly, either as the solvent itself (coordinating solvent) or diluted in a non-coordinating solvent (*e.g.*, octadecene, ODE), but can also be part of the precursor compound (*e.g.*, cadmium oleate).

The parameter space for controlling the nucleation and growth rates of colloidal NCs and HNCs is quite large: nature and concentration of precursors, rate (and method) of addition of precursors, reaction temperature (which may be different at different reaction stages), and composition of the coordinating solvent (*i.e.*, nature and concentration of surfactants). This complexity renders the nucleation and

growth kinetics quite sensitive to variations and inhomogenities in concentrations, temperature, and heating and cooling rates. Therefore, the preparation of high-quality colloidal NCs and HNCs is far from trivial, since seemingly small variations may tip the system out of control, limiting the reproducibility of many synthetic protocols. Nevertheless, this complexity is also a very attractive feature, since it offers plenty of room for judicious and systematic manipulation.

As will be discussed below, achieving an optimum balance between nucleation and growth is a vital and usually challenging problem, which is still empirically addressed. The underlying mechanisms leading to nucleation and growth of colloidal NCs are still poorly understood and, consequently, a general theoretical model that accurately describes the formation of colloidal NCs is not yet available. However, the colloidal synthesis of NCs has been extensively investigated over the last three decades and has developed into a rather mature field. As a result, a number of fundamental principles has emerged to guide the rational development of synthetic methodologies for colloidal NCs and HNCs. These principles will be discussed in section 3.1 below. The utility of this set of concepts as guidelines for the design of preparation protocols for colloidal HNCs will be illustrated in section 3.3. The impact of unintentional impurities on the reproducibility of synthetic protocols will be analysed on section 3.2. Considering that the nucleation and growth of colloidal NCs and HNCs has been treated extensively in several recent works,[27–28,31] we will here only outline the essential concepts, emphasizing the correlations between them, and highlighting recent developments that provide further insight into the topic.

3.1 Fundamental concepts

The formation of colloidal NCs consists of a long chain of chemical steps, in which earlier events determine the fate of later events. However, the overall process can be divided into a small number of elementary kinetic steps.[27–28,205,206] Basically, four consecutive stages can be recognized:

1. Induction or pre-nucleation period. It is the time before the existence of stable crystal nuclei can be discerned, and encompasses a complex chain of coupled chemical reactions, the first of which being the decomposition of precursors into monomers (*i.e.*, basic units of the NC) with rate k_1 (see section 3.1.1). This is followed by assembly of the monomers into smaller clusters (subcritical nuclei or NC embryos) with an average rate k_2. The rate limiting step will determine the overall rate k_i. It has been experimentally demonstrated[206] that the length of the induction period is inversely proportional to k_i.

2. Nucleation period: formation of stable crystal nuclei (*i.e.*, critical nuclei). The critical nucleus is the size of the cluster at the end of the induction period.[205] Therefore, from this perspective, nucleation is a singular event marking the end of the induction period. We will thus define it as the final step prior to the formation of the critical nucleus: either the addition of one more monomer unit to the largest possible subcritical nucleus or the assembly of 2 (or more) smaller clusters, with a rate k_{rc}, which may be larger or smaller than k_i. The effective nucleation rate k_n will be equal to the slower rate (k_{rc} or k_i) (section 3.1.2).

3. Growth of the nuclei into larger NCs. Growth may proceed by sequential addition of monomer species to the growing NC or by agglomeration of smaller NCs. In any case, this process will be characterized by an average rate k_g. Typically, growth is terminated when the desired size (and shape) is achieved by quickly cooling the reaction mixture (section 3.1.3).

4. Annealing stage. Annealing requires equilibrium conditions, in which the growth has effectively stopped. It may be useful to improve the crystallinity and surface quality of the NC and to fabricate complex colloidal HNCs, but is not always possible or desirable, as it may lead to broadening of the size and shape distribution (section 3.1.4).

The temporal separation of the nucleation and growth stages is required for a narrow size distribution.[5,19,27,28,205,206] This can be achieved by the so-called hot injection technique, which involves the rapid injection of a cold solution of precursors into a hot coordinating solvent, or by steady heating of the reaction mixture (“heating-up” method). It should also be realized that the monomers available for growth are those not consumed during the nucleation stage. Therefore, nucleation and growth rates should be kinetically balanced in order to yield good control over the size and shape of the NCs. The final size is related to the rate constants k_n and k_g, as well as the initial precursor concentration $[P]_0$,[206] so that when $k_g[P]_0/k_n$ is large relatively few nuclei grow quickly into larger NCs, whereas when $k_g[P]_0/k_n$ is small a larger concentration of smaller NCs is obtained. If the imbalance is too large the synthesis fails, leading to either uncontrolled growth of large crystals or no NCs at all. As it will be discussed below (section 3.1.3), the monomer concentration during the growth stage strongly affects the growth rates, thereby determining not only the final size of the NCs, but also their shape.

These four stages can also be identified in the colloidal synthesis of HNCs, but the nature of the nucleation stage is fundamentally different, since homogenous nucleation is undesirable in this case. Moreover, the optimum balance requires conditions that are quite different from those needed in the synthesis of single component NCs. To clarify the fundamental reasons for these requirements and for the differences between the synthesis of HNCs and NCs we will address each stage in detail below.

3.1.1 Induction period: the precursor decomposition. As mentioned above, the induction period involves two distinct kinetic steps: (a) decomposition of precursors into monomers, and (b) assembly of monomers into crystal nuclei of increasing size. The latter step is better discussed in the context of the nucleation process, so we will focus here on the first fundamental step. The mechanism of monomer formation and the nature of the monomer itself are often not well understood, since comprehensive mechanistic studies have been undertaken only for very few cases.

Recently, the mechanism of formation of ME NCs (M = Cd or Zn; E = S, Se, Te) from ML_2 and TBP-E in octadecene (TBP = tributylphosphine, L = OA or ODPA) has been investigated in detail (Scheme 1).[207] The cleavage of the P═E bond is shown to be activated by the Lewis acidic

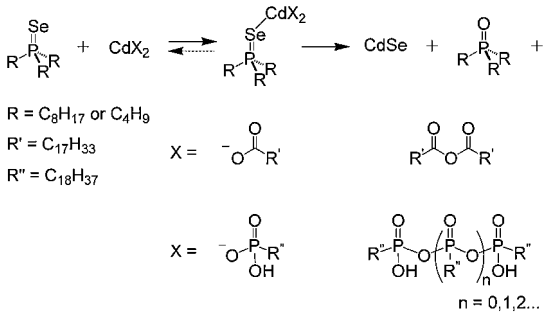

Scheme 1 Proposed reaction pathway for precursor conversion in the colloidal synthesis of CdSe NCs. Reproduced with permission from ref. 207. Copyright 2007 American Chemical Society.

character of the metal centre. This activation facilitates the nucleophilic attack by the L^- group. Evidence is presented for a bimolecular decomposition mechanism, *i.e.*, a second L^- group must bind to the P atom for the cleavage to take place. The reaction rates increase with increasing temperature. Further, the cleavage rates increase from S to Te (S < Se < Te) and are substantially lower for the Zn-complexes. Oleate complexes are observed to be more reactive than phosphonate complexes, in agreement with other studies.[134] These results show that the surfactants may also have a role as reagents. Therefore, changing their concentration in the reaction mixture will likely affect the P=E cleavage rate, in addition to the binding of surfactants to the NC surface. This may have a large impact on the nucleation and growth rates, since the cleavage of the P=E bond is likely the rate limiting step in the formation of the monomers. Indeed, several experimental studies have established a relationship between the concentration of surfactants and the precursor reactivity. For instance, higher concentrations of phosphonic acids have been reported to decrease the stability of Cd–phosphonate complexes.[208] Similarly, high concentrations of OA increase the reactivity of $Cd(OA)_2$.[209] Further, amines have been shown to enhance the reactivity of Cd–carboxylate salts,[134] while depressing the reactivity of In–myristate.[210]

The reaction mechanism has also been studied for the formation of PbSe NCs from $Pb(OA)_2$ and TOP-Se.[211] Two mechanisms were identified and observed to occur simultaneously: (a) nucleophilic attack of the P=Se bond by the metal complex and (b) reduction of lead oleate to Pb^0 by phosphines, followed by reaction with TOP-Se. This highlights the fact that phosphines are reducing agents and that some impurities in TOP may be much stronger reducing agents than TOP itself, thereby strongly affecting the reaction rates (see section 3.2. below).

It should be emphasized that both mechanistic studies[207,211] imply that the monomer is at least one ME unit stabilized by a number of surfactant molecules. Moreover, considering that the induction periods observed for the colloidal syntheses of CdSe NCs vary dramatically depending on the reactivity of the precursors (*viz.*, $\leq$40 ms, $\sim$1s, and $\sim$10s, for TOP-Se with $Cd(CH_3)_2$, $Cd(OA)_2$, or $Cd(TDPA)_2$, respectively, section 3.1.2, and minutes for $Cd(TDPA)_2$ and TOP-S [57]), we suggest that the monomer formation is likely the rate limiting step in the nucleation process of colloidal semiconductor NCs.

3.1.2 Nucleation stage. Nucleation is stochastic in nature, and can be homogeneous or heterogeneous.[19,22,23,27,28] Heterogeneous nucleation occurs at surfaces of foreign nuclei, bubbles or pre-existing NCs. Homogeneous nucleation requires spontaneous density fluctuations of the medium that lead several atoms to assemble into a crystal nucleus. This nucleus must be sufficiently large to be stable. The minimum size for a stable nucleus is called critical radius (r_C). Nuclei smaller than r_C redissolve, while nuclei larger than r_C can undergo further growth and are typically referred to as seeds.

3.1.2.I Homogeneous nucleation. Homogeneous nucleation is undesirable in the synthesis of HNCs, as the homogeneously nucleated NCs will compete with the growing HNCs for the limited supply of monomers. Although the focus of this review is the colloidal synthesis of HNCs, it is still useful to address the process of homogeneous nucleation, as this facilitates the understanding of the heterogeneous nucleation process and of the conditions necessary to prevent homogenous nucleation. It should be noted that in some cases (*e.g.*, concentric core/shell QDs), even heterogeneous nucleation should be prevented, as a slow heteroepitaxial growth leads to higher quality shells (section 3.1.3 below).

Various models have been used in the past to describe the NC formation process: classical nucleation theory (CNT), single particle growth laws, and rate equation based models. Each of these models has advantages, drawbacks and limitations.[205,212] Nevertheless, the basic physics of nucleation is best illustrated with the help of the simplest, and possibly the most inaccurate, of these models: CNT. CNT is described in a number of books and reviews,[205] so we will not address it here in any detail, but merely use it to qualitatively discuss the underlying principles involved in the nucleation of colloidal NCs, and to rationalize the large body of empirical knowledge available. However, one should keep in mind that CNT has several shortcomings, even for the seemingly simple case of nucleation of liquids from gas, and therefore cannot provide a quantitative description.[205]

The first requisite for nucleation is oversaturation. The driving force for nucleation is the difference in free energy between the crystal components (monomers) in the crystal and in solution. The total change in free energy, ΔG_{TOT}, for the formation of a spherical crystal nucleus of radius r with n monomers M (*viz.*, an atom, molecule, or ionic pair) from a solution of M is given by

$$\Delta G_{TOT} = (4/3)\pi r^3 \Delta G_V + \Delta G_S = (4/3)\pi r^3 \rho \Delta\mu + 4\pi r^2 \gamma \quad (1)$$

where ΔG_V is the volume excess free energy and ΔG_S is the surface excess free energy. ΔG_V will be negative due to the energy freed by the chemical bonds formed in the crystal nucleus, which largely compensates the energy spent to break the bonds between the monomers and the solvent (or surfactant) molecules. ΔG_S will be positive due to the fact that monomers at the surface have unsaturated bonds. The term ρ gives the density of the crystalline phase and $\Delta\mu$ represents the chemical potential difference between the nucleus and the monomers in solution, which can be approximated to $-kT$ ln S. The parameter S is a measure for the degree of oversaturation,

and can be expressed as $S = S_T/S_0$, where S_T is the monomer concentration in the growth solution and S_0 the concentration in equilibrium with a macroscopic crystal at temperature T. This implies that it is also possible to achieve a high S by using an excess of one of the precursors, since the relevant quantity to define S_0 is the solubility product of the crystal (*e.g.*, for the prototypical case of CdSe the product [Cd][Se]).

The term γ is the interfacial tension between the developing crystal and the supersaturated solution. Because ΔG_V and ΔG_S have opposite signs and different size dependences, ΔG_{TOT} will reach a maximum for nuclei with critical radius r_C and then decrease with increasing radius. This imposes an energy barrier for nucleation ΔG_C, as it implies that crystal embryos with $r < r_C$ redissolve to monomers, while those with $r > r_C$ grow out to mature NCs, or even macroscopic crystals if no constraints are imposed on the growth process.

The critical radius is given by:

$$r_C = -2\gamma/(\rho kT \ln S) \quad (2)$$

The size distribution of the critical nuclei can be very small (smaller than 10%).[19] Eqn (2) shows that higher T and/or higher supersaturations lead to smaller r_C, in agreement with experimental results.[213] Also, the concentration of critical nuclei formed during the nucleation stage is directly proportional to the monomer concentration.[19]

By analogy to Arrhenius expressions used to describe thermally activated processes the steady state nucleation rate J (number of critical nuclei per unit time in a unit volume of solution) can be expressed as

$$J = J_0 \exp(-\Delta G_C/kT) \cong J_0 \exp[-16\pi\gamma^3/3k^3T^3(\ln S)^2] \quad (3)$$

The pre-exponential factor J_0 depends on the number of monomer units per critical nucleus and the diffusion coefficient of the monomers. Although eqn (3) is only qualitatively valid, it provides useful guidelines for the manipulation of the nucleation rates, since it shows that J is strongly dependent on the interfacial tension γ, the reaction temperature T, and the degree of supersaturation S. This explains the success of the hot-injection technique, since supersaturation at high T results in small r_C and high nucleation rates, leading to a burst of nucleation, which lowers S and is accompanied by fast cooling. The combination of lower S and lower T decreases the nucleation rates to negligible values, effectively separating the nucleation and growth stages. The concentration of nuclei after nucleation has been shown to remain constant.[19,213] It is interesting to note that recent work has demonstrated that separation between nucleation and growth also occurs in the "heating-up" method.[214]

The separation between nucleation and growth is further facilitated by using less reactive precursors and suitable surfactants. As discussed above (section 3.1.1), the monomer formation from the precursors is likely the rate limiting step in the induction period and nucleation stages, and is also thermally activated. Therefore, the drop in T will also slow down the monomer formation, increasing the impact of the drop in S. This is probably the reason why less reactive precursors (*e.g.*, $Cd(OA)_2$) require a relatively smaller T drop than more reactive precursors (*e.g.*, $Cd(CH_3)_2$). A similar reasoning applies to the adjuvant role of surfactants in separating nucleation and growth, since the binding between surfactants and metal atoms is also stronger at lower T's.

The reactivity of the precursors may also affect the reproducibility of the synthesis. If the nucleation is very fast, the effective reaction volume for nucleation will be only slightly larger than the injection volume, and mixing will quickly lower the concentration while simultaneously increasing T. This may give rise to inhomogeneities due to T and concentration gradients, which will be reflected in larger size dispersions and poorer reproducibility. This is more problematic if highly reactive precursors (*e.g.*, $Cd(CH_3)_2$ and TOP-Se) are used, because then the monomer formation is very fast and consequently the induction period is short. Analysis of a slow motion movie (provided as Electronic Supplementary Information) shows that in this case nucleation takes place in $\leq$40 ms, which is much faster than the whole injection ($\sim$700 ms for 10 mL). This means that when using highly reactive precursors, such as $Cd(CH_3)_2$, the duration of the nucleation stage is essentially determined by the time span of the injection itself. Therefore, the use of less reactive precursors, such as $Cd(OA)_2$, is beneficial because it increases the induction times (see 3.1.1 above), allowing for good homogenization before nucleation takes place.

Surfactants may lower or increase the nucleation rates, depending on the nature of both the precursor and the surfactant. As mentioned above (section 3.1.1), the surfactant molecule also act as reactant, modifying the precursor reactivity. If the precursor reactivity is enhanced by the surfactants (*e.g.*, primary alkylamines on Cd(II) carboxylate complexes[134]) the nucleation rate increases due to higher rates of monomer formation.[215] Conversely, if the surfactant depresses the precursor reactivity (*e.g.*, amines on In(III) myristate complexes[210]) the nucleation rate decreases. Additionally, the surfactant molecules affect the nucleation rates by coordinating to the monomer species, which increases the stability of the monomers in solution with respect to the nucleus. This translates into a lower $\Delta\mu$ and a larger r_C, therefore increasing ΔG_C and lowering the nucleation rate. Consequently, a higher surfactant concentration will lower the concentration of nuclei and increase their size.[213,215] The stronger the interaction surfactant-monomer, the more pronounced the effect.[215] This may become apparent even for surfactants that enhance the precursor reactivity, provided their concentration is sufficiently high.[134]

This complex interplay between precursors, surfactants and nascent NCs is clearly illustrated by a recent study investigating the growth of colloidal CdSe NCs in a diluted ternary surfactant system (TOP, OA, and Bis-(2,2,4-trimethylpentyl)-phosphinic acid, TMPPA).[209] The deprotonated forms of OA and TMPPA are also part of the Cd precursor (*i.e.*, $Cd(OA)_2$ and $Cd(TMPPA)_2$). The final NC size and size dispersion were observed to depend strongly on the concentration of surfactants and the TMMPA/OA ratio, being larger for higher OA concentrations. Further, the nuclei concentration initially increased and then decreased to an equilibrium value. These results can be understood in terms of a competition between redissolution and growth, due to the acidity of both coordinating agents and the different precursor stabilities.

The higher stability of the $Cd(TMPPA)_2$ complex decreases both the growth and the dissolution rates, and therefore stabilizes smaller nuclei. The weaker acidic character of TMPPA further decreases the dissolution rates. Conversely, OA is a stronger acid, while the $Cd(OA)_2$ complex is less stable. This shifts the equilibrium towards larger critical sizes and facilitates Ostwald ripening, since the higher acidity favours dissolution and the weaker OA–Cd bond offers less protection to the surface ions.

It should be noted that the validity of the qualitative conclusions drawn above is not affected by the shortcomings of CNT. The greatest flaw of CNT is that it treats nuclei as bulk material having macroscopic properties.[205] The key assumptions are: nuclei are spherical particles with uniform and size-independent density and sharp interfaces. The interfacial tension γ is also assumed to be size independent. Further, interactions with surfactants and solvents are neglected. These assumptions become unreasonable when considering a nucleus of only several atoms. Most likely, both ΔG_V and γ are size dependent,[19,205] varying considerably with the size and inherent structure of the growing nuclei, as well as with the particular arrangement of the surface atoms and the surfactant molecules.

3.1.2.II Heterogeneous nucleation. Nucleation is facilitated by surfaces. The nucleating agent provides a low-energy interface with the crystal phase, thereby lowering the activation energy for nucleation ΔG_C.[25–28] Heterogeneous nucleation will thus happen at lower supersaturations and/or lower T's than homogeneous nucleation, making it possible to use reaction conditions that effectively suppress homogeneous nucleation. ΔG_C for heterogeneous nucleation is given by:[27]

$$\Delta G_C(\text{hetero}) = \Delta G_C(\text{hom}) \times f(\Theta) \quad (4)$$

where $f(\Theta)$ is a parameter that depends on the contact angle Θ between the nucleating crystal and the adjuvant surface. The contact angle Θ is related to the ability of the growing material to wet the substrate, which increases with decreasing interfacial tension. Higher wettabilities result in lower contact angles, leading to more pronounced reduction in the nucleation barrier, and faster nucleation rates.

The interfacial tension in solid-solid interfaces is primarily related to the lattice mismatch between the two materials. Therefore, heterogeneous nucleation will be more effective if the lattice mismatch between the nascent NC and the substrate is small. Considering that different crystallographic facets differ in terms of free energies and interatomic distances, it is clear that the activation energy for heteronucleation will be strongly dependent on the nature of the adjuvant facet. Moreover, the crystallographic orientation of the nucleating crystal will be imposed by the substrate in order to minimize the interfacial tension. It should also be pointed out that heterogeneous nucleation is facilitated on high energy sites, such as defects and corners, and may dominate if the concentration of such sites is too high. It is thus important in the synthesis of colloidal HNCs that the NCs used as seeds have a high-quality surface and excellent crystallinity.

As discussed in the previous section, surfactants have an essential role in homogeneous nucleation, performing a number of functions. Their impact on heterogeneous nucleation is even more dramatic, since they will not only regulate the monomer chemical potential in solution, but also the free energy and accessibility of the adjuvant surfaces. The surfactant molecules modify the free energies of the different facets of the seed NC, thereby enhancing or depressing the heteronucleation rates on specific facets. Moreover, surfactant molecules sterically hinder incoming monomers, limiting or even blocking the access to certain facets or surface sites. This makes it possible to use surfactants to control the accessibility of adjuvant surfaces, thereby accelerating, slowing down, or preventing heteronucleation on selected facets of a NC seed. For instance, it has been recently demonstrated that thermally induced heteronucleation of Au NCs at defects along the body of CdS nanorods is suppressed at temperatures sufficiently low to ensure that the alkylamine surfactant monolayer is organized in a densely packed phase that blocks the access of the Au precursor to the surface sites.[140] Long-chain amines show effective blocking at higher T's than short-chain ones, consistent with a higher phase transition temperature (section 2.2.8).[131] In another recent study, the surfactant concentration was used to control the site-selectivity of heterogeneous nucleation of Co NCs on TiO_2 nanorods (Fig. 14).[63] For low surfactant concentrations, the growth of the Co NCs occurred non-selectively at the sides and tips of the nanorods. At concentrations sufficiently high to densely coat the sides of the rods, nucleation occurred selectively at the tips. At even higher concentrations, heterogeneous nucleation was impeded and homogeneous nucleation dominated.[63]

3.1.2.III Magic size clusters. Under some circumstances the so-called "magic size clusters" (MSCs) are transiently formed in the early stages of the nucleation and growth of colloidal NCs, when the NC sizes are below 2 nm. MSCs are clusters containing a well-defined number of atoms and characterized by a higher stability than slightly larger or smaller clusters. Their presence in the reaction mixture is inferred from their narrow and well defined optical absorption transitions. Growth in the MSC regime is stepwise, since the clusters grow from one magic-size to the next. The stability of MSCs is typically explained by the closed shell configuration model.[27] This model works well for metal MSCs, but is inadequate to explain the structure of MSCs of semiconductors, which seem to be based on small tetramers as the basic unit (*e.g.*, the adamantane cage, as observed for the family of selenophenol capped CdSe MSCs isolated by Soloviev *et al.*[216]). The contribution of ligand molecules to the stability of MSCs is also probably significant. Density functional theory calculations of

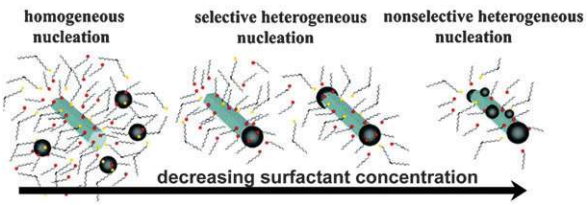

Fig. 14 Mechanism for surfactant-controlled Co NC heteronucleation and growth on TiO_2 nanorod seeds. Adapted with permission from ref. 63. Copyright 2007 American Chemical Society.

the morphology and electronic structure of $Cd_{33}Se_{33}$ clusters (bare and capped with amine and phosphine oxide ligands) have shown that the electronic states are strongly affected by cluster-ligand interactions.[220]

It has been suggested that semiconductor MSCs correspond to local thermodynamic minima in the progression from precursors to nanorods and are formed only at the high monomer chemical potentials needed to form the rod morphology.[208,217] Recent work, however, suggests that MSCs are not intermediates in the growth of nanorods, but rather kinetic "dead ends", that must decompose again to release the monomers needed for growth, and therefore work as monomer reservoirs, thereby modulating the growth kinetics.[208]

Further, semiconductor MSCs (primarily CdSe and CdTe) have been observed under a variety of different conditions.[92,218,219,221] Typically, high monomer oversaturations and low T's ($\sim$50–100 °C) are used. Under these conditions r_C is very small and growth rates are very slow, so that MSCs can be stabilized. However, reactive precursors must be used to ensure that monomer oversaturation is achieved at low T's. Stabilization by suitable surfactants is probably also a requisite.

3.1.2.IV Nucleation mechanism. Understanding the nucleation mechanism of colloidal NCs is an essential prerequisite to rationally design and fabricate HNCs with controlled size, morphology and architecture. Accordingly, the nucleation and growth of colloidal NCs in solution has been attracting increasing attention,[212–214,222–225] but is nevertheless still poorly understood due to the small sizes and inherently transient nature of the nuclei present at the early stages of NC formation.[205] An additional complication is that the nature of the monomeric species that participate in the nucleation and growth is still largely unknown, since studies aiming at unravelling the chemical mechanism of colloidal NC formation are scarce (section 3.1.1). As a result, a quantitative and general picture of what happens during the nucleation and growth of NCs in solution has yet to emerge, although remarkable advances in this direction have been made in the last few years.

Recent work on both PbSe and CdSe colloidal QDs[207,211] has provided convincing evidence that in the case of semiconductor NCs the monomer is at least one ME unit stabilized by a number of surfactant molecules (section 3.1.1). It is therefore reasonable to speculate that the nuclei involved as intermediates during the formation of semiconductor NC seeds (*i.e.*, critical nuclei) may be similar to magic size clusters, originating from the assembly of increasingly larger $[ME]_n$ clusters (*e.g.*, n = 1, 4, 8, 17, 32, as observed for solid state selenophenol CdSe MSCs[216]). This raises the possibility that sub-critical nuclei could break out into smaller clusters rather than completely redissolve into monomers. However, it remains a critical challenge to identify and monitor such clusters *in situ*, as this requires techniques capable of tracking the growth dynamics of very small clusters with fast temporal-resolution *in situ*. Such techniques have only recently become available. For example, NMR spectroscopy and mass spectrometry have been used to show that cyclic tetramers are produced in the pre-nucleation stage in systems such as Aluminium- and Gallium Phosphate.[205]

Recently, the nucleation kinetics of colloidal Au NCs was investigated *in situ* by continuous flow time-resolved XAFS (X-Ray absorption fine structure) spectroscopy.[223] The Au NCs were obtained through the reduction of $AuCl_4^-$ by citrate ions in water in the presence of poly(vinylpyrrolidone) as a stabilizer. The reaction is very slow, with the induction period lasting 80 min. During this stage, $AuCl_6^{-2}$ dimers are initially formed and then react with $AuCl_4^-$ ions to form trimers. In a subsequent stage higher order 'Au_nCl_{n+x}'' oligomers and small Au clusters (*e.g.*, Au_{13}) are formed by sequential addition of $AuCl_3^-$ units. Once the Au clusters are formed, the growth rates accelerate, presumably due to coalescence of smaller clusters into larger NCs.[223]

The nucleation and growth of colloidal Au NCs was also recently probed by *in situ* time-resolved UV-vis absorption and SAXS/WAXS spectroscopy (time resolution: 3, 130 and 800 ms, respectively).[224] In this study the Au NCs were obtained through the reduction of a gold salt by borohydride in the presence of a cationic surfactant (DDAB) and an excess of a alkyl derivative ligand (decylamine, DAm, or decanoic acid, DAc) in toluene. The results show that the nucleation rates are strongly affected by the ligands, being two orders of magnitude larger for the amine than for the acid. The difference between the two ligands is ascribed to the stronger reducing power of DAm. The rate limiting step in the formation of the Au NCs is the monomer formation from precursors, *i.e.*, reduction of the Au(III)-DDAB ion pair to Au(I) or Au(0) species. This step occurs in 150–250 ms in the presence of DAc, but is faster than 50 ms in the presence of DAm, leading to a shorter induction period and a burst of nucleation that nearly depletes the monomer supply for further growth. Accordingly, when DAm is used, 2 nm diameter Au NCs are already observed after 50 ms and a final size of 2.8 nm is achieved after 3 s. In contrast, in the case of DAc, the formation of 2 nm Au NCs starts only after 400 ms and lasts for $\sim$1.5 s, consuming only 10% of the available Au atoms. Subsequently, the number of NCs remains almost constant while their size steadily increases, reaching 7 nm after 16 s.[224] This behaviour clearly indicates a separation between the nucleation and growth stages (see above), which can be rationalized in terms of the balance between the rate of monomer production from precursors (instantaneous monomer flux) and the rate of monomer consumption by growth. After the first 1.5 s all the monomers produced are consumed for growth therefore preventing the concentrations to reach the oversaturation levels required for nucleation.

3.1.3 Growth stage. The NC growth is a deterministic process, whose outcome is dictated by the initial conditions at the onset of the growth stage: temperature, composition of the reaction medium (surfactant system and solvents), concentration, size, shape and structure of the NC seeds, and remaining concentration of monomers and precursors. It is thus clear that the fate of the NCs is largely determined by the nucleation stage. However, one should realize that these initial conditions are not sharply defined, as a result of a spread in nucleation time and fluctuations or inhomogeneities in the reaction conditions during the induction period and nucleation stage. Most importantly, the reaction flask in which

the synthesis of colloidal NCs and HNCs is taking place is not a thermodynamically isolated system, since its temperature must be tightly controlled. In fact, it nearly always is an open system, either due to addition of fresh precursors (*e.g.*, to grow a HNC) or simply because the reaction is carried out under an inert gas flow. This makes it a very dynamic system, and offers plenty of opportunities for judicious manipulation of the growth rates.

3.1.3.I Growth dynamics. The growth rate of a NC increases with the monomer concentration and the temperature, and is strongly size dependent, since it depends on the surface area of the NC. It is also strongly affected by the presence of surfactants, which slow down the growth. The specific impact of a surfactant system, however, will depend on its nature and concentration. To understand the effect of the various reaction parameters on the growth rates it is necessary to consider the growth mechanism. Two elementary steps can be distinguished in the growth process of a colloidal NC:[22,27] (a) monomer diffusion to the NC surface, and (b) incorporation of the monomer into the NC. It should be noted that the competing process of NC dissolution (removal of monomers from the NC followed by diffusion away from the NC surface) will also occur, but will become important only at low monomer concentrations.

The driving force for diffusion is the concentration gradient between the NC surface and the bulk of the solution. Therefore, the monomer diffusion rate is determined by the monomer concentration and the diffusion constant in the reaction medium, which is a function of the temperature and the composition of the growth solution (solvents, surfactants, precursors). Diffusion rates can be increased by increasing T and/or monomer concentration, or decreasing the surfactant concentration in the growth medium. If the rate limiting step is the monomer diffusion, the growth is said to be in the diffusion controlled regime. It must be pointed out, however, that recent theoretical modelling has challenged the concept of diffusion limitation, since the typical experimental growth rates under conditions presumed to be diffusion controlled are several orders of magnitude slower than the diffusion limited theoretical estimate.[212]

The incorporation of the monomer into the NC involves a reaction between the monomer-surfactant complex and the NC surface and thus involves a certain activation energy. It also implies the release of at least one surfactant molecule. The rate of this process is determined by the reaction rates between the monomers and the NC surface sites. It is also possible that precursors decompose directly at the NC surface. The microscopic mechanism of monomer addition is still not well understood. Nevertheless, it is clear that the reaction rates will vary widely, depending on the different crystallographic facets of the NC, and possibly also on the specific position of the reaction site (*e.g.*, centre of a facet, corner, *etc.*). If the rate limiting step is the incorporation of monomers into the NC, the growth is under reaction control.

The reaction controlled growth dominates at high concentrations of monomers, when the diffusion rates become so fast that the diffusion process can be neglected. Therefore, it may be expected that the initial NC growth will be primarily reaction controlled. As the monomers are consumed, the concentration drops, and the monomers in the immediate vicinity of the growing NC are depleted. Under these conditions monomer diffusion is expected to become the rate limiting step. The growth rates will then be determined by the diffusion rates and rates of dissolution and deposition.

The monomer concentration during the growth stage also determines the size distribution of the NCs.[22,26–28] At high concentrations an initially broad size distribution can undergo size distribution focusing. Due to the high concentration, r_C is small (see section 3.1.2), and all NCs grow. However, since the growth rates are proportional to the surface area of the NC, smaller NCs grow relatively faster than larger ones. At low concentrations r_C becomes large, and therefore the size distribution broadens, since NCs larger than r_C will grow at expense of the smaller ones (defocusing regime or Ostwald ripening). At lower concentrations dissolution rates accelerate, and smaller NCs will dissolve faster due to their higher surface/volume ratio. Recent theoretical modelling of the nucleation and growth of colloidal NCs has shown that diffusion limitation is not required for size distribution focusing, which can also be achieved under pure reaction controlled conditions.[212,222]

Size defocusing can be prevented by two strategies: (a) growth is terminated while the monomer concentration is still in the focussing regime; and (b) the monomer concentration is maintained high. To maintain concentrations in the focussing regime some groups use repeated injections of fresh monomers.[27] However, this may lead to new nucleation events if the concentration exceeds the nucleation threshold. An alternative is to use a large excess of one of the precursors.[143] In this case, growth will be limited by depletion of one of the NC components and the final concentration product of monomers will still be sufficiently high to prevent defocusing.[143]

There are two models for the growth of colloidal NCs: kinetic control and thermodynamic control. In the kinetic control model, growth occurs under conditions far from equilibrium, so that the size and shape of the NC (or HNC) are determined by the kinetic balance between several competing processes. In contrast, the thermodynamic control model is based on the concept of equilibrium and assumes that the binding between the surfactant molecules and the NC surface is sufficiently strong to thermodynamically drive the system toward a particular average size under a given set of conditions.[225] Both models are valid, depending on the growth conditions. The kinetic control regime occurs under conditions that promote fast growth (*viz.*, high monomer concentration), while thermodynamic control will be active under slow growth conditions (*viz.*, low monomer concentration).[226] Therefore, it is possible that the NC growth starts under kinetic control and later switches to thermodynamic control as the monomers are consumed.

Several colloidal NC systems (*e.g.*, MnO, CdSe[92,143,212]) have been observed to reach a steady state at the end of the growth stage. This is clearly demonstrated, for instance, by the influence of the growth temperature on the final size of CdSe NCs,[19] which has been observed to increase with T (*viz.*, 1.2, 1.7, 2.5, 3.2, and 4 nm in diameter at 100, 150, 200, 240 and 260 °C, respectively[92,143]). Moreover, the evolution of the NC size in response to a sudden increase in T is very similar to that

following a sudden increase in monomer concentration.[19,143] The occurrence of a (pseudo) steady state following the focusing regime has been recently supported by theoretical modelling.[212] In many cases the steady state is short lived and is followed by an increase in size dispersion (defocusing regime). This is particularly pronounced at higher T's (>260 °C in the CdSe system mentioned above[143]). However, the use of an excess of one of the precursors, in combination with relatively low T's (*viz*., 240 °C), has been observed to substantially increase the duration of the equilibrium state, thereby preventing defocusing.[143]

The reaction mechanism is also crucial for the growth stage. Recent work on the mechanisms underlying the formation of InP QDs from In(III)–myristate and tris(trimethylsilyl)-phosphine suggests that the broad size distributions typically obtained are due to the high reactivity of the precursors.[210] If the precursors are completely depleted during the pre-nucleation and nucleation stages, subsequent growth of the NCs will be possible only *via* ripening and/or aggregation of nuclei. This results in a large size distribution. It was also demonstrated that amines hinder precursor decomposition, thereby partially mitigating the deleterious effects of the exceedingly fast conversion of precursors into monomers.[210] This emphasizes the important role of surfactants as reagents (sections 3.1.1 and 3.1.2.I), which in turn may strongly affect the growth rates, given that the precursor conversion into monomers may continue throughout the growth stage. A high precursor stability results in higher activation energies for monomer addition to the NC, decreasing the growth rates and enhancing the differences between the growth rates of different crystallographic facets.[134,215,227]

Surfactants also affect the NC growth by binding to monomer species in solution and to the NC surface, thereby decreasing both the reaction and the diffusion rates. Further, the surfactant layer also depresses the reaction rates by limiting access to the NC surface and by actively competing with the monomers for the reaction sites. As mentioned above (section 2.2), the functionality of the surfactant molecules depends on both the polar head (coordinates to metal atoms) and the apolar tail (affects the diffusion properties). The interactions between the surfactant molecules will also have a profound impact on the growth rates, because they determine the surfactant dynamics in the reaction medium and at the NC surface. Faster dynamics result in faster growth, since the residence times of the surfactant at the NC surface will be shorter (see section 2.2.4), thus making the surface more accessible to monomers. The surfactant dynamics are determined both by the polar head group and the apolar chain length, so that weakly coordinating head groups and/or shorter chains result in faster dynamics, and consequently faster growth at relatively lower T's.[134] The dynamics also depend on the concentration of the surfactant and the temperature, so that higher T's or lower concentrations lead to faster dynamics. However, for surfactants capable of enhancing the precursor reactivity (section 3.1.2.I), concentrations below a certain threshold will depress the growth rates.[134]

3.1.3.II Crystalline phase control. Due to the high surface to volume ratio of NCs the overall surface energy can dramatically modify the stability of crystalline phases, making it possible to obtain NCs with crystal structures that are metastable for the bulk material. As it will be discussed below (3.1.3.III), this has important consequences for the shape control of NCs and HNCs.

The most common reaction parameter to control the crystalline phase of a NC is the growth temperature. Typically, growth at higher T's yield the phase that is thermodynamically stable for bulk at ambient conditions, while NCs produced at sufficiently low T's crystallize in the metastable phase (*e.g*., CdSe NCs are wurtzite, WZ, and zinc-blende, ZB, and MnS NCs are rock-salt, RS, and WZ, at high and low T's, respectively).[1,24,57] Surfactants can also have a large impact on the crystal structure of a NC, by modifying the surface energies of the facets, thereby changing the relative stability of a given phase. For example, CdSe NCs have been synthesized with either the ZB or the WZ structure, without changing the growth T, by simply adding TDPA to the Se precursor.[228] In the absence of TDPA or with TDPA in the Cd precursor solution WZ is obtained. Surfactants have also been reported to control the crystal structure of CdTe NCs (ZB or WZ).[215] Phase (and shape) control of NCs has also been achieved without changing the growth T or the nature of the surfactants, by tuning the nucleation and growth kinetics.[226] Very high supersaturations were observed to yield ZB ZnSe NCs, suggesting that the initial nuclei have the ZB structure, which is then kinetically frozen due to the fast growth. Conversely, very low supersaturations lead to ZnSe nanorods with the WZ structure, which for bulk ZnSe is stable only at high T's (>1420 °C).[226]

3.1.3.III Growth and shape control. The ability to control the shape of colloidal NCs has grown dramatically in recent years, yielding a plethora of 0-dimensional (*e.g*., cubes, stars, pyramids), 1-dimensional (*e.g*., straight or zig-zag wires), and 2-dimensional (*e.g*., platelets and disks) NCs, as well as more complex morphologies (*e.g*., multipods and nanorings).[21–26] Shape control has been recently extended to colloidal HNCs, producing a wide variety of sophisticated nanostructures, in which the composition, morphology, and connectivity of the individual segments of the HNC can be varied (*viz*., concentric core/multishell QDs, heterodimers, nanodumbbells, hetero-nanorods and multipods, Fig. 15).[25–30]

Although colloidal NCs are very often referred to as spherical, they are never truly so, since a NC is always highly facetted, and therefore should better be described as nearly spherical. In fact, NCs frequently present shapes that, albeit isotropic, cannot be approximated to spherical (*e.g*., cubes, tetrahedra, octahedra, truncated cubes, *etc*.). Therefore, to understand the mechanisms underlying the shape control of colloidal NCs, it is more insightful to classify the morphology of a NC in just two categories: nearly-spherical or isotropic (*i.e*., low aspect ratio) and anisotropic (*i.e*., high aspect ratio).

According to Wulff's theorem, the equilibrium shape of a crystal is the one that minimizes the overall surface free energy, and will thus be dictated by the relative surface energies of the various facets.[27] Therefore, under thermodynamic control, when the growth rates are sufficiently slow to allow equilibrium to be achieved, the shape of colloidal NCs

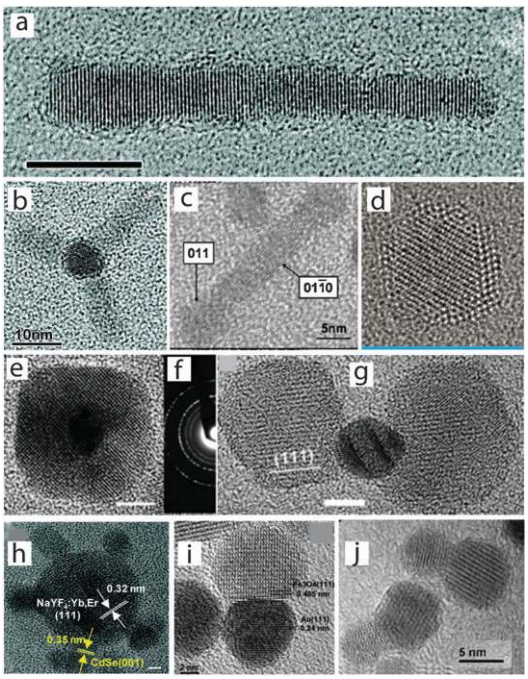

Fig. 15 Gallery of HRTEM images of colloidal HNCs of various compositions: (a) dot core/rod shell CdSe/CdS nanorod (scale bar: 5 nm). Reproduced with permission from ref. 57, Copyright 2007 American Chemical Society. (b) CdSe/CdS nanotetrapod. Reproduced with permission from ref. 57, Copyright 2007 American Chemical Society. (c) CdTe–CdSe–CdTe dumbbells. The images show that the CdTe dots are neither wurtzite nor oriented along the c-axis of the CdSe rod. Reproduced with permission from ref. 60, Copyright 2006 American Chemical Society. (d) PbSe/CdSe core/shell QDs. Courtesy of M. A. van Huis, Delft University of Technology, Netherlands. (e) Au–Fe_3O_4 core/shell HNCs (scale bar: 4 nm). Reproduced with permission from ref. 51, Copyright 2006 American Chemical Society. (f) electron diffraction pattern of the HNC shown in (e). Reproduced with permission from ref. 51, Copyright 2006 American Chemical Society. (g) Fe_3O_4–Au–Fe_3O_4 HNC (scale bar: 4 nm). Reproduced with permission from ref. 51, Copyright 2006 American Chemical Society. (h) CdSe NCs grown onto a $NaYF_4$: Yb,Er NC (scale bar: 3 nm). Reproduced with permission from ref. 229, Copyright 2010 American Chemical Society. (i) Au–Fe_3O_4 (scale bar: 2 nm). Reproduced with permission from ref. 52, Copyright 2005 American Chemical Society. (j) γ-Fe_2O_3–CdS. Reproduced with permission from ref. 56, Copyright 2005 American Chemical Society.

and HNCs will be isotropic, although facetted, both because this minimizes surface area and because low-energy facets of the NC are relatively close to each other in energy.[22,27] However, the shape of colloidal NCs or HNCs is frequently not the equilibrium one, because usually the growth is quenched while the growth rates are still significant, resulting in metastable anisotropic morphologies that are kinetically controlled.[22,27] The growth rate of a crystal facet depends exponentially on the surface free energy,[22] so that at high growth rates high-energy facets grow more quickly than low-energy facets, typically yielding high aspect ratio shapes. These shapes can still be rationalized in terms of Wulff constructions, by replacing free energies by growth rates, since fast growing facets tend to disappear.[27] It is worth noting that the NC shape is ultimately determined by the surface free energies, both under thermodynamic and kinetic control, since in the first case the NC surface consists primarily of low-energy facets, while in the latter the high-energy facets exhibit the fastest growth rates.

It is thus clear that the shape of a NC (or HNC) can be controlled by manipulating the surface free energies and the growth kinetics. This can be achieved by tuning a number of reaction parameters: temperature, concentration and nature of precursors, concentration and nature of the surfactants, crystal structure of the growing material, and concentration, shape, faceting and structure of the seeds (nucleated *in situ* or added). The impact of each parameter depends on the growth mechanism. In the discussion above, it was implicitly assumed that the growth proceeds *via* monomer addition to an existing NC seed, so that the crystallographic orientation of the growing monolayer is dictated by the substrate facet, resulting in homo- or heteroepitaxial growth, depending on whether or not the compositions of the growing material and the seed are the same. The possibility of growth through NC aggregation is often overlooked, based on the assumption that the surfactant molecules provide an effective steric barrier to NC coalescence. However, there is substantial evidence that particle coalescence or even oriented attachment can also play an important role in the growth and shape control of colloidal NCs.[38,206,225]

To date, several mechanisms have been proposed for the shape controlled growth of NCs.[23–28,31] These mechanisms are typically addressed separately, but it should be noted that there is no fundamental reason for them to be mutually exclusive. In fact, the coexistence of different growth mechanisms is probably a common occurrence. Furthermore, although a single universal mechanism is unlikely to exist, the shape control of NCs (and HNCs) can be rationalized in terms of a few general principles. Given that the various approaches developed for the size and shape control of colloidal NCs and HNCs have been extensively reviewed in several recent works,[23–28,31] we will here only outline the underlying principles involved in the shape control under each of the different growth regimes (homoepitaxy, heteroepitaxy, and oriented attachment), and discuss recent developments providing further insight into the topic.

Shape control and homoepitaxy. The shape of a NC under homoepitaxial growth can be understood in terms of the general principles described above. The growth regime is determined by the monomer flux towards the NC surface.[27,217] The monomer flux is defined by the monomer diffusion rate, which increases with the effective monomer concentration and the temperature. High monomer fluxes favour anisotropic growth, while low fluxes lead to isotropic growth. Monomer fluxes that are too low to sustain growth, but are still sufficiently high to prevent NC dissolution, lead to a process of internal ripening in which material is transported from high-energy facets to low-energy facets, causing the aspect ratio to slowly decrease towards a roughly isotropic shape. Very low fluxes result in inter-NC ripening, because the dissolution rates increase (see above).

It is interesting to note that very high monomer fluxes may induce branching, leading to the formation of multipods or even hyperbranched NCs. To understand this phenomenon

one has to consider that the growing NC is facetted, but is embedded inside an isotropic diffusion sphere, so that different parts of the NC are exposed to different concentration gradients.[27] These differences are negligible at low concentrations, but increase dramatically with increasing concentrations, because the spatial extension of the diffusion layer is inversely proportional to the diffusion rates. Consequently, different parts of the NC will grow slower or faster. A fast growing region will produce a flux from the slower growing regions towards itself and simultaneously move towards the boundaries of the diffusion sphere, where the concentrations are even higher. At sufficiently high concentrations, this will lead to self-sustained branching from high-energy facets or sites (*e.g.*, corners, edges or defects) of the NC and may lead to hyperbranching, since any defect (*e.g.*, kinks, stacking faults) in the fast growing branches will serve as a nucleation site.

In the effective concentration model[217] the need for strong surfactants to produce anisotropic shapes is explained simply by their ability to yield high monomer concentrations after the nucleation stage.[27,217] Therefore, the same surfactant may lead to either isotropic or anisotropic shapes, depending on the effective monomer concentration. In this context, the precursor stability and the surfactant-precursor interactions are also very important, since they will affect both the nucleation and the growth stages (sections 3.1.2 and 3.1.3.I). A slow nucleation leads to fewer nuclei and higher residual monomer concentration, and therefore favours anisotropic growth. Conversely, fast nucleation leads to higher concentration of smaller nuclei and lower residual monomer concentration, thereby favouring isotropic growth.

The surfactant molecules may also have a more direct impact on the NC shape. As mentioned above (section 2.3), the surface free energies of the various crystallographic facets of a NC can be remarkably different and may be strongly modified by surfactants and surface reconstruction. This affects the equilibrium shape of the NC (section 2.3),[158] and also kinetically controls the NC shape during growth. Further, some surfactants may bind more strongly to certain facets, thereby restricting their accessibility to monomers and increasing the activation energy for monomer addition to surface sites located on these facets.[23,25–27] This is usually referred to in the literature as the "selective adhesion model". The different bonding strengths of the surfactants to different facets will enhance or depress their relative growth rates, which may lead to highly anisotropic shapes, particularly under high monomer fluxes. The decisive role of selective adhesion in the shape control of colloidal NCs has been clearly established on a number of studies, leading to rods, tetrapods, platelets, bullets, and other complex shapes.[23,25–27] For example, CdTe NCs grown in ODPA : TOPO mixtures are dot shaped, while growth in ODPA : TOPO : Methylphosphonic acid (MPA) leads to multipods (bipods, tripods and tetrapods).[230] The growth rates and number and length of arms was observed to increase with the concentration of MPA.[230] Similarly, the controlled synthesis of hyperbranched CdTe and CdSe NCs, with shapes ranging from "thorny balls" to tree and "spider net"-like ramified dendrimers, has been recently achieved by varying the amount and type of surfactant (*e.g.*, mixtures of TDPA and 2-carboxyethylphosphonic acid, CEPA, yield different degrees of branching depending on the CEPA : TDPA ratio).[161] Further, CdSe nanoplatelets have been recently obtained by carrying out the growth in the presence of acetate.[231]

The impact of the surfactant molecule on the NC shape depends on the head group and the apolar tail. For strongly binding head groups the ability to boost anisotropic growth and branching increases with decreasing chain length. This has been extensively investigated for the anisotropic growth of CdSe NCs using TOPO and phosphonic acids (PA's) as surfactants and Cd–phosphonate complexes and TOP-Se as precursors.[208,217,232] These studies have clearly established that shorter chain PA's lead to higher aspect ratio nanorods and favour branching, facilitating the growth of tetrapods. This is due to a combination of factors.[208,232] First, shorter alkyl chains result in lower precursor stability (*e.g*, reactivity of Cd-hexylphosphonate is *ca.* 3 orders of magnitude larger than that of Cd-tetradecylphosphonate) and faster diffusion rates, leading to faster nucleation and growth. Further, shorter chain PA's bind more dynamically than their longer chain counterparts, enhancing the impact of selective adhesion on the growth rates of different facets. Therefore, shape control is easier to achieve using a mixture of short and long chain PA's.[232]

Anisotropic growth is also favoured by lower growth temperatures, since the reaction rates decrease.[25] Therefore, the free energy differences between different facets and the selective adhesion of surfactants become more discriminatory, strongly affecting the growth rates of different facets.[25,233,234] However, short chain ligands are needed as well,[233] since the reactivity of precursors based on long chain ligands is negligible at low temperatures. For instance, it has been observed that in a diluted monosurfactant system (*viz.*, 2-hexenoic acid, 2-octenoic acid or 2-decenoic acid in ODE) spherical NCs are obtained at 300 °C, while at lower T's (*viz.*, 270 and 220 °C) rods are obtained (lower T's and/or shorter chains lead to longer rods).[233]

As mentioned above, high-aspect ratio shapes are rarely the equilibrium shape and therefore the morphology of anisotropic NCs will evolve in response to changes in their solution environment (see section 3.1.4 below). For example, annealing of CdSe nanorods at 300 °C at low monomer concentration leads to a process of internal ripening in which the aspect ratio slowly decreases until a roughly isotropic shape is achieved.[26–28,217,235] If annealing is carried out while keeping a high monomer concentration but slowly replacing the surfactant (*e.g.*, TDPA by acetate[235]), the nanorods evolve to nanobullets, trigonal pyramids and eventually multipods in which the arms grow in the 101 direction (in contrast to the 002 orientation normally observed for rods and multipods grown in the presence of phosphonic acids).[235]

Finally, the crystalline phase of the seed also influences the final shape of the NC.[24,27] Non-centrosymmetric crystal structures, such as WZ (*e.g.*, CdSe and CdTe), are inherently polar and tend to grow anisotropically, easily yielding rods and multipods. In fact, NCs of materials with the WZ structure are rarely truly isotropic, commonly yielding prolate NCs (aspect ratio: 1.2–1.5). Conversely, centrosymmetric crystal structures, such as ZB (*e.g.*, CdTe, CdS) and rock-salt (*e.g.*, PbSe, MnS),

tend to grow isotropically along the three crystalographic axes, resulting in nearly spherical NCs, cubes or tetrahedra (commonly with truncated edges). Nevertheless, centrosymmetric materials are also often observed to yield anisotropic shapes such as rods and wires,[24,27,37,164] sometimes under low monomer fluxes. This cannot be explained by kinetic arguments, and is usually ascribed to oriented attachment (see below).

Structural polytypism and twinning can also be exploited to yield branched NCs.[25–27] This is well illustrated by CdSe and CdTe NCs, which can crystallize in either the WZ or the ZB crystal structures. The two structures are very close in energy and therefore switching between them can be driven kinetically or by selective adhesion of surfactants, allowing the fabrication of complex shaped NCs, such as tetrapod, dendrimer and hyperbranched NCs.[25–27,161] The final shape of a NC is also critically affected by the morphology and faceting of the NC seeds. For example, upon fast growth conditions tetrahedral ZB CdSe NC seeds, with four {111} facets, yield tetrapods,[106] while cuboctahedral ZB CdSe NC seeds, with eight {111} facets, yield octapods.[234]

Shape control and heteroepitaxy. The principles discussed above for homoepitaxial growth also apply to heteroepitaxial growth, but shape control of HNCs is inherently more challenging, since the requirement for lattice matching at the heterointerface imposes larger constraints on the morphology of a HNC. The essential difference between homo- and heteroepitaxial growth is that the latter depends on both the surface and the heterointerfacial free energies. Therefore, the shape of a colloidal HNC is extremely sensitive to the characteristics of the seed (crystal structure, size, shape and faceting, surface defects, *etc.*) and the nature of the growing material. Nevertheless, the current understanding of the impact of the seeds on the shape of HNCs is still limited, although it is clear that misfit strain at the heterojunction is very relevant. Moreover, several other complex mechanisms, such as solid-state atomic diffusion and/or exchange, redox processes, phase separation, and oriented attachment may intervene in the heteroepitaxial growth process.[25,27,28]

Interfacial strain due to lattice mismatch is an important issue in nanostructures grown by heteroepitaxy, as the wealth of data on QDs and quantum wells grown by vapour phase (VP) deposition methods clearly illustrates.[236,237] The growth mode and shape evolution is dictated by the interfacial strain, which is in turn determined by the interface free energies and the lattice mismatch.[236] Depending on the latter, three different heteroepitaxial growth modes can be distinguished:[236] (a) layer-by-layer growth (Frank van der Merwe mode, FM, for lattice matched systems); (b) layer growth followed by self-organization in islands (Stranski-Krastanow mode, SK, for lattice mismatched systems with relatively small mismatches, *i.e.*, $\leq$10%); and (c) island growth (Volmer-Weber mode, VW, for lattice mismatched systems with larger mismatches, *i.e.*, $\geq$10%). In the case of the FM mode the strain is negligible and therefore the thickness of the heteroepitaxial layer is in principle unlimited. Conversely, in the VW mode the growing material will minimize the interfacial area, therefore growing as islands. In the SK mode a thin heteroepitaxial layer grows, but is strained due to the lattice mismatch. Strain builds up as the thickness increases, and, as a result, self-reorganization of the layer into islands will occur to relieve strain, if the thickness exceeds a critical value. This critical thickness is determined by the strain energy and is therefore smaller for larger mismatches, but is typically just a few monolayers (MLs). For example, the critical thickness for the growth of InAs over GaAs (7% lattice mismatch) is 2 MLs.[238]

Strain relaxation in VP-grown layers can occur by energy minimization mechanisms that yield defect free islands, such as elastic relaxation on facet edges and renormalization of the surface (or interface) free energy, but it can also occur through the formation of misfit dislocations and other defects, especially as the islands grow larger.[238] These defects can severely compromise the properties of heterojunction nanostructures by, *e.g.*, increasing nonradiative recombination rates.[237] It should be noted that strain relaxation is a dynamic process that occurs concomitantly with the growth, and therefore is under strong kinetic control. As a result, relaxation by formation of misfit dislocations and other defects is favoured under fast growth conditions, because they involve the reorganization of fewer atoms than interface and surface reconstruction processes and island formation.

Heteroepitaxial growth of colloidal HNCs is expected to be analogous to that observed *via* VP techniques,[25,28] but one should keep in mind that colloidal HNCs are much smaller and more facetted than their VP-grown counterparts. Consequently, colloidal HNCs are able to accommodate larger degrees of interfacial strain, and therefore heteroepitaxial growth may occur for larger lattice mismatches. For example, ZnS shells can be grown over CdSe cores despite the large lattice mismatch (*viz.*, 12%), although the shell thickness will be limited to 2 or 3 MLs.[30] Further, the critical thickness for the self-reorganization will be larger in colloidal HNCs than in VP-grown heteronanostructures, making it possible to grow relatively thick shells of lattice-mismatched materials over NC seeds. To minimize the strain field in the shell, the chemical bonds in the HNC core become also partially strained. This induces an axial compressive or tensile stress in the HNC core, depending on whether the bonds are shorter or longer than normal.

Recently, the PL of Mn^{2+} doped at radially controlled positions in the shell of CdS/ZnS core/shell NCs (7% lattice mismatch) has been used as a local probe of the pressure in the shell.[239] This pressure is induced by compressive stress, since the lattice parameters of ZnS are smaller than those of CdS. The redshift of the Mn^{2+} PL with increasing shell thickness indicates a pressure of more than 4 GPa for 7.5 MLs of ZnS.[239] It is interesting to note that this thickness is much larger than the critical value observed for InAs heteropitaxial layers grown over GaAs substrates by VP methods (*i.e.*, 2 MLs), despite similar lattice mismatches ($\sim$7%). This demonstrates that colloidal HNCs can indeed accommodate larger lattice mismatches than their VP-counterparts. The radial dependence and magnitude of the pressure derived from the Mn^{2+} PL shift were shown to be in good agreement with theoretical models, which allowed the authors to estimate that the pressure induced by a hypothetical 7.5 MLs thick ZnS heteroepitaxial shell on CdSe would be 10 GPa.[239]

This explains why the ZnS shell is experimentally observed to grow smoothly over CdSe only for a couple of MLs. The strain for thicker ZnS shells over CdSe cores is thus likely to exceed the threshold for creation of misfit dislocations. On the other hand, for CdSe/CdS and CdSe/ZnSe the mismatches are smaller (3.9% and 6.3%, respectively), and therefore the maximum interfacial pressure remains smaller, possibly allowing unlimited thick shells. Accordingly, CdSe/CdS core/shell HNCs consisting of 19 CdS MLs overcoating a 3 nm CdSe core have been recently obtained.[86]

The facetted nature of colloidal NCs also makes the heteroepitaxial growth over colloidal seeds much more complex than under VP conditions, since different facets will not only have different free energies and reactivities, but will also offer different lattice mismatches. Further, as discussed above, surfactant molecules may bind more strongly to certain facets of the NC seed, thereby decreasing their growth rates and availability for heteroepitaxial growth,[25] irrespective of their suitability in terms of lattice mismatch. The combination of these constraints may result in anisotropic growth or the formation of complex morphologies even under conditions that would yield isotropic growth under homoepitaxy. For instance, it has been experimentally demonstrated that anisotropic HNCs, such as heterorods, can accommodate much larger lattice mismatches (as large as 11%) than concentric structures such as core/shell QDs.[65] Consequently, the length of colloidal heteronanorods or multipods is less limited than the shell thickness of core/shell HNCs and typically reach several tens of nm, or even hundreds, allowing the fabrication of narrow colloidal nanowires. Strain relaxation in this case occurs primarily by the periodical formation of stacking faults and dislocations, which do not preclude the continued growth of the nanorod or nanowire.

The different susceptibilities to heteroepitaxial growth of the various facets of a seed NC have been exploited to fabricate complex HNCs. For example, the tips of nanorods with the wurtzite structure typically consist of the polar facets, which are more reactive than other facets. This fact has been successfully utilized to grow a number of different materials (*e.g.*, PbSe,[61] Au,[140] or CdTe[60]) selectively at the tips of CdSe and CdS nanorods, yielding dumbbell or matchsticks HNCs. To prevent nucleation on the lateral facets a relatively low temperature is needed (*e.g.*, 130 °C for PbSe on CdSe).[61] Similarly, a number of different materials (*e.g.*, Co) has been grown on the tips of TiO_2 nanorods.[25–28,63] When the lattice mismatch between the NC seed and the material to be deposited is too large, heterogeneous nucleation will dominate over heteroepitaxial growth. In this case, preferential nucleation may occur on selected facets that offer the smallest possible mismatch, yielding heterodimers or oligomers.[25,27,28] It is then also possible that growth occurs only on high energy sites such as corners and/or defects.

The monomer concentration also has a crucial impact on the shape control of HNCs, since fast growth rates may be incompatible with slow mechanisms of strain minimization (*e.g.*, interfacial reconstruction and strain redistribution). The resulting shape and structure of the overgrown material will then be the one that is more effective in terms of dynamically minimizing the overall strain energy. Under such conditions the growth of concentric HNCs is precluded, and very often homogeneous nucleation followed by homoepitaxial growth prevails. It is also possible that under fast growth conditions and/or large mismatches the deposited material grows as an amorphous shell, which later undergoes crystallization and shape change under annealing conditions.[26,27] It should be noted that the residual strain energy after the growth stage will be decisive for the shape evolution under annealing conditions (section 3.1.4).

It may also be expected that the mechanisms for strain relaxation will be different in colloidal HNCs. The investigation of type-I core/shell QDs has clearly established that the lattice mismatch induces strain at the core-shell interface, which negatively affects both the QY and the stability of the QD and limits the shell thickness.[30,239] Nevertheless, the mechanisms by which interfacial strain relaxation affect the properties of colloidal HNCs are still poorly understood, since very few studies have addressed this topic. The shell distribution on CdSe/ZnS core/shell QDs has been investigated by a few groups.[35,160,240] These studies have provided a clear structural basis for near unity PL QY on CdSe based core/shell HNCs, showing that high PL QYs require uniform coating by a reasonably thick (≥ 5 MLs) heteroepitaxial shell.[35,160,240] This requirement is not met by CdSe/ZnS core/shell HNCs. Due to the large lattice mismatch, the distribution of ZnS around the CdSe core is highly anisotropic. The ZnS shell appears to be located more on one side of the NCs and form irregular patches on the core that in general do not uniformly surround the CdSe core.[240] Moreover, ZnS NCs are also present, implying that very often homogenous nucleation of ZnS NCs has prevailed over heteroepitaxial growth and/or heterogeneous nucleation. An uniform shell coverage is obtained only for a graded CdS/ZnS shell material. In this case preferential growth takes place on the anion terminated facets, yielding bullet shape core/shell HNCs.[35,160] Further, the Se polar facet is observed to have the fastest growth rate, followed by the Se-rich (10−1) facets.

Shape control and oriented attachment. Oriented attachment of smaller NCs into larger nanostructures has been proposed to explain the formation of anisotropic and complex shaped colloidal NCs of a number of different materials (*viz.*, TiO_2, PbSe, PbS, CdSe, CdTe, Au, MnO, ZnS, *etc.*).[38,43,241,242] For example, the formation of PbSe nanowires and nanorings,[243] nanostars,[244] and, more recently, nanorods,[245] has been attributed to growth through oriented attachment. There are also reports on the formation of narrow nanowires ($\sim$1.5–3 nm diameter and up to 200 nm long) by oriented attachment of NCs during growth at mild temperatures ($\sim$100–150 °C) and long times (4 to 70 h) (*e.g*, ZnSe : Mn nanowires[246] and CdSe nanorods[247] by heating-up single-source precursors in HDA, CdSe nanowires[248] by reacting Cd acetate and selenourea in amines). Oriented attachment has also been observed during post-preparative treatments, leading to the formation of single-crystalline CdSe[249] and CdTe nanowires.[250] The nanowire growth occurred spontaneously at room temperature and took several days to be completed.[249,250] The diameter of the wires was determined by the diameter of the parent NCs (1.6 nm and 3–5 nm for CdSe and CdTe, respectively[249,250]).

Surfactants have been observed to play a decisive role in the growth of NCs by oriented attachment, possibly by destabilizing or selectively exposing certain facets.[38] For instance, it has been clearly established that the acetate concentration is by far the most important parameter for the formation of PbSe star-shaped NCs, presumably due to a pronounced reduction in steric hindrance.[244] Moreover, oriented attachment appears to be facilitated by shorter chain and/or relatively weak surfactants (*e.g.*, pyridine,[249] thioglycolic acid,[250] or acetate[244]).

Three different stages have been identified in the growth of CdSe and CdTe nanowires through oriented attachment.[248,250] Initially, small NCs (sometimes as small as MSC's[246–249]) are generated, or added to the growth medium in case of post-synthesis growth. This is followed by oriented attachment of the parent NCs in pearl necklace aggregates, which subsequently reorient and fuse, yielding single crystalline nanowires. The fusion process is accompanied by recrystallization from ZB to WZ. The overall process is probably driven by the reduction of the surface and interfacial energy, thereby minimizing the total free energy of the system. Most likely, these three stages are a general feature in the mechanism of formation of nanostructures through oriented attachment. Indeed, this general mechanism is corroborated by a recent *in situ* study of the low-temperature (100 °C) unification of PbSe NCs through oriented attachment,[164] which allowed the direct observation of a complex chain of processes: NC coalescence, followed by multiple rotations to achieve proper lattice orientation, interfacial relaxation to eliminate misfits and finally fusion into larger single-crystalline NCs.

Growth by NC coalescence in solution has also been recently observed *in situ* by using solution TEM.[225] Coalescence events were more common for smaller Pt NCs, due to their larger surface-to-volume ratio and greater mobility. After a coalescence event the resulting particle underwent a relaxation process, during which the individual NCs fused and recrystallized, along with a shape change and slight loss of monomers.[225] The results show that individual nearly-spherical Pt NCs can grow either by monomer attachment from solution or by particle coalescence.[225]

It is generally accepted that the oriented attachment process is driven by a dipolar interaction between the parent NCs. The recent observation of the transient formation of short strings of NCs in solutions of both PbSe and CdSe colloidal NCs provides further support to this idea.[251] A size-dependent permanent dipole moment has been reported for WZ CdSe NCs and nanorods,[252,253] and ascribed to the intrinsic polar character of the WZ lattice. However, dipole moments have also been observed for NCs of materials with centro-symmetric crystal structures, such as ZnSe (ZB)[252] or PbSe (rock-salt).[251,254] The origin of these dipole moments is still under debate, but it is generally attributed to an asymmetric distribution of the polar facets,[38,164,243,251] or to shape asymmetry.[255]

Novel mechanistic insights into the epitaxial growth of shape-controlled colloidal NCs. Experimental results show that the growth on the Se terminated polar facets of a nanorod or NC is faster than on the Cd terminated polar facets, both under homo- and heteroepitaxy.[35,57,58,160] For example, during the growth of CdS rod shells on CdSe NC seeds the volume increase in one direction is 6–9 times larger than in the other direction, so that the seed NC ends up closer to one side of the rod.[57–59] The selective adhesion model explains well why the growth in the c-direction is faster (selective adhesion stabilizes the non-polar side facets more and hinders diffusion of the precursors and/or monomers to the NC side). However, it does not explain the differences between the growth rates of the Se (00-1) and Cd (001) facets, if the growth proceeds by incorporation of atomic units. This would convert a Se polar facet into a Cd polar facet, and vice-versa. This reversal of the facets' composition would cause the growth rates to be roughly the same on both sides, in contradiction with the experimental observations.

This discrepancy can be solved by considering that the growth proceeds by addition of CdSe units rather than atomic species (Fig. 16). This is in line with the reaction mechanisms proposed for both CdSe and PbSe QDs (section 3.1.1). This is also consistent with the recent observation that the sublimation of PbSe NCs proceeds by sequential release of PbSe molecules, whereby the termination at the newly exposed surface is retained, so that the sublimation of one complete facet exposes an identical one.[159] It is possible that the attachment of the CdSe units is directed by the dipole moment of the NC, which would prevent the reversal in the composition of the facets. We note that this brings the epitaxial growth and the oriented attachment mechanisms together in a more unified view of the growth of anisotropic NCs, since the growth can proceed by addition of CdSe molecular units or larger $[CdSe]_n$ units. Higher precursor concentrations will lead to larger n values, thereby favouring fast anisotropic growth by oriented attachment of larger units. In this context it is interesting to note that a recent investigation of the atomic structure of CdSe nanorods

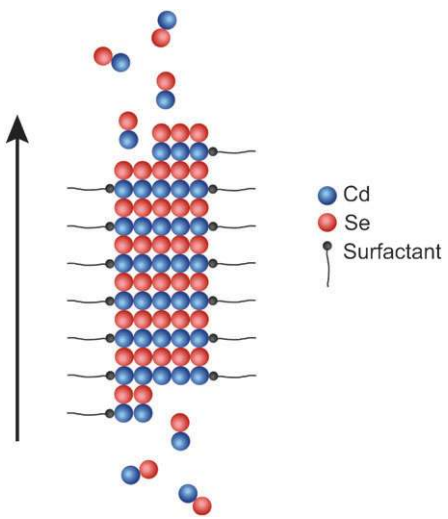

Fig. 16 Schematic diagram of a possible growth mechanism for CdSe nanorods, explaining the fact that the growth rates are faster on the Se terminated tips and that the facet composition is preserved throughout the growth (see text for details). The arrow indicates the intrinsic dipole moment of the nanorods. Surfactant molecules attached to monomers are omitted for simplicity. Courtesy of E. Groeneveld (Utrecht University, Netherlands).

by Z-STEM and electron nanodiffraction has provided strong evidence that long CdSe nanorods grow both by monomer incorporation from solution and by oriented attachment driven by dipole–dipole interactions.[256]

3.1.4 Annealing stage. As discussed in section 3.1.3.I above, a steady state will be reached when the monomer concentration drops to a level that is insufficient to sustain growth. If the monomer concentration is so low that the dissolution rates become significant, the steady state will be short lived and the system will enter an inter-NC ripening regime, in which larger NCs (or HNCs) grow at the expense of the smaller ones.[22,27,217] This is undesirable, as it will lead to an increase in size and shape dispersion, while preventing surface annealing. In order to allow the annealing stage to be reached the steady state must be maintained, which requires monomer concentrations that are sufficiently high to slow down the dissolution rates, but still insufficient to sustain growth. This may be achieved by using a combination of lower T's and a large excess of one of the precursors (see section 3.1.3.I). Under such conditions, inter-NC mass transport processes and growth rates are negligible, but the surface atoms still have enough mobility. This allows surface annealing and reconstruction to take place, leading to high PL QYs.[143]

As mentioned above (section 3.1.3.III), shape evolution becomes possible under annealing conditions, since the high mobilities of the surface atoms allow for intraparticle ripening. This is often undesirable because it decreases the aspect ratio of anisotropic NCs and HNCs, but it may also be useful to improve the quality of shells, induce oriented attachment or modify the shape of HNCs. For example, γ-Fe_2O_3–CdS heterodimers are obtained by first growing an amorphous and isotropic Fe_2O_3 shell over a CdS NC. Upon subsequent annealing the shell crystallizes and retracts to one side of the seed.[27]

Diffusion may also occur during the annealing stage. Although diffusion processes have been extensively investigated in bulk materials, little is known about diffusion in nanomaterials. However, there are several recent studies reporting on the observation of a variety of diffusion processes in NCs and HNCs. Diffusion of Au from the inner core of concentric core/shell Au/Ag_2S HNCs to the surface, yielding a heterodimer, has been observed at room temperature, taking 72 h to be completed.[257] Conversely, inwards diffusion of Au from the surface to the core of a NC, yielding core/shell HNCs, has been reported for both Au/InAs[258] and Au/PbTe.[259] Diffusion may also lead to ejection of the dopant ion in doped NCs (*e.g.*, ZnSe : Mn NCs containing 15 Mn^{2+} ions/NC loose all dopants if heated to 300 °C).[72] Further, thermally activated interdiffusion may convert concentric core/shell QDs into gradient alloy QDs (*e.g.*, CdSe/ZnSe upon heating above 270 °C).[114] Similarly, Se–Te interdiffusion across the heterojunction has been observed in linear CdTe/CdSe/CdTe heteronanorods, upon continued heating under annealing conditions.[66] Interdiffusion is quite fast and is already observable after 10 min at 300 °C, well before internal ripening has led to appreciable changes in the aspect ratio.

3.2 The hidden variable: adventitious impurities

The complex nature of the reaction systems typically used in the colloidal synthesis of NCs and HNCs renders many synthetic protocols difficult to reproduce. The variability in the synthesis can partially be traced to unintentional variations in the reaction parameters. Indeed, careful and systematic optimization leads to highly reproducible synthetic protocols (3–5% standard deviation for manual syntheses, and as small as 0.2% for automated syntheses[260]). Nevertheless, the largest source of irreproducibility is the presence of adventitious impurities in the chemicals used.

The critical role of impurities was recognized already in the early years. Phosphonic acids were originally adventitious impurities in technical TOPO, bringing a bit of alchemy to the nascent field of colloidal nanoscience, and giving rise to a rich scientific lore, full of anecdotal tales about "good" and "bad" batches of TOPO. After their presence and impact was recognized they became essential additives to control the shape of colloidal NCs (section 3.1.3.III). The intentional addition of ligands presumed to be analogous to the impurities in technical TOPO (*i.e.*, alkylphosphonic acids) led to the first controlled synthesis of colloidal QRs and tetrapods, initiating extensive research activites on understanding and controlling the anisotropic growth of NCs.[261]

The reproducibility problems associated with the use of TOPO as a surfactant became more and more evident over the years, despite the improved purity of commercially available TOPO (99%). However, it was only recently that efforts were undertaken to identify the impurities present in TOPO 99%.[227] Up to now, ten different impurities have been identified, going from simple molecules such as H_3PO_3 to larger molecules such as 1-methylheptyl-di-*n*-octylphosphineoxide (MDOPO). More importantly, some of those impurities have turned out to be essential for the synthesis of high-quality shape controlled CdSe NCs (*e.g.*, di-*n*-octylphosphinic acid, at levels of 0.2 wt%, for nanowires; and di-*n*-octylphosphine oxide, at levels of 0.8 wt%, for nearly spherical NCs).[227] It is also worth mentioning that the composition of the surfactant layer on colloidal CdSe NCs prepared in technical TOPO has been shown to consist primarily of P-containing impurities (*viz.*, *n*-octylphosphonate, OPA, and P,P′-(di-*n*-octyl)dihydrogen pyrophosphonic acid, PPA).[170] The impact of impurities has also been identified in other commonly used surfactants. For instance, it has been recently demonstrated that phosphine impurities in commercially available TOP (shorter chain phosphines, dialkylphosphines, and phenylphosphines) can strongly influence the synthesis of colloidal PbSe NCs, affecting the reaction yield, the number of NCs formed and their sizes.[211]

Impurities may also be inadvertently introduced during preparation of the precursors. For example, in the synthesis of PbSe NCs the lead oleate precursor is prepared by reacting Pb-acetate and oleic acid. This reaction produces also water and acetic acid, which must be removed by heating under vacuum. If this process is not properly done, the residual acetic acid will strongly affect the NC size and shape.[244] Heating the surfactant mixture may also lead to unsuspected changes, since organic molecules may be highly reactive at the temperatures

used in some synthetic protocols (*viz*., 300–340 °C). Accordingly, the main component of the surfactant layer of CdSe NCs prepared in technical TOPO (*viz*., PPA) is actually formed *in situ* during the NC synthesis *via* the dehydrative condensation of an impurity (OPA) present in technical TOPO at concentrations of ~1 mol%.[170] The *in situ* formation of DOPA and OPA by oxidation of TOPO has also been observed by heating a mixture of TDPA and TOPO (both 99%) to 280–300 °C under a weak vacuum (1000 mTorr).[262] It is worth noting that the oxidation took place even though the reaction mixture had been subjected to three nitrogen purge and degassing cycles (vacuum ≥ 1000 mTorr),[262] so it is conceivable that *in situ* formation of impurities may inadvertently happen during sub-optimal degassing.

It should also be realized that the early work on, *e.g*., shape control using phosphonic acids was also affected by the limited purity of the chemicals available at the time. For example, the growth of CdTe tetrapods, previously reported to take place in ODPA,[263] has been recently shown to be actually determined by methylphosphonic acid,[230] an impurity present in commercially available ODPA until *ca*. 2005. The extent to which impurities in the surfactants are still biasing the conclusions currently published in the literature is unclear. To improve the reproducibility of synthetic protocols, some groups advocate the purification of starting chemicals and intentional addition of impurities.[227] An alternative is the use of protocols using diluted surfactant systems (*e.g*., ODA in ODE), which are more robust and less sensitive to impurities than those based on neat surfactant systems.

3.3 General considerations on the preparation of colloidal heteronanocrystals

3.3.1 Strategies for the synthesis of high-quality colloidal heteronanocrystals. There are essentially two strategies for the synthesis of colloidal HNCs: the single-stage (or "one-pot") approach, and the multistage seeded growth approach. In the first one the HNC is fabricated by sequentially adding the precursors of the different components in the same reaction flask. Although this approach may be appealing for its simplicity, it cannot provide the degree of control required for the targeted synthesis of high-quality colloidal HNCs. As discussed in the previous sections, the heteroepitaxial growth of high-quality shells (or branches) on seed NCs requires physical-chemical conditions that substantially differ from those needed for the growth of single composition NCs (*i.e*., the seeds). Moreover, uncontrolled interfacial alloying is usually unavoidable in a single-stage synthesis, since the concentration of monomers of the first component should still be substantial when the second component is added (otherwise inter-NC ripening would have set in, see section 3.1.3). In contrast, the multistage approach is highly versatile and provides several advantages over the single-stage strategy:

1. The addition of preformed nuclei to the reaction mixture (*i.e*., seeded growth) is a very effective way of separating nucleation and growth, and leads to a better control over the growth stage, both under homo- and heteroepitaxy.

2. Different conditions can be used to grow each segment of the HNC. Therefore, the targeted synthesis of complex multicomponent HNCs, in which NCs of different composition and shape are sequentially combined, becomes possible.

3. The seeds (NCs or HNCs) can be subjected to post-synthetic processing (purification, size-selection, ligand exchange or annealing). This can be used to improve the quality of the seeds and allows for judicious surface manipulation. This is a key advantage, as the seed characteristics have a decisive impact on the growth kinetics and the final shape of the HNCs (section 3.1.3.III).

4. The heterointerface is better controlled, since the possibility of unintentional interfacial alloying is almost eliminated (provided the temperature is low enough and the excess of unreacted precursors has been removed from the surface of the seed NCs[82]). Additionally, controlled hetero-interfacial alloying becomes possible by a proper choice of growth temperature or by controlling the ratio between the added precursors.[82]

5. The method is highly flexible regarding the choice of synthesis techniques. These techniques will be briefly discussed below.

Precursor addition to seeds. This is the most commonly used technique to grow HNCs, being particularly well suited when slow growth is required. The precursor solution for the new component of the HNC is added to the seed NCs dissolved in a suitable surfactant mixture and under vigorous stirring. The reaction temperature is typically set prior to the precursor addition, but it may also be increased following it (the so-called "heating-up" or "thermal cycling" method[107,264]). The heteroepitaxial growth may also be photo- rather than thermally-induced.[140] Photoassisted growth has been recently reported to lead to selective deposition of Au NCs on the sulfur-rich end facets of CdS nanorods.[140] The precursor addition must keep relatively constant growth rates, while preventing homogeneous nucleation, and can be performed in several ways: (a) dropwise addition of mixed precursors, (b) alternate injections of each precursor separately (the so-called "SILAR" method), or (c) dropwise and alternate addition. The effectiveness of each method depends primarily on the precursor reactivity. If the precursor is highly reactive, all three methods will fail to completely suppress homogeneous nucleation, but (c) is the most effective. Conversely, if the precursor is too stable, the differences between (a) and (c) vanish, and all three methods will fail if the time allowed for growth between two subsequent additions is too short (*i.e*., if the addition rates exceed the monomer consumption rates). Specific examples will be discussed in more detail below.

Seeded injection. In this method seed NCs and one of the precursors are injected together in a hot solution containing the second precursor and surfactants, under vigorous stirring. Anisotropic growth can be ensured by using a high concentration of precursors and suitable surfactants. This technique has been successfully used to obtain anisotropic HNCs with well defined length and diameter for a number of compositions (*viz*., dot core/rod shell nanorods: CdSe/CdS,[57–59] ZnSe/CdS;[59] tetrapods: CdSe/CdS,[57] CdSe/CdTe,[106] ZnTe/CdTe,[106] ZnTe/CdSe,[106] ZnTe/CdS,[106] CdTe/CdSe;[85] octapods: CdSe/CdS[234]).

Ion exchange. This method consists of adding a large excess of the cation precursor of the new component to a solution of the seed NC in a solvent (*e.g.*, methanol or toluene), typically at mild temperatures (25–100 °C). This leads to an exchange reaction in which the new cation diffuses into the parent NC and displaces the parent cation, while keeping the anionic sublattice unaffected.[64,265,266] The size and shape of the parent NC is preserved. Therefore, cation exchange offers a way to make shape-controlled NCs which would otherwise not be possible (*e.g.*, Ag_2S nanorods,[265] PbS nanorods,[265] or cuboctahedral ZB CdSe NCs[234]). The extent of the conversion depends on the reaction time and the ratio between parent and new cations, and can be total or partial.[265] The exchange rates may also strongly depend on the crystallographic facets, as observed for CdS/Cu_2S,[267] PbTe/CdTe,[268] and PbSe/CdSe.[49] Moreover, the NC composition can be controlled through successive cation exchange reactions (*e.g.*, Cd^{2+} by Cu^{+}, and subsequently Cu^{+} by Pb^{2+}).[265] Therefore, cation exchange offers a very attractive route to fabricate shape-controlled HNCs which are not attainable by conventional seeded growth methods, and has successfully yielded a number of novel colloidal HNCs (*viz.*, core/shell QDs: PbSe/CdSe,[49] and PbTe/CdTe;[268] heterorods: CdS/Ag_2S,[64] CdS/Cu_2S,[265] CdS/PbS,[265] and PbSe/PbS[266]).

Replacement of sacrificial domains. This method consists of obtaining a HNC through the replacement of a sacrificial component of a parent HNC by the desired component.[25,29] Since the shape and location of the sacrificial domain are preserved, this approach allows the fabrication of colloidal HNCs which would be unfeasible by direct heteroepitaxial growth methods. For example, concentric Au/Ag_2S and Au/Ag_2Se core/shell nanorods have been fabricated by reacting the silver shell of Au/Ag core/shell nanorods with sodium sulfide or selenourea.[269] Similarly, metal/metal oxide core/shell HNCs can be obtained by the controlled oxidation of metal NCs (*e.g.*, Co/CoO; Ni/NiO; MnO/Mn_3O_4).[25] Further, Au-tipped CdSe and CdS based dumbbell HNCs have been obtained by first growing PbSe or CdTe NCs on the tips of CdSe and CdS nanorods, and subsequently replacing them by Au NCs through a redox reaction.[270] It should be noted that the ion exchange method discussed above can also be regarded as an example of the sacrificial replacement strategy.

3.3.2 Guidelines for the design of synthesis protocols for colloidal heteronanocrystals. The development of a novel synthesis protocol for a colloidal HNC is still a largely empirical endeavour, in which a set of original conditions are judiciously chosen and put to practice. Depending on the outcome of these exploratory experiments, the initial choices are refined and optimized, or drastically revised. The success of this development process requires a stringent approach that takes full advantage of the complex nature of colloidal NCs by systematically exploring and mapping their multidimensional synthetic parameter space. In this section, we will discuss how the fundamental principles presented above can be used as guidelines both for the original choices and for the subsequent optimization process, allowing for a rational design of novel synthesis schemes.

I. Choosing the seeds. The choice is in principle unlimited, since any colloidal NC can be used as seed, regardless of shape or composition (single-component, alloy, doped or hetero-NCs). However, as discussed above (section 3.1.3.III), the characteristics of the seeds strongly influence the final morphology of the HNC and impose constraints on the nature of the overgrowing segment. To illustrate the decisive role of the seeds in the colloidal synthesis of HNCs, we will focus on one particular system (*viz.*, CdSe), out of the plethora of possible material combinations. CdSe QDs and CdSe based HNCs have been work horses of colloidal nanoscience since the inception of the field, and continue to lead to new insights and fundamental advances. Therefore, CdSe based HNCs are ideal to showcase the limits and possibilities of the colloidal synthesis of HNCs, since a large variety of sophisticated HNCs have been grown based on CdSe seeds (*e.g.*, concentric core/shell QDs, heterodimers, heterotetrapods, dot core/rod shell HNCs, heterorods, dumbbells, matchsticks, *etc.*, Fig. 17)[25–30] For example, as illustrated in Fig. 17, the morphology and connectivity of the colloidal HNC can be directed by using shape controlled NCs as seeds. The impact of the seeds on the fate of the HNC growth will be discussed in more detail below.

II. Choosing the HNC's architecture: composition, morphology and connectivity of the overgrowing segment. The composition and shape of the overgrowing segment are chosen based on the properties desired for the HNC and the role to be

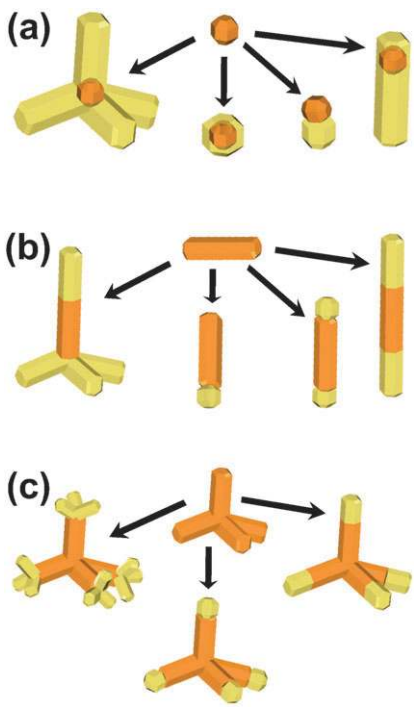

Fig. 17 Scheme showing the HNC morphologies that can be obtained by seeded growth using shape controlled CdSe nanocrystals as seeds: (a) nearly spherical NCs, (b) nanorods, and (c) tetrapods. See text for details regarding the growth pathways. Courtesy of M. Casavola (Utrecht University, Netherlands).

fulfilled by the new segment. From this perspective, the essential parameters to be considered are the nature (*viz*., metal, semiconductor, *etc*.), chemical composition, and properties (*e.g*., band positions, electron and hole effective masses, magnetic susceptibility, optical transitions, *etc*.) of the overgrowing material (section 2.1). Further, as mentioned above (section 2.2), the surfactant layer may also be utilized to impart properties to the HNC, and therefore must be taken into account when designing the HNC's architecture.

The choice of composition is ample but not unrestricted, as the overgrowing material must be chemically and structurally compatible with the seed surface. Moreover, the composition of the HNC imposes limitations on the morphologies attainable. These constraints are particularly strict if the overgrowing material is intended to form a concentric shell around the seed NC, since this requires small lattice mismatches (section 3.1.3.III). However, there are strategies to circumvent or minimize compatibility issues. Some of these strategies will be discussed below.

III. Choosing the reaction parameters: precursors, surfactants, and temperature. A different synthesis technique must be adopted depending on the intended morphology and composition of the HNC. The CdSe–PbSe combination offers an insightful illustration of the constraints imposed by the desired HNC architecture on the synthesis methodology. The lattice mismatch between CdSe and PbSe is very small (*viz*., 1%), and alloying between the two materials is prevented due to a lattice-type mismatch (CdSe is WZ or ZB, while PbSe is rock-salt, RS). The difference in the coordination numbers of the atoms in the two types of crystal structure (4-fold in ZB or WZ, 6-fold in RS) precludes interdiffusion and makes it possible to obtain atomically flat CdSe-PbSe interfaces by heteroepitaxial growth. Consistently, CdSe/PbSe dumbbells can be obtained by seeded growth using CdSe nanorods as seeds.[61] However, concentric PbSe/CdSe core/shell QDs cannot be obtained by seeded heteroepitaxial growth, because the temperatures needed are too high for PbSe QDs. Nevertheless, concentric PbSe/CdSe core/shell QDs (Fig. 15d) can be easily obtained by cation exchange.[49] Once the PbSe/CdSe core/shell QD is obtained, other morphologies become attainable because then the outer surface consists of CdSe (*e.g*., PbSe/CdSe/CdS core/shell/shell and core/shell/tetrapod HNCs[271]).

As discussed above (sections 3.1.2 and 3.1.3), the heterogeneous nucleation rates and heteroepitaxial growth dynamics are determined by a number of reaction parameters: concentration and characteristics of the seeds, nature and concentration of precursors and surfactant species, and the growth temperature. These variables are strongly interdependent, and the optimum balance between them depends on the HNC's composition and architecture. To highlight the essential aspects to be considered when optimizing the reaction parameters, we will briefly discuss illustrative examples of CdSe based HNCs for different morphology categories.

Concentric core/shell QDs. The majority of the investigations on colloidal HNCs has focused on concentric nearly spherical core/shell QDs, leading to the development of synthetic strategies that allow a high degree of control over the heteroepitaxial shell growth, yielding highly luminescent and stable QDs.[30] High-quality shells can only be obtained by slow heteroepitaxial growth on the facets of highly crystalline nearly spherical seeds (Fig. 17a). The lattice mismatch between the shell and the seed must be small, especially if thick shells (>3 ML) are desired (section 3.1.3.III). Alternatively, the lattice mismatch can be gradually adapted by using gradient shells and a multishell strategy (*e.g*., CdSe/CdS/(Cd,Zn)S/ZnS core/multishell QDs[97]).

The growth temperature must be low enough to avoid alloying, inter-particle ripening, and homogeneous nucleation, but sufficiently high to allow the precursors to react, and heterointerfacial annealing and relaxation to occur. Too low temperatures may lead to island or anisotropic growth, or simply no growth at all. The surfactant system should be chosen such as not to bind too strongly or too selectively to the surface of the seed NC or to the overgrowing material at the growth temperature (see section 2.2.1). Long-chain amines (*e.g*., octadecylamine or oleylamine) diluted in a non-coordinating solvent (*e.g*., ODE) are particularly well suited, especially if Zn containing shells are used, since surfactants containing Oxygen as the donor atom bind too strongly to Zn (section 2.2.1). Further, low monomer fluxes should be used to prevent homogeneous nucleation and ensure that heteroepitaxial growth prevails.

The monomer flux is determined by the precursor reactivity and addition rate, so that high reactivity precursors must be added at slower rates and at lower temperatures. For example, high-quality colloidal CdSe/CdS core/shell QDs (shell thickness ≤ 3 ML) can be prepared by slow addition of high reactivity precursors (*viz*., bis(trimethylsilyl)sulfide, $(TMS)_2S$, and $Cd(CH_3)_2$) to a solution of TOPO capped CdSe NCs in pyridine at 100 °C.[272] In contrast, the use of low reactivity precursors (*e.g*., $Cd(OA)_2$ and elemental sulfur in ODE) allows faster addition rates, provided that the cationic and anionic precursors are added in alternate and separate injections. This gave rise to the so-called SILAR (successive ion layer adsorption and reaction) technique,[98] which is based on alternate injections of low reactivity cationic and anionic precursors in sufficient amounts to produce one ML at a time. Due to the low precursor reactivity a higher growth temperature is needed (*viz*., 240 °C). Moreover, a sufficiently long growth time between subsequent additions is essential to avoid homogeneous nucleation due to high concentrations of unconsumed monomers.[98]

The use of less reactive precursors increases the flexibility of the synthesis protocols, since there are many different precursors currently available. The reactivity of metal carboxylate salts (*e.g*., $Cd(OA)_2$ or $Cd(Ac)_2$)[98,273] increases with decreasing chain length, allowing the use of lower growth temperatures for shorter chain salts. For example, $Cd(OA)_2$ does not react below 200 °C,[98] while $Cd(Ac)_2$ is highly reactive already at 150 °C.[50,107] The choice of chalcogenide precursors is more limited, being restricted to phosphine complexes (*e.g*., TOP-E or TBP-E; E = S, Se, Te)[207] or elemental Se and S dissolved in ODE.[274] Further, a variety of single-source precursors for II–VI, III–V and IV–VI semiconductor materials is available (*e.g*., zinc diethyldithiocarbamate, and other thiolato and thiocarbamato metal complexes),[275] but have only recently been used in the synthesis of colloidal HNCs.[107,264]

Another advantage of less reactive precursors is that their reactivity may be modulated by surfactants (see sections 3.1.2 and 3.1.3). This has been recently exploited to sequentially grow 11 ML CdS, 6 ML gradient (Cd,Zn)S and 2 ML ZnS over a 3 nm CdSe core, yielding very stable and robust nearly spherical QDs.[276] The large increase in volume during the growth implies the addition of increasingly larger amounts of precursors. In conjunction with the fact that the growth rate of colloidal NCs decreases with increasing size, this may lead to accumulation of unconsumed monomers during the growth of thick shells, if the monomer addition rates exceed the growth rates. Under such conditions homogeneous nucleation is facilitated and will effectively compete with the HNCs for the monomers. To prevent monomer accumulation, the reactivity of the metal-oleate complexes was decreased by utilizing a secondary amine (dioctylamine) instead of a primary amine as surfactant, while increasing the growth time allowed for each ML (3 h for cation precursors, 1 h for S precursor, at 240 °C).[276] Surfactant molecules may also lead to structural changes. For example, primary alkylamines seem to induce a structural transformation of CdSe seeds from ZB into WZ, thereby precluding the overgrowth of CdS ZB shells.[277] In contrast, CdSe/CdS ZB core/shell QDs are readily obtained from CdSe ZB seeds by using trioctylamine as surfactant.[277]

An alternative strategy to prevent monomer accumulation during the growth of thick shells is to increase the growth rates by increasing the reaction temperature. This implies the use of higher growth T's for larger HNCs.[84,109,278] This approach, however, may also have undesired effects, since higher temperatures increase not only the reactivity of the growing NCs, but also the mobility of surface atoms, the NC solubility, and the monomer formation rates. Therefore, higher growth T's may also enhance inter-NC ripening, interfacial alloying, and homogeneous nucleation.

CdSe/ZnS/ZnSe/CdSe core/multishell colloidal QDs provide an elegant illustration of the thoughtful design of a colloidal HNC for a specific goal.[84] The composition and dimensions of each component of this colloidal HNC were judiciously chosen in order to slow down the intraband cooling of hot electrons. Due to the requirement that the S-exciton peak be at 550–555 nm, 2.8 nm diameter CdSe NCs were used as seeds. A thin (1 ML) ZnS shell was then added to improve the stability of the cores at the high T's (*viz*., 280 °C) needed to grow thick shells, while still allowing hole tunnelling out of the core. Subsequently, 9 ML of ZnSe were grown as a hole extracting shell. A final 1 ML CdSe shell was used to passivate surface electron traps. Finally, the inorganic HNC was coated with dodecanethiol, chosen for its effectiveness as hole trapping agent, while lacking vibrational transitions in resonance with the $1S_e$-$1P_e$ intraband transition of the CdSe core.

Heterodimers. In case the overgrowing material does not wet the seed, growth may occur only on a precisely defined facet, so that the lattice mismatch is minimized (Fig. 17a). This mechanism is involved in the growth of Au NCs on CdSe seeds (lattice mismatch: ~50%),[54] yielding CdSe/Au heterodimers. The reverse process (*i.e*., heterogeneous nucleation of CdSe NCs on seeds) has also been observed, leading to the formation of CdSe@Fe_2O_3 heterodimers[53] and CdSe@$NaYF_4$:Yb,Er heteronanostructures (Fig. 15h).[229] Alternatively, the material can initially grow as an amorphous shell, thereby circumventing the lattice mismatch problem. Subsequent annealing induces crystallization of the shell, accompanied by a de-wetting and retraction process which leads to the formation of a heterodimer. This latter mechanism is responsible for the formation of CdSe@FePt heterodimers,[55] in which the first step consists of growth of an amorphous CdSe shell over FePt NCs.

Core/shell nanorods. Shell growth on a nanorod is carried out under conditions similar to those used to grow concentric shells over a nearly spherical NC seed. However, shell growth on nanorods or heteronanorods of II–VI semiconductor materials (*e.g*., CdSe, CdSe/CdS, *etc*.) occurs primarily in the length direction due to the higher reactivity of the polar facets.[279,280]

Heteronanorods, heterotetrapods, and nanodumbbells. Nearly spherical CdSe NCs can also be employed as seeds for the heteroepitaxial growth of anisotropic HNCs (Fig. 17a), such as dot core/rod shell CdSe/CdS nanorods[57] (Fig. 15a) and CdSe/CdS heterotetrapods[57,58] (Fig. 15b). The essential difference with respect to growing concentric core/shell QDs is the use of growth conditions that promote anisotropic growth:[57,58] high monomer concentration, high growth T's (315–350 °C) and surfactants that selectively bind to the non-polar facets of II–VI WZ semiconductors (*viz*., mixture of short and long chain phosphonic acids, such as propylphosphonic acid and ODPA or hexylphosphonic acid and TDPA). Under such conditions, the morphology of the HNC is dictated by the crystal structure and shape of the seed (WZ yields rods,[57,58] while ZB leads to tetrapods[57,234] or octapods,[234] for tetrahedral or cuboctahedral seed NCs, respectively). Growth of CdS rod shells on WZ CdSe seeds has also been observed at low T's (*viz*., 120–130 °C), using highly reactive precursors ($Cd(CH_3)_2$ and $(TMS)_2S$) and TOPO, TOP and HDA as surfactants.[281] In this case anisotropic growth took place only when an excess of the S precursor was used (Cd : S = 1.5).[281]

The use of CdSe nanorods as seeds (Fig. 17b) yields nanomatchsticks, nanodumbbells, heteronanorods, or heterotetrapods, depending on the growth conditions. Heterorods and heterotetrapods form under conditions that promote anisotropic growth, with branched heterojunctions dominating at very high precursor concentrations (*e.g*., CdSe/CdTe heteronanorods and heterotetrapods).[65,282] Due to the different reactivities of the anion-terminated and cation-terminated polar facets linear heteroepitaxial growth may occur on one tip of the nanorod while branching takes place at the other.[65] In contrast, conditions that favour isotropic growth (*viz*., low monomer concentrations and lower T's) will lead to nucleation and growth of nearly spherical NCs at both tips of the rods, yielding dumbbells (*e.g*., CdSe–CdTe, Fig. 15c,[60,282] CdSe–PbSe,[61] and CdSe–Au[140]). Under special conditions (*viz*., low *T* and fast injection of low concentration of precursors) some materials may selectively grow on only one tip of the nanorod, yielding nanomatchsticks (*e.g*., CdSe–PbSe,[61] and CdSe–Au[29,140]). Heteroepitaxial growth on CdSe tetrapod seeds (Fig. 17c) may occur either by linear extension of each arm or by branching at the tips of the arms, depending on the

precursor concentration (*e.g.*, CdSe/CdTe tetrapods[65]). Growth of spherical NCs at the tips of the arms has been reported only for Au on CdTe tetrapods.[26]

IV. Controlling the dimensions of the overgrowing segment. The dimensions of the HNCs can be controlled by the total amount of precursors added in relation to the concentration of seeds, the growth T and the reaction time. In this context, the knowledge of the size and shape of the NCs used as seeds and of their concentration in the reaction medium is essential. The concentration of seeds can be easily determined by absorption spectroscopy, provided the molar absorption coefficients of the NCs are known. It is common practice to use the band edge absorption coefficient for this purpose.[30] However, this may lead to potentially large errors in the concentrations determined, especially if peak intensities and wavelength scales are used, because the band edge absorption coefficient is strongly size and shape dependent, and therefore inherently sensitive to the size dispersion of the NC ensemble.[96] In contrast, the absorption coefficient at energies far above the band edge scales linearly with the NC volume, both for nearly spherical NCs[96] and for nanorods,[283] making it a more reliable parameter, irrespective of size and shape dispersion. Further, the absorption cross section at high energies can be directly determined from the bulk optical constants.[96] Therefore, the use of the molar absorption coefficient at energies far above the band gap is strongly recommended,[96] in order to minimize the inaccuracies in the concentration of seeds. These inaccuracies may have deleterious consequences for the HNC growth, particularly when the SILAR methodology is used, since small initial errors are propagated and amplified in the course of the reaction, eventually leading to a significant excess of unconsumed monomers, which may trigger undesired processes such as homogeneous nucleation or island growth.

4. Outlook

The past decades have witnessed remarkable progress in the colloidal synthesis of shape-controlled NCs and HNCs. Several principles have emerged from these studies, which provide useful guidelines for the design of novel HNCs. The field is now moving towards more sophisticated nanostructures where size, shape, composition and connectivity of multiple segments of a HNC must be tailored in an independent and controllable way. However, there are still a number of challenges that must be addressed before the targeted synthesis of complex multicomponent colloidal HNCs reaches its full potential.

The most critical of these challenges is the development of a coherent theoretical framework that allows the rational design and fabrication of colloidal HNCs. As discussed in this review, the understanding of a number of fundamental issues is still quite fragmentary, despite the large body of accumulated knowledge. Therefore, future progress in the field will require further research on a variety of topics. First, the dynamics of the NC surface and of the organic–inorganic interface must be better understood and controlled. Second, the reaction mechanisms for the formation of colloidal NCs and HNCs are largely unknown, and should be investigated in more detail. Further, the elucidation of the nucleation and growth mechanisms remains a critical challenge, which only recently became addressable. Moreover, the role of strain and alloying on nanoheterojunctions and the correlation between atomic scale structure and the properties of HNCs are crucial issues that merit a systematic and comprehensive investigation. Future work will certainly shed more light on these issues, paving the way to a myriad of novel colloidal HNCs that will in turn give rise to new phenomena and open up many application possibilities.

References

1 A. P. Alivisatos, *J. Phys. Chem.*, 1996, **100**, 13226.
2 E. Roduner, *Chem. Soc. Rev.*, 2006, **35**, 583.
3 P. Schapotschnikow, B. Hommerson and T. J. H. Vlugt, *J. Phys. Chem. C*, 2009, **113**, 12690.
4 Z. Nie, A. Petukhova and E. Kumacheva, *Nat. Nanotechnol.*, 2010, **5**, 15.
5 D. V. Talapin, J. Lee, M. V. Kovalenko and E. V. Shevchenko, *Chem. Rev.*, 2010, **110**, 389.
6 R. C. Somers, M. G. Bawendi and D. G. Nocera, *Chem. Soc. Rev.*, 2007, **36**, 579.
7 A. L. Rogach, T. A. Klar, J. M. Lupton, A. Meijerink and J. Feldmann, *J. Mater. Chem.*, 2009, **19**, 1208.
8 N. A. Frey, S. Peng, K. Cheng and S. Sun, *Chem. Soc. Rev.*, 2009, **38**, 2532.
9 I. L. Medintz, H. Mattoussi and A. R. Clapp, *Int. J. Nanomedicine*, 2008, **3**, 151.
10 X. Michalet, F. F. Pinaud, L. A. Bentolila, J. M. Tsay, S. Doose, J. J. Li, G. Sundaresan, A. M. Wu, S. S. Gambhir and S. Weiss, *Science*, 2005, **307**, 538.
11 X. Peng, J. Chen, J. A. Misewich and S. S. Wong, *Chem. Soc. Rev.*, 2009, **38**, 1076.
12 E. Holder, N. Tessler and A. L. Rogach, *J. Mater. Chem.*, 2008, **18**, 1064.
13 V. Wood, M. J. Panzer, J. Caruge, J. E. Halpert, M. G. Bawendi and V. Bulovic, *Nano Lett.*, 2010, **10**, 24.
14 P. V. Kamat, *J. Phys. Chem. C*, 2008, **112**, 18737.
15 W. G. J. H. M. van Sark, K. W. J. Barnham, L. H. Slooff, A. J. Chatten, A. Büchtemann, A. Meyer, S. J. McCormack, R. Koole, D. J. Farrell, R. Bose, E. E. Bende, A. R. Burgers, T. Budel, J. Quilitz, M. Kennedy, T. Meyer, C. de Mello Donegá, A. Meijerink and D. Vanmaekelbergh, *Opt. Express*, 2008, **16**, 21773.
16 H. Goesmann and C. Feldmann, *Angew. Chem. Int. Ed.*, 2010, **49**, 1362.
17 H. W. Hillhouse and M. C. Beard, *Curr. Opin. Colloid Interface Sci.*, 2009, **14**, 245.
18 G. Konstantatos and E. H. Sargent, *Nat. Nanotechnol.*, 2010, **5**, 391.
19 C. de Mello Donegá, P. Liljeroth and D. Vanmaekelbergh, *Small*, 2005, **1**, 1152.
20 C. Burda, X. Chen, R. Narayanan and M. A. El-Sayed, *Chem. Rev.*, 2005, **105**, 1025.
21 A. R. Tao, S. Habas and P. Yang, *Small*, 2008, **4**, 310.
22 Y. Yin and A. P. Alivisatos, *Nature*, 2005, **437**, 664.
23 S. Kumar and T. Nann, *Small*, 2006, **2**, 316.
24 Y. Jun, J. Choi and J. Cheon, *Angew. Chem., Int. Ed.*, 2006, **45**, 3414.
25 M. Casavola, R. Buonsanti, G. Caputo and P. D. Cozzoli, *Eur. J. Inorg. Chem.*, 2008, 837.
26 P. D. Cozzoli, T. Pellegrino and L. Manna, *Chem. Soc. Rev.*, 2006, **35**, 1195.
27 L. Manna and S. Kudera, in *Advanced Wet-Chemical Synthetic Approaches to Inorganic Nanostructures*, ed. P. D. Cozzoli, Transworld Research Network, Kerala, 2008, ch. 1, pp. 1–53.
28 G. Caputo, R. Buonsanti, M. Casavola and P. D. Cozzoli, in *Advanced Wet-Chemical Synthetic Approaches to Inorganic Nanostructures*, ed. P. D. Cozzoli, Transworld Research Network, Kerala, 2008, ch. 14, pp. 407–453.

29 R. Costi, A. E. Saunders and U. Banin, *Angew. Chem., Int. Ed.*, 2010, **49**, 4878.
30 P. Reiss, M. Protière and L. Li, *Small*, 2009, **5**, 154.
31 J. Park, J. Joo, S. G. Kwon, Y. Jang and T. Hyeon, *Angew. Chem., Int. Ed.*, 2007, **46**, 4630.
32 *Semiconductor Nanocrystal Quantum Dots: Synthesis, Assembly, Spectroscopy and Applications*, ed. A. L. Rogach, Springer Verlag, New York, 2008.
33 *Semiconductor nanomaterials*, in *Nanomaterials for the Life Sciences*, ed. C. Kumar, Wiley-VCH, Weinheim, vol. 6, 2010.
34 G. D. Scholes, *Adv. Funct. Mater.*, 2008, **18**, 1157.
35 S. J. Rosenthal, J. McBride, S. J. Pennycook and L. C. Feldman, *Surf. Sci. Rep.*, 2007, **62**, 111.
36 C. Carrillo-Carrión, S. Cárdenas, B. M. Simonet and M. Valcárcel, *Chem. Commun.*, 2009, 5214.
37 Y. Xia, Y. Xiong, B. Lim and S. E. Skrabalak, *Angew. Chem., Int. Ed.*, 2009, **48**, 60.
38 Q. Zhuang, S.-J. Liu and S.-H. Yu, *J. Mater. Chem.*, 2009, **19**, 191.
39 R. Klajn, J. F. Stoddart and B. A. Grzybowski, *Chem. Soc. Rev.*, 2010, **39**, 2203.
40 C. L. Choi and A. P. Alivisatos, *Annu. Rev. Phys. Chem.*, 2010, **61**, 369.
41 J. A. Dahl, B. L. S. Maddux and J. E. Hutchison, *Chem. Rev.*, 2007, **107**, 2228.
42 V. I. Klimov, *Annu. Rev. Phys. Chem.*, 2007, **58**, 635.
43 Z. Tang and N. A. Kotov, *Adv. Mater.*, 2005, **17**, 951.
44 D. Vanmaekelbergh and P. Liljeroth, *Chem. Soc. Rev.*, 2005, **34**, 299.
45 U. Banin and O. Millo, *Annu. Rev. Phys. Chem.*, 2003, **54**, 465.
46 E. Lifshitz, L. Fradkin, A. Glozman and L. Langof, *Annu. Rev. Phys. Chem.*, 2004, **55**, 509.
47 M. Kuno, *Phys. Chem. Chem. Phys.*, 2008, **10**, 620.
48 H. Kim, M. Achermann, L. P. Balet, J. A. Hollingsworth and V. I. Klimov, *J. Am. Chem. Soc.*, 2005, **127**, 544.
49 J. M. Pietryga, D. J. Werder, D. J. Williams, J. L. Casson, R. D. Schaller, V. I. Klimov and J. A. Hollingsworth, *J. Am. Chem. Soc.*, 2008, **130**, 4879.
50 P. T. K. Chin, C. de Mello Donegá, S. S. van Bavel, S. C. J. Meskers, N. A. J. M. Sommerdijk and R. A. J. Janssen, *J. Am. Chem. Soc.*, 2007, **129**, 14880.
51 W. Shi, H. Zeng, Y. Sahoo, T. Y. Ohulchanskyy, Y. Ding, Z. L. Wang, M. Swihart and P. N. Prasad, *Nano Lett.*, 2006, **6**, 875.
52 H. Yu, M. Chen, P. M. Rice, S. X. Wang, R. L. White and S. Sun, *Nano Lett.*, 2005, **5**, 379.
53 S. T. Selvan, P. K. Patra, C. Y. Ang and J. Y. Ying, *Angew. Chem., Int. Ed.*, 2007, **46**, 2448.
54 J. Zeng, J. Huang, C. Liu, C. Hao Wu, Y. Lin, X. Wang, S. Zhang, J. Hou and Y. Xia, *Adv. Mater.*, 2010, **22**, 1936.
55 M. Zanella, A. Falqui, S. Kudera, L. Manna, M. F. Casula and W. J. Parak, *J. Mater. Chem.*, 2008, **18**, 4311.
56 Kwan-Wook Kwon and Moonsub Shim, *J. Am. Chem. Soc.*, 2005, **127**, 10269.
57 D. V. Talapin, J. H. Nelson, E. V. Shevchenko, S. Aloni, B. Sadtler and A. P. Alivisatos, *Nano Lett.*, 2007, **7**, 2951.
58 L. Carbone, C. Nobile, M. De Giorgi, F. D. Sala, G. Morello, P. Pompa, M. Hytch, E. Snoeck, A. Fiore, I. R. Franchini, M. Nadasan, A. F. Silvestre, L. Chiodo, S. Kudera, R. Cingolani, R. Krahne and L. Manna, *Nano Lett.*, 2007, **7**, 2942.
59 D. Steiner, D. Dorfs, U. Banin, F. D. Sala, L. Manna and O. Millo, *Nano Lett.*, 2008, **8**, 2954.
60 J. E. Halpert, V. J. Porter, J. P. Zimmer and M. G. Bawendi, *J. Am. Chem. Soc.*, 2006, **128**, 12590.
61 S. Kudera, L. Carbone, M. F. Casula, R. Cingolani, A. Falqui, E. Snoeck, W. J. Parak and L. Manna, *Nano Lett.*, 2005, **5**, 445.
62 T. Mokari, E. Rothenberg, I. Popov, R. Costi and U. Banin, *Science*, 2004, **304**, 1787.
63 M. Casavola, V. Grillo, E. Carlino, C. Giannini, F. Gozzo, E. F. Pinel, M. A. Garcia, L. Manna, R. Cingolani and P. D. Cozzoli, *Nano Lett.*, 2007, **7**, 1386.
64 R. D. Robinson, B. Sadtler, D. O. Demchenko, C. K. Erdonmez, L. Wang and A. P. Alivisatos, *Science*, 2007, **317**, 355.
65 D. J. Milliron, S. M. Hughes, Y. Cui, L. Manna, J. Li, L. Wang and A. P. Alivisatos, *Nature*, 2004, **430**, 190.
66 B. Koo and B. A. Korgel, *Nano Lett.*, 2008, **8**, 2490.
67 R. Koole, M. M. van Schooneveld, J. Hilhorst, C. de Mello Donegá, D. C. 't Hart, A. van Blaaderen, D. Vanmaekelbergh and A. Meijerink, *Chem. Mater.*, 2008, **20**, 2503.
68 J. Lee, M. I. Bodnarchuk, E. V. Shevchenko and D. V. Talapin, *J. Am. Chem. Soc.*, 2010, **132**, 6382.
69 M. Casavola, A. Falqui, M. A. Garcia, M. García-Hernández, C. Giannini, R. Cingolani and P. D. Cozzoli, *Nano Lett.*, 2009, **9**, 366.
70 E. Zych, A. Meijerink and C. de Mello Donegá, *J. Phys.: Condens. Matter*, 2003, **15**, 5145.
71 D. J. Norris, A. L. Efros and S. C. Erwin, *Science*, 2008, **319**, 1776.
72 D. Chen, R. Viswanatha, G. L. Ong, R. Xie, M. Balasubramaninan and X. Peng, *J. Am. Chem. Soc.*, 2009, **131**, 9333.
73 C. Dong and F. C. J. M. Van Veggel, *ACS Nano*, 2009, **3**, 123.
74 R. Kumar, M. Nyk, T. Y. Ohulchansky, C. A. Flask and P. N. Prasad, *Adv. Funct. Mater.*, 2009, **19**, 853.
75 S. B. Orlinskii, J. Schmidt, E. J. J. Groenen, P. G. Baranov, C. de Mello Donegá and A. Meijerink, *Phys. Rev. Lett.*, 2005, **94**, 097602.
76 R. Beaulac, L. Schneider, P. I. Archer, G. Bacher and D. R. Gamelin, *Science*, 2009, **325**, 973.
77 R. Beaulac, P. A. Archer, J. van Rijssel, A. Meijerink and D. R. Gamelin, *Nano Lett.*, 2008, **8**, 2949.
78 S. T. Ochsenbein, Y. Feng, K. M. Whitaker, E. Badaeva, W. K. Liu, X. Li and D. R. Gamelin, *Nat. Nanotechnol.*, 2009, **4**, 681.
79 V. A. Vlaskin, R. Beaulac and D. R. Gamelin, *Nano Lett.*, 2009, **9**, 4376.
80 D. A. Bussian, S. A. Crooker, M. Yin, M. Brynda, A. L. Efros and V. I. Klimov, *Nat. Mater.*, 2009, **8**, 35.
81 U. E. H. Laheld, F. B. Pedersen and P. C. Hemmer, *Phys. Rev. B*, 1995, **52**, 2697.
82 S. A. Ivanov, A. Piryatinski, J. Nanda, S. Tretiak, K. R. Zavadil, W. O. Wallace, D. Werder and V. I. Klimov, *J. Am. Chem. Soc.*, 2007, **129**, 11708.
83 C. de Mello Donegá, *Phys. Rev. B*, 2010, **81**, 165303.
84 A. Pandey and P. Guyot-Sionnest, *Science*, 2008, **322**, 929.
85 H. Zhong and G. D. Scholes, *J. Am. Chem. Soc.*, 2009, **131**, 9170.
86 F. Garcia-Santamaria, Y. Chen, J. Vela, R. D. Schaller, J. A. Hollingsworth and V. I. Klimov, *Nano Lett.*, 2009, **9**, 3482.
87 A. G. Winbow, A. T. Hammack, L. V. Butov and A. C. Gossard, *Nano Lett.*, 2007, **7**, 1349.
88 V. I. Klimov, S. A. Ivanov, J. Nanda, M. Achermann, I. Bezel, J. A. McGuire and A. Piryatinski, *Nature*, 2007, **447**, 441.
89 Y. Zhang, L. W. Wang and A. Mascarenhas, *Nano Lett.*, 2007, **7**, 1264.
90 J. M. Klostranec, Q. Xiang, G. A. Farcas, J. A. Lee, A. Rhee, E. I. Lafferty, S. D. Perrault, K. C. Kain and W. C. W. Chan, *Nano Lett.*, 2007, **7**, 2812.
91 X. Wang, X. Ren, K. Kahen, M. A. Hahn, M. Rajeswaran, S. Maccagnano-Zacher, J. Silcox, G. E. Cragg, A. L. Efros and T. D. Krauss, *Nature*, 2009, **459**, 686.
92 C. de Mello Donegá, M. Bode and A. Meijerink, *Phys. Rev. B*, 2006, **74**, 085320.
93 A. Narayanaswamy, L. F. Feiner, A. Meijerink and P. J. van der Zaag, *ACS Nano*, 2009, **3**, 2539.
94 J. S. Steckel, J. P. Zimmer, S. Coe-Sullivan, N. E. Stott, V. Bulovic and M. G. Bawendi, *Angew. Chem., Int. Ed.*, 2004, **43**, 2154.
95 A. Pandey and P. Guyot-Sionnest, *J. Chem. Phys.*, 2007, **127**, 104710.
96 C. de Mello Donegá and R. Koole, *J. Phys. Chem. C*, 2009, **113**, 6511.
97 R. Xie, U. Kolb, J. Li, T. Basché and A. Mews, *J. Am. Chem. Soc.*, 2005, **127**, 7480.
98 J. J. Li, Y. A. Wang, W. Guo, J. C. Keay, T. D. Mishima, M. B. Johnson and X. Peng, *J. Am. Chem. Soc.*, 2003, **125**, 12567.
99 D. V. Talapin, A. L. Rogach, A. Kornowski, M. Haase and H. Weller, *Nano Lett.*, 2001, **1**, 207.
100 J. Bleuse, S. Carayon and P. Reiss, *Phys. E.*, 2004, **21**, 331.

101 J. Müller, J. M. Lupton, P. G. Lagoudakis, F. Schindler, R. Koeppe, A. L. Rogach, J. Feldmann, D. V. Talapin and H. Weller, *Nano Lett.*, 2005, **5**, 2044.
102 I. Swart, Z. Sun, D. Vanmaekelbergh and P. Liljeroth, *Nano Lett.*, 2010, **10**, 1931.
103 D. Oron, M. Kazes and U. Banin, *Phys. Rev. B*, 2007, **75**, 035330.
104 J. He, S. S. Lo, J. Kim and G. D. Scholes, *Nano Lett.*, 2008, **8**, 4007.
105 N. N. Hewa-Kasakarage, P. Z. El-Khoury, A. N. Tarnovsky, M. Kirsanova, I. Nemitz, A. Nemchinov and M. Zamkov, *ACS Nano*, 2010, **4**, 1837.
106 A. Fiore, R. Mastria, M. G. Lupo, G. Lanzani, C. Giannini, E. Carlino, G. Morello, M. de Giorgi, Y. Li, R. Cingolani and L. Manna, *J. Am. Chem. Soc.*, 2009, **131**, 2274.
107 W. Zhang, G. Chen, J. Wang, B. Ye and X. Zhong, *Inorg. Chem.*, 2009, **48**, 9723.
108 M. Jones, S. Kumar, S. S. Lo and G. D. Scholes, *J. Phys. Chem. C*, 2008, **112**, 5423.
109 S. Kim, B. Fisher, H. Eisler and M. Bawendi, *J. Am. Chem. Soc.*, 2003, **125**, 11466.
110 R. Xie, U. Kolb and T. Basché, *Small*, 2006, **2**, 1454.
111 J. Bang, J. Park, J. H. Lee, N. Won, J. Nam, J. Lim, B. Y. Chang, H. J. Lee, B. Chon, J. Shin, J. B. Park, J. H. Choi, K. Cho, S. M. Park, T. Joo and S. Kim, *Chem. Mater.*, 2010, **22**, 233.
112 N. N. Hewa-Kasakarage, M. Kirsanova, A. Nemchinov, N. Schmall, P. Z. El-Khoury, A. N. Tarnovsky and M. Zamkov, *J. Am. Chem. Soc.*, 2009, **131**, 1328.
113 R. E. Bailey and S. Nie, *J. Am. Chem. Soc.*, 2003, **125**, 7100.
114 X. Zhong, M. Han, Z. Dong, T. J. White and W. Knoll, *J. Am. Chem. Soc.*, 2003, **125**, 8589.
115 D. V. Petrov, B. S. Santos, G. A. L. Pereira and C. de Mello Donegá, *J. Phys. Chem. B*, 2002, **106**, 5325.
116 W. K. Bae, K. Char, H. Hur and S. Lee, *Chem. Mater.*, 2008, **20**, 531.
117 N. Al-Salim, A. G. Young, R. D. Tilley, A. J. McQuillan and J. Xia, *Chem. Mater.*, 2007, **19**, 5185.
118 P. Viste, J. Plain, R. Jaffiol, A. Vial, P. M. Adam and P. Royer, *ACS Nano*, 2010, **4**, 759.
119 P. Pompa, L. Martiradonna, A. Della Torre, F. Della Sala, L. Manna, M. De Vittorio, F. Calabi, R. Cingolani and R. Rinaldi, *Nat. Nanotechnol.*, 2006, **1**, 126.
120 E. Shaviv and U. Banin, *ACS Nano*, 2010, **4**, 1529.
121 E. Elmalen, A. E. Saunders, R. Costi, A. Salant and U. Banin, *Adv. Mater.*, 2008, **20**, 4312.
122 L. Amirav and A. P. Alivisatos, *J. Phys. Chem. Lett.*, 2010, **1**, 1051.
123 R. Koole, B. Luigjes, M. Tachiya, R. Pool, T. J. H. Vlugt, C. de Mello Donegá, A. Meijerink and D. Vanmaekelbergh, *J. Phys. Chem. C*, 2007, **111**, 11208.
124 B. A. Kairdolf, A. M. Smith and S. Nie, *J. Am. Chem. Soc.*, 2008, **130**, 12866.
125 M. V. Kovalenko, M. Scheele and D. V. Talapin, *Science*, 2009, **324**, 1417.
126 D. F. Shriver, P. W. Atkins, T. L. Overton, J. P. Rourke, M. T. Weller and F. A. Armstrong, *Inorganic Chemistry*, Oxford University Press, Oxford, 4th edn, 2006.
127 L. G. Wade, Jr., *Organic Chemistry*, Pearson Prentice Hall, New Jersey, 5th edn, 2003.
128 A. Dubavik, V. Lesnyak, W. Thiessen, N. Gaponik, T. Wolff and A. Eychmüller, *J. Phys. Chem. C*, 2009, **113**, 4748.
129 S. F. Wuister, I. Swart, F. van Driel, S. G. Hickey and C. de Mello Donegá, *Nano Lett.*, 2003, **3**, 503.
130 R. Koole, P. Schapotschnikow, C. de Mello Donegá, T. J. H. Vlugt and A. Meijerink, *ACS Nano*, 2008, **2**, 1703.
131 S. F. Wuister, A. van Houselt, C. de Mello Donegá, D. Vanmaekelbergh and A. Meijerink, *Angew. Chem., Int. Ed.*, 2004, **43**, 3029.
132 B. Fritzinger, I. Moreels, P. Lommens, R. Koole, Z. Hens and J. C. Martins, *J. Am. Chem. Soc.*, 2009, **131**, 3024.
133 A. Hassinen, I. Moreels, C. de Mello Donegá, J. C. Martins and Z. Hens, *J. Phys. Chem. Lett.*, 2010, **1**, 2577.
134 N. Pradhan, D. Reifsnyder, R. Xie, J. Aldana and X. Peng, *J. Am. Chem. Soc.*, 2007, **129**, 9500.
135 R. L. Donkers, Y. Song and R. W. Murray, *Langmuir*, 2004, **20**, 4703.
136 G. A. Devries, M. Brunnbauer, Y. Hu, A. M. Jackson, B. Long, B. T. Neltner, O. Uzun, B. H. Wunsch and F. Stellaci, *Science*, 2007, **315**, 358.
137 D. K. Schwartz, *Annu. Rev. Phys. Chem.*, 2001, **52**, 107.
138 A. M. Jackson, Y. Hu, P. J. Silva and F. Stellacci, *J. Am. Chem. Soc.*, 2006, **128**, 11135.
139 S. F. Wuister, C. de Mello Donegá and A. Meijerink, *J. Am. Chem. Soc.*, 2004, **126**, 10397.
140 G. Menagen, J. E. Macdonald, Y. Shemesh, I. Popov and U. Banin, *J. Am. Chem. Soc.*, 2009, **131**, 17406.
141 W. J. M. Mulder, R. Koole, R. J. Brandwijk, G. Storm, P. Chin, G. J. Strijkers, C. de Mello Donegá, K. Nicolay and A. W. Griffioen, *Nano Lett.*, 2006, **6**, 1.
142 R. Koole, M. M. van Schooneveld, J. Hilhorst, K. Castermans, D. P. Cormode, G. J. Strijkers, C. de Mello Donegá, D. Vanmaekelbergh, A. W. Griffioen, K. Nicolay, Z. A. Fayad, A. Meijerink and W. J. M. Mulder, *Bioconjugate Chem.*, 2008, **19**, 2471.
143 C. de Mello Donegá, S. G. Hickey, S. F. Wuister, D. Vanmaekelbergh and A. Meijerink, *J. Phys. Chem. B*, 2003, **107**, 489.
144 C. Bullen and P. Mulvaney, *Langmuir*, 2006, **22**, 3007.
145 A. M. Munro, I. J. Plante, M. S. Ng and D. S. Ginger, *J. Phys. Chem. C*, 2007, **111**, 6220.
146 G. Kalyuzhny and R. W. Murray, *J. Phys. Chem. B*, 2005, **109**, 7012.
147 F. Seker, K. Meeker, T. F. Kuech and A. B. Ellis, *Chem. Rev.*, 2000, **100**, 2505.
148 A. Kahn, *Surf. Sci.*, 1994, **299/300**, 469.
149 W. J. Huang, R. Sun, J. Tao, L. D. Menard, R. G. Nuzzo and J. M. Zuo, *Nat. Mater.*, 2008, **7**, 308.
150 D. D. Lovingood, R. Achey, A. K. Paravastu and G. F. Strouse, *J. Am. Chem. Soc.*, 2010, **132**, 3344.
151 V. V. Matylitsky, L. Dworak, V. V. Breus, T. Basché and J. Wachtveitl, *J. Am. Chem. Soc.*, 2009, **131**, 2424.
152 S. F. Wuister, C. de Mello Donegá and A. Meijerink, *J. Phys. Chem. B*, 2004, **108**, 17393.
153 M. T. Frederick and E. A. Weiss, *ACS Nano*, 2010, **4**, 3195.
154 P. Guyot-Sionnest, B. Wehrenberg and D. Yu, *J. Chem. Phys.*, 2005, **123**, 074709.
155 I. Moreels, B. Fritzinger, J. C. Martins and Z. Hens, *J. Am. Chem. Soc.*, 2008, **130**, 15081.
156 J. Y. Rempel, B. L. Trout, M. G. Bawendi and K. F. Jensen, *J. Phys. Chem. B*, 2005, **109**, 19320.
157 L. Manna, L. W. Wang, R. Cingolani and A. P. Alivisatos, *J. Phys. Chem. B*, 2005, **109**, 6183.
158 C. Fang, M. A. Van Huis, D. Vanmaekelbergh and H. W. Zandbergen, *ACS Nano*, 2010, **4**, 211.
159 M. A. van Huis, N. P. Young, G. Pandraud, J. F. Creemer, D. Vanmaekelbergh, A. I. Kirkland and H. W. Zandbergen, *Adv. Mater.*, 2009, **21**, 4992.
160 J. McBride, J. Treadway, L. C. Feldman, S. J. Pennycook and S. J. Rosenthal, *Nano Lett.*, 2006, **6**, 1496.
161 A. G. Kanaras, C. Sonnichsen, H. Liu and A. P. Alivisatos, *Nano Lett.*, 2005, **5**, 2164.
162 Y. Khalavka and C. Sonnichsen, *Adv. Mater.*, 2008, **20**, 588.
163 W. H. Evers, H. Friedrich, L. Filion, M. Dijkstra and D. Vanmaekelbergh, *Angew. Chem. Int. Ed.*, 2009, **48**, 9655.
164 M. A. van Huis, L. T. Kunneman, K. Overgaag, Q. Xu, G. Pandraud, H. W. Zandbergen and D. Vanmaekelbergh, *Nano Lett.*, 2008, **8**, 3959.
165 B. Gilbert, F. Huang, Z. Lin, C. Goodell, H. Zhang and J. F. Banfield, *Nano Lett.*, 2006, **6**, 605.
166 H. Zhang, B. Gilbert, F. Huang and J. F. Banfield, *Nature*, 2003, **424**, 1025.
167 J. Rockenberger, L. Troger, A. L. Rogach, M. Tischer, M. Grundmann, A. Eychmüller and H. Weller, *J. Chem. Phys.*, 1998, **108**, 7807.
168 K. S. Hamad, R. Roth, J. Rockenberger, T. van Buuren and A. P. Alivisatos, *Phys. Rev. Lett.*, 1999, **83**, 3474.
169 C. McGinley, M. Riedler, T. Möller, H. Borchert, S. Haubold, M. Haase and H. Weller, *Phys. Rev. B*, 2002, **65**, 245308.
170 J. T. Kopping and T. E. Patten, *J. Am. Chem. Soc.*, 2008, **130**, 5689.
171 M. Jones and G. D. Scholes, *J. Mater. Chem.*, 2010, **20**, 3533.

172 S. F. Wuister, C. de Mello Donegá and A. Meijerink, *J. Chem. Phys.*, 2004, **121**, 4310.
173 S. F. Wuister, R. Koole, C. de Mello Donegá and A. Meijerink, *J. Phys. Chem. B*, 2005, **109**, 5504.
174 G. Jiang, A. S. Susha, A. A. Lutich, F. D. Stefani, J. Feldmann and A. L. Rogach, *ACS Nano*, 2009, **3**, 4127.
175 S. F. Wuister, C. de Mello Donegá and A. Meijerink, *Phys. Chem. Chem. Phys.*, 2004, **6**, 1633.
176 D. Oron, A. Aharoni, C. de Mello Donegá, J. van Rijssel, A. Meijerink and U. Banin, *Phys. Rev. Lett.*, 2009, **102**, 177402.
177 O. Labeau, P. Tamarat and B. Lounis, *Phys. Rev. Lett.*, 2003, **90**, 257404.
178 S. A. Crooker, T. Barrick, J. A. Hollingsworth and V. I. Klimov, *Appl. Phys. Lett.*, 2003, **82**, 2793.
179 M. Furis, J. A. Hollingsworth, V. Klimov and S. Crooker, *J. Phys. Chem. B*, 2005, **109**, 15332.
180 J. H. Blokland, V. I. Claessen, F. J. P. Wijnen, E. Groeneveld, C. de Mello Donegá, D. Vanmaekelbergh, A. Meijerink, J. C. Maan and P. C. M. Christianen, *Phys. Rev. B*, 2010, submitted.
181 F. J. P. Wijnen, J. H. Blokland, P. T. K. Chin, P. C. M. Christianen and J. C. Maan, *Phys. Rev. B*, 2008, **78**, 235318.
182 C. de Mello Donegá, A. A. Bol and A. Meijerink, *J. Lumin.*, 2002, **96**, 87.
183 W. G. J. H. M. Van Sark, P. L. T. M. Frederix, D. J. Van den Heuvel, H. C. Gerritsen, A. A. Bol, J. N. J. van Lingen, C. de Mello Donegá and A. Meijerink, *J. Phys. Chem. B*, 2001, **105**, 8281.
184 J. Zhao, G. Nair, B. R. Fisher and M. G. Bawendi, *Phys. Rev. Lett.*, 2010, **104**, 157403.
185 B. Mahler, P. Spinicelli, S. Buil, X. Quelin, J. P. Hermier and B. Dubertret, *Nat. Mater.*, 2008, **7**, 659.
186 R. Osovsky, D. Cheskis, V. Kloper, A. Sashchiuk, M. Kroner and E. Lifshitz, *Phys. Rev. Lett.*, 2009, **102**, 197401.
187 H. Wang, C. de Mello Donegá, A. Meijerink and M. Glasbeek, *J. Phys. Chem. B*, 2006, **110**, 733.
188 E. Hendry, M. Koeberg, F. Wang, H. Zhang, C. de Mello Donegá, D. Vanmaekelbergh and M. Bonn, *Phys. Rev. Lett.*, 2006, **96**, 057408.
189 G. Morello, F. Della Sala, L. Carbone, L. Manna, G. Maruccio, R. Cingolani and M. De Giorgi, *Phys. Rev. B*, 2008, **78**, 195313.
190 C. Mauser, E. Da Como, J. Baldauf, A. L. Rogach, J. Huang, D. V. Talapin and J. Feldmann, *Phys. Rev. B*, 2010, **82**, 081306.
191 J. L. Blackburn, D. C. Selmarten and A. J. Nozik, *J. Phys. Chem. B*, 2003, **107**, 14154.
192 J. J. H. Pijpers, R. Koole, W. H. Evers, A. J. Houtepen, S. Boehme, C. de Mello Donegá, D. Vanmaekelbergh and M. Bonn, *J. Phys. Chem. C*, 2010, in press.
193 C. Harris and P. V. Kamat, *ACS Nano*, 2010, **3**, 682.
194 G. Nair and M. G. Bawendi, *Phys. Rev. Lett.*, 2007, **76**, 081304.
195 J. J. H. Pijpers, R. Ulbricht, K. J. Tielrooij, A. Osherov, Y. Golan, C. Delerue, G. Allan and M. Bonn, *Nat. Phys.*, 2009, **5**, 811.
196 M. T. Trinh, A. J. Houtepen, J. M. Schins, T. Hanrath, J. Piris, W. Knulst, A. P. L. M. Goossens and L. D. A. Siebbeles, *Nano Lett.*, 2008, **8**, 1713.
197 C. Delerue, G. Allan, J. J. H. Pijpers and M. Bonn, *Phys. Rev. B*, 2010, **81**, 125306.
198 J. A. McGuire, M. Sykora, J. Joo, J. M. Pietryga and V. I. Klimov, *Nano Lett.*, 2010, **10**, 2049.
199 M. Califano, *ACS Nano*, 2009, **3**, 2706.
200 B. S. Santos, G. A. L. Pereira, D. V. Petrov and C. de Mello Donegá, *Opt. Commun.*, 2000, **178**, 187.
201 Y. Fu, S. Hellstrom and H. Agren, *J. Nonlinear Opt. Phys. Mater.*, 2009, **18**, 195.
202 S. B. Orlinskii, J. Schmidt, P. G. Baranov, D. M. Hofmann, C. de Mello Donegá and A. Meijerink, *Phys. Rev. Lett.*, 2004, **92**, 047603.
203 K. M. Whitaker, S. T. Ochsenbein, V. Z. Polinger and D. R. Gamelin, *J. Phys. Chem. C*, 2008, **112**, 14331.
204 S. B. Orlinskii, H. Blok, J. Schmidt, P. G. Baranov, C. de Mello Donegá and A. Meijerink, *Phys. Rev. B*, 2006, **74**, 045204.
205 E. E. Finney and R. G. Finke, *J. Colloid Interface Sci.*, 2008, **317**, 351.
206 M. A. Watzky, E. E. Finney and R. G. Finke, *J. Am. Chem. Soc.*, 2008, **130**, 11959.
207 H. Liu, J. S. Owen and A. P. Alivisatos, *J. Am. Chem. Soc.*, 2007, **129**, 305.
208 Z. Jiang and D. F. Kelley, *ACS Nano*, 2010, **4**, 1561.
209 J. van Embden and P. Mulvaney, *Langmuir*, 2005, **21**, 10226.
210 P. M. Allen, B. J. Walker and M. G. Bawendi, *Angew. Chem.*, 2010, **122**, 772.
211 J. S. Steckel, B. K. H. Yen, D. C. Oertel and M. G. Bawendi, *J. Am. Chem. Soc.*, 2006, **128**, 13032.
212 J. Y. Rempel, M. G. Bawendi and K. F. Jensen, *J. Am. Chem. Soc.*, 2009, **131**, 4479.
213 C. Bullen and P. Mulvaney, *Nano Lett.*, 2004, **4**, 2303.
214 S. G. Kwon, Y. Piao, J. Park, S. Angappane, Y. Jo, N. M. Hwang, J. G. Park and T. Hyeon, *J. Am. Chem. Soc.*, 2007, **129**, 12571.
215 W. W. Yu, Y. A. Wang and X. Peng, *Chem. Mater.*, 2003, **15**, 4300.
216 V. N. Soloviev, A. Eichhofer, D. Fenske and U. Banin, *J. Am. Chem. Soc.*, 2001, **123**, 2354.
217 Z. A. Peng and X. Peng, *J. Am. Chem. Soc.*, 2002, **124**, 3343.
218 S. Kudera, M. Zanella, C. Giannini, A. Rizzo, Y. Li, G. Gigli, R. Cingolani, G. Ciccarella, W. Spahl, W. J. Parak and L. Manna, *Adv. Mater.*, 2007, **19**, 548.
219 S. F. Wuister, F. van Driel and A. Meijerink, *Phys. Chem. Chem. Phys.*, 2003, **5**, 1253.
220 S. Kilina, S. Ivanov and S. Tretiak, *J. Am. Chem. Soc.*, 2009, **131**, 7717.
221 M. Li, J. Ouyang, C. I. Ratcliffe, L. Pietri, X. Wu, D. M. Leek, I. Moudrakovski, Q. Lin, B. Yang and K. Yu, *ACS Nano*, 2009, **3**, 3832.
222 J. van Embden, J. E. Sader, M. Davidson and P. Mulvaney, *J. Phys. Chem. C*, 2009, **113**, 16342.
223 T. Yao, Z. Sun, Y. Li, Z. Pan, H. Wei, Y. Xie, M. Nomura, Y. Niwa, W. Yan, Z. Wu, Y. Jiang, Q. Liu and S. Wei, *J. Am. Chem. Soc.*, 2010, **132**, 7696.
224 B. Abécassis, F. Testard, O. Spalla and P. Barboux, *Nano Lett.*, 2007, **7**, 1723.
225 H. Zheng, R. K. Smith, Y. Jun, C. Kisielowski, U. Dahmen and A. P. Alivisatos, *Science*, 2009, **324**, 1309.
226 P. D. Cozzoli, L. Manna, M. L. Curri, S. Kudera, C. Giannini, M. Striccoli and A. Agostiano, *Chem. Mater.*, 2005, **17**, 1296.
227 F. Wang, R. Tang, J. L.-F. Kao, S. D. Dingman and W. E. Buhro, *J. Am. Chem. Soc.*, 2009, **131**, 4983.
228 M. B. Mohamed, D. Tonti, A. Al-Salman, A. Chemseddine and M. Chergui, *J. Phys. Chem. B*, 2005, **109**, 10533.
229 C. Yan, A. Dadvand, F. Rosei and D. F. Perepichka, *J. Am. Chem. Soc.*, 2010, **132**, 8868.
230 L. Carbone, S. Kudera, E. Carlino, W. J. Parak, C. Giannini, R. Cingolani and L. Manna, *J. Am. Chem. Soc.*, 2006, **128**, 748.
231 S. Ithurria and B. Dubertret, *J. Am. Chem. Soc.*, 2008, **130**, 16504.
232 W. Wang, S. Banerjee, S. Jia, M. L. Steigerwald and I. P. Herman, *Chem. Mater.*, 2007, **19**, 2573.
233 S. Sapra, J. Poppe and A. Eychmüller, *Small*, 2007, **3**, 1886.
234 S. Deka, K. Miszta, D. Dorfs, A. Genovese, G. Bertoni and L. Manna, *Nano Lett.*, 2010, **10**, 3770, DOI: 10.1021/nl102539a.
235 P. S. Nair, K. P. Fritz and G. D. Scholes, *Small*, 2007, **3**, 481.
236 R. Nötzel, *Semicond. Sci. Technol.*, 1996, **11**, 1365.
237 P. Bhattacharya, S. Ghosh and A. D. Stiff-Roberts, *Annu. Rev. Mater. Res.*, 2004, **34**, 1.
238 I. A. Ovidko and A. G. Sheinerman, *Adv. Phys.*, 2006, **55**, 627.
239 S. Ithurria, P. Guyot-Sionnest, B. Mahler and B. Dubertret, *Phys. Rev. Lett.*, 2007, **99**, 265501.
240 Z. Yu, L. Guo, H. Du, T. Krauss and J. Silcox, *Nano Lett.*, 2005, **5**, 565.
241 J. H. Yu, J. Joo, H. M. Park, S. Baik, Y. W. Kim, S. C. Kim and T. Hyeon, *J. Am. Chem. Soc.*, 2005, **127**, 5662.
242 C. Schliehe, B. H. Juarez, M. Pelletier, S. Jander, D. Greshnykh, M. Nagel, A. Meyer, S. Foerster, A. Kornowski, C. Klinke and H. Weller, *Science*, 2010, **329**, 550.
243 K. S. Cho, D. V. Talapin, W. Gaschler and C. B. Murray, *J. Am. Chem. Soc.*, 2005, **127**, 7140.
244 A. J. Houtepen, R. Koole, D. Vanmaekelbergh, J. Meeldijk and S. G. Hickey, *J. Am. Chem. Soc.*, 2006, **128**, 6792.
245 W. Koh, A. C. Bartnik, F. W. Wise and C. B. Murray, *J. Am. Chem. Soc.*, 2010, **132**, 3909.

246 P. T. K. Chin, J. W. Stouwdam and R. A. J. Janssen, *Nano Lett.*, 2009, **9**, 745.
247 S. G. Thoma, A. Sanchez, P. P. Provencio, B. L. Abrams and J. P. Wilcoxon, *J. Am. Chem. Soc.*, 2005, **127**, 7611.
248 N. Pradhan, H. Xu and X. Peng, *Nano Lett.*, 2006, **6**, 720.
249 F. S. Riehle, R. Bienert, R. Thomann, G. A. Urban and M. Krüger, *Nano Lett.*, 2009, **9**, 514.
250 Z. Tang, N. A. Kotov and M. Giersig, *Science*, 2002, **297**, 237.
251 M. Klokkenburg, A. Houtepen, R. Koole, J. W. De Folter, B. H. Erné, E. Van Faasen and D. Vanmaekelbergh, *Nano Lett.*, 2007, **7**, 2931.
252 M. Shim and P. Guyot-Sionnest, *J. Chem. Phys.*, 1999, **111**, 6955.
253 L. Li and A. Alivisatos, *Phys. Rev. Lett.*, 2003, **90**, 0974021.
254 D. V. Talapin, E. V. Shevchenko, C. B. Murray, A. V. Titov and P. Král, *Nano Lett.*, 2007, **7**, 1213.
255 S. Shanbhag and N. A. Kotov, *J. Phys. Chem. B*, 2006, **110**, 12211.
256 Z. Yu, M. A. Hahn, S. E. Maccagnano-Zacher, J. Calcines, T. D. Krauss, E. S. Alldredge and J. Silcox, *ACS Nano*, 2008, **2**, 1179.
257 J. Yang and J. Y. Ying, *J. Am. Chem. Soc.*, 2010, **132**, 2114.
258 T. Mokari, A. Aharoni, I. Popov and U. Banin, *Angew. Chem., Int. Ed.*, 2006, **45**, 8001.
259 I. R. Franchini, G. Bertoni, A. Falqui, C. Giannini, L. W. Wang and L. Manna, *J. Mater. Chem.*, 2010, **20**, 1357.
260 E. M. Chan, C. Xu, A. W. Mao, G. Han, J. S. Owen, B. E. Cohen and D. J. Milliron, *Nano Lett.*, 2010, **10**, 1874.
261 X. Peng, L. Manna, W. Yang, J. Wickham, E. Scher, A. Kadavanich and A. P. Alivisatos, *Nature*, 2000, **404**, 59.
262 A. Wolcott, R. C. Fitzmorris, O. Muzaffery and J. Z. Zhang, *Chem. Mater.*, 2010, **22**, 2814.
263 L. Manna, D. J. Milliron, A. Meisel, E. C. Scher and A. P. Alivisatos, *Nat. Mater.*, 2003, **2**, 382.
264 D. Chen, F. Zhao, H. Qi, M. Rutherford and X. Peng, *Chem. Mater.*, 2010, **22**, 1437.
265 J. M. Luther, H. Zheng, B. Sadtler and A. P. Alivisatos, *J. Am. Chem. Soc.*, 2009, **131**, 16851.
266 P. K. Jain, L. Amirav, S. Aloni and A. P. Alivisatos, *J. Am. Chem. Soc.*, 2010, **132**, 9997.
267 B. Sadtler, D. O. Demchenko, H. Zheng, S. M. Hughes, M. G. Merkle, U. Dahmen, L. Wang and A. P. Alivisatos, *J. Am. Chem. Soc.*, 2009, **131**, 5285.
268 K. Lambert, B. de Geyter, I. Moreels and Z. Hens, *Chem. Mater.*, 2009, **21**, 778.
269 M. Z. Liu and P. Guyot-Sionnest, *J. Mater. Chem.*, 2006, **16**, 3942.
270 L. Carbone, S. Kudera, C. Giannini, G. Ciccarella, R. Cingolani, P. D. Cozzoli and L. Manna, *J. Mater. Chem.*, 2006, **16**, 3952.
271 D. C. Lee, I. Robel, J. M. Pietryga and V. I. Klimov, *J. Am. Chem. Soc.*, 2010, **132**, 9960.
272 X. Peng, M. C. Schlamp, A. V. Kadavanich and A. P. Alivisatos, *J. Am. Chem. Soc.*, 1997, **119**, 7019.
273 I. Mekis, D. V. Talapin, A. Kornowski, M. Haase and H. Weller, *J. Phys. Chem. B*, 2003, **107**, 7454.
274 C. Bullen, J. van Embden, J. Jaseniak, J. E. Cosgriff, R. J. Mulder, E. Rizzardo, M. Gu and C. L. Raston, *Chem. Mater.*, 2010, **22**, 4135.
275 M. A. Malik, M. Afzaal and P. O'Brien, *Chem. Rev.*, 2010, **110**, 4417.
276 Y. Chen, J. Vela, H. Htoon, J. L. Casson, D. J. Werder, D. A. Bussian, V. I. Klimov and J. A. Hollingsworth, *J. Am. Chem. Soc.*, 2008, **130**, 5026.
277 B. Mahler, N. Lequeux and B. Dubertret, *J. Am. Chem. Soc.*, 2010, **132**, 953.
278 J. van Embden, J. Jasieniak and P. Mulvaney, *J. Am. Chem. Soc.*, 2009, **131**, 14299.
279 S. Deka, A. Quarta, M. G. Lupo, A. Falqui, S. Boninelli, C. Giannini, G. Morello, M. de Giorgi, G. Lanzani, C. Spinella, R. Cingolani, T. Pellegrino and L. Manna, *J. Am. Chem. Soc.*, 2009, **131**, 2948.
280 P. T. K. Chin, R. A. M. Hikmet, S. C. J. Meskers and R. A. J. Janssen, *Adv. Funct. Mater.*, 2007, **17**, 3829.
281 D. V. Talapin, R. Koeppe, S. Götzinger, A. Kornowski, J. M. Lupton, A. L. Rogach, O. Benson, J. Feldmann and H. Weller, *Nano Lett.*, 2003, **3**, 1677.
282 S. Kumar, M. Jones, S. S. Lo and G. D. Scholes, *Small*, 2007, **3**, 1633.
283 E. Shaviv, A. Salant and U. Banin, *ChemPhysChem*, 2009, **10**, 1028.

